Multi-objective H_∞/GH_2 preview control of active vehicle suspensions

Ahmad Akbari Alvanagh

Multi-objective H_∞/GH_2 preview control of active vehicle suspensions

Ahmad Akbari Alvanagh

This work concerns with multi-objective H_∞/GH_2 control of preview-based active vehicle suspensions. This control scheme has two main features:

1. It allows the constrained outputs of the system, namely, suspension working space, to vary freely as long as they remain within their given bounds, in order that the best possible performance could be delivered.

2. The optimization as well as constraint fulfillment is done for the worst case road disturbances in order that the designed system perform satisfactorily for a wide range of road irregularities. The H_∞ norm of (sub)system is minimized wherever minimization is required. Also, for the constrained outputs, the GH_2-norm measure is used to fulfill system constraints for the worst case disturbances.

Moreover, it allows for considering pole location constraints to guarantee sufficient stability margins for the system.

Output feedback nature of the design here makes it more convenient for practical implementation.

The proposed approach is first evaluated numerically on a quarter car model and compared to the state-of-the-art preview control algorithm in the literature, namely, LQG-preview, and finally it is verified experimentally.

ACKNOWLEDGMENTS

Firstly I wish to thank gratefully and sincerely my supervisor, Prof. Boris Lohmann for his guidance, understanding, patience, and most importantly, his friendship during my graduate studies. I have been amazingly fortunate to have a supervisor who gave me the freedom to develop on my own, and at the same time the guidance to recover when my steps faltered and helped me enrich my ideas.

I am grateful to all members of the institute of automatic control who accepted me with open arms and provided support in many different ways. They provided me with one of the most comfortable working places and friendly working atmosphere I have ever had.

Particularly, I wish to extend my warmest thanks to Guido Koch, Sebastian Spirk and Enrico Pellegrini, who built up and prepared the test-rig for the experimental verification of this work.

Also, I owe my gratitude to all other friends in a wider community in Munich who have made my life there both fruitful and enjoyable.

Most importantly, this wouldn't have been possible without the love and patience of my family. My family to whom this dissertation is dedicated, has been a constant source of love, concern, support and strength all these years. I would like to express my heart-felt gratitude to my family.

Ahmad Akbari   Munich, October 2008

TABLE OF CONTENTS

II Potential Assessment

LIST OF FIGURES

vii

LIST OF TABLES

Part I

Preliminaries

Chapter 1

INTRODUCTION AND MOTIVATION

A vehicle suspension system, apart from its static task of carrying car body, has to:

- isolate car body (and occupants) from road induced shocks and vibrations to provide **ride comfort** and pleasure for the occupants.

- ensure firm, uninterrupted contact of wheels to the road surface (good handling or good road holding) leading to **ride safety**.

- prevent excessive suspension bottoming. An important feature of real world car suspension design problem is that only a fixed and limited working space is available. The suspension working space is defined as the relative distance between axle and vehicle body and is limited by **structural constraints**. Hitting these constraints can lead to considerable deterioration of ride comfort and possible structural damage.

Clearly, these requirements should be fulfilled for any road type and any driving speed.

A suspension system in its most basic form consists of two basic components of spring and shock absorber (also known as damper). A vehicle is suspended over its wheels by springs, usually coil, leaf or air springs. Irregularities in the road surface are transmitted mechanically to the springs. The energy in the compressed springs is dissipated by shock absorbers. Fig. 1.1 shows two typical suspensions. The left one is a double-A or double-wishbone suspension. It has two parallel wishbone-shaped

arms to locate the wheel. The shock absorber and coil spring are mounted to the wishbones to control the vertical movement. The right one is called McPherson strut suspension. A strut suspension system combines the control arms and shock absorbers of a conventional suspension into one unit, thereby leading to a low-mass and space-saving design. In this approach, the whole damper/spring assembly turns with the steering. This unit is utilized in a large number of cars up to the midsize category.
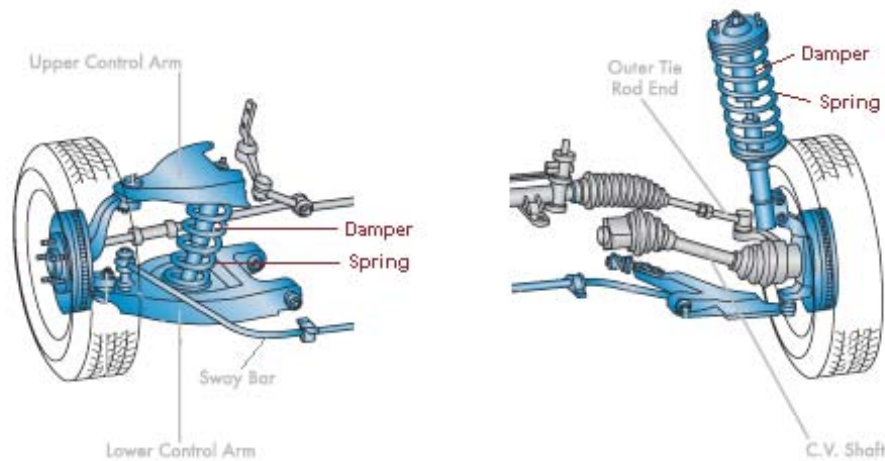
Figure 1.1: Two most common front suspension types. Left: Control arm type, Right: (McPherson) strut type. Figure from www.midas.com

1.1 Suspension strategies

The design requirements of vehicle suspensions are highly conflicting, for example enhancing ride comfort calls for larger suspension stroke and smaller damping of wheel-hop mode [11] and hence leads to a degradation in ride safety. Therefore, the design of a vehicle suspension calls for a trade-off between these conflicting objectives.

Different suspension strategies satisfy this indispensable trade-off to differing degrees, mainly influenced by the type or class of suspension used. Suspension systems can be classified into 3 groups: *Passive*, *semi-active* and *active*. This classification is based on similar definitions of passivity as used in electrical networks and mathematics [31]. Remember that a a system with input u and output y is called passive if

$$\int_0^T u^T y \, dt, \quad \forall T > 0$$

is lower bounded. In the case of suspensions, the force and displacement (or velocity) are considered as input and output respectively. Such a system, can only dissipate or absorb the input energy. Unlike passive systems that can only store or dissipate energy, active suspensions can continually vary the flow of energy and can supply energy to the system when required and therefore require an external power force. In other words, energy consumption of the systems is the main feature for their classification.

1.1.1   Passive suspensions

A passive suspension consists of spring and shock absorber. Ride comfort, i.e. better isolation of the sprung mass from road disturbances, requires a soft damping which is achieved by allowing a larger suspension deflection. But ride safety, i.e. keeping the tire in contact with road surface, can be achieved with a stiff damping by avoiding any unnecessary suspension deflections. Fig. 1.2 illustrates this conflict for a passive system. It shows how changing the elements of a passive system, namely damper coefficient b_s and spring stiffness k_s influences the ride comfort and safety. Elements of a passive suspension system are tuned as a trade off between these two conflicting criteria. When we refer to a traditional or a passive suspension system, we mean a system that comes as is. Once it has been installed in the car, its characteristics changes very little. Because of this inherent compromise, passive suspensions may only satisfy the essential requirements. For example, luxury limousines use soft suspensions to offer good ride comfort, while sport cars usually have stiff suspensions to achieve superior handling performance.
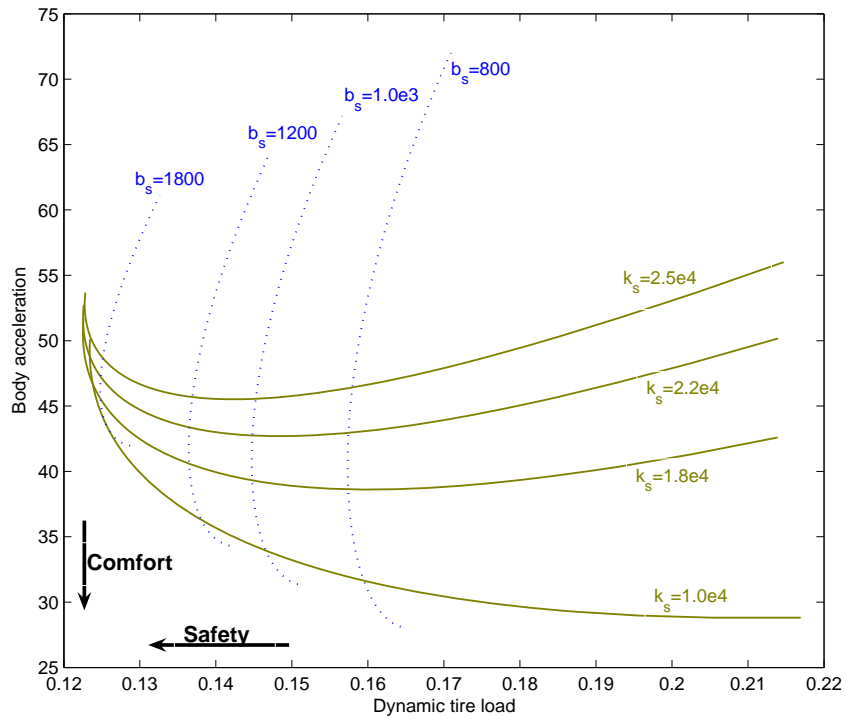
Figure 1.2: Ride comfort vs. safety for different values of the suspension elements

1.1.2 Semi-active suspensions

The aforementioned conflict in performance requirements of a suspension system can be improved by employing a damper with variable damping characteristics. This strategy is referred to as semi-active suspension. Depending on the road excitation, damping is adjusted to increase performance. Fig. 1.3 shows the characteristics of the semi-active damper compared to a passive one.

The damping force in a shock absorber is generated when the oil flow through the hydraulic orifices in the shock absorber. The lower the oil flow is, the larger damping force can be generated. Therefore, the damper coefficient can be controlled through
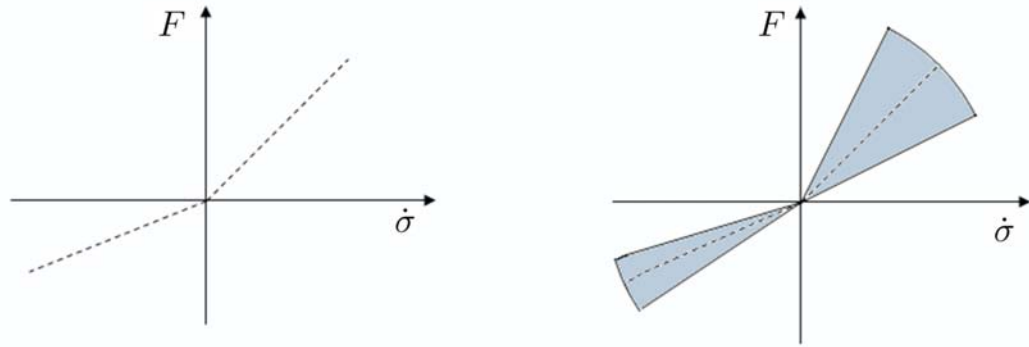
Figure 1.3: Damper characteristics, left:passive suspension, right:semi-active suspension; $\sigma := z_s - z_u$

either the control of fluid viscosity or adjusting the orifice.

Dampers with controllable orifice

Early semi-active dampers are based on the latter regulation technique. One distinguishes two types of semi-active dampers in this category: *on/off controlled (switchable)*, where various throttles are switched on or off to control the restrictiveness of the damper. and *continuously controlled*, which employs a continuous valve. The adjustment of the throttle is achieved using an electric motor or by means of magnet valves[17]. The change speed, because of mechanical motion, is slow. However, currently ZF Sachs offers a state of the art variable dampers under the name of CDC (continuously damping control) [9], having high switching times between 11 and 40 ms.

Dampers with controllable fluid

ER (Electro-rheological) and MR (Magneto-rheological) fluids are two kinds of smart materials, which can be used for this purpose. There are polarizable particles of a few microns in the oil, which are made by mixing fine particles into a synthetic

hydrocarbon oil. The working principle of this type of dampers is illustrated in Fig. 1.4. When this fluid is subjected to an electrical or magnetic field, the particles will be polarised and distributed in a sequential order, leading to a stiffer suspension system. The fluid can react within 1 ms and can be easily controlled. Both ER and MR fluids were initially developed independently in the 1940's. Initially, it was ER fluids that received the most attention, but soon they were found to be not so well suited to most applications as MR fluids [63]. In their non-activated or "off" state, both have typically similar viscosity, but MR fluids exhibit a much greater increase in viscosity. For a typical ER fluid, the maximum yield stress is about 10 kPa, but it is about 100 kPa for a typical MR damper.

MR dampers were firstly came into series production in the 2002 Cadillac Seville STS. It was based on first version of Delphi's MagneRide system. In 2006, Audi launched the new TT model, which is based on the refined Delphi's MagneRide system.

Other types of semi-active suspensions:

A semi-active suspension system may also utilize a semi-active (air) spring. Its principle is simple. Different spring stiffnesses is realized by alteration of air volume. But, this leads to a change in initial deflection. To cope with the problem, hydropneumatic systems can be used, in which the removed air is replaced with hydraulic liquid. For more details, refer to [42]. Other types of semi-active suspensions include various self-leveling solutions. Suspensions systems like Hydrolastic, and Hydragas (an evolution of Hydrolastic)[36] can be classified in the category of semi-active suspensions.

The criterion determining the change of suspension stiffness is known as control law. Many control laws have been presented in the literature for adjusting a semi-active system, e.g. [43, 50]. However, a well known control law to change the damper coefficient, is based on sky-hook theory. The principle of this approach is to reduce the oscillations of body and wheel independently of each other. This is done by assuming that the body is linked to the sky and tuning the damper so that the same performance is obtained in real case, i.e., when no such a link exists. For more details and relation see e.g. [45].
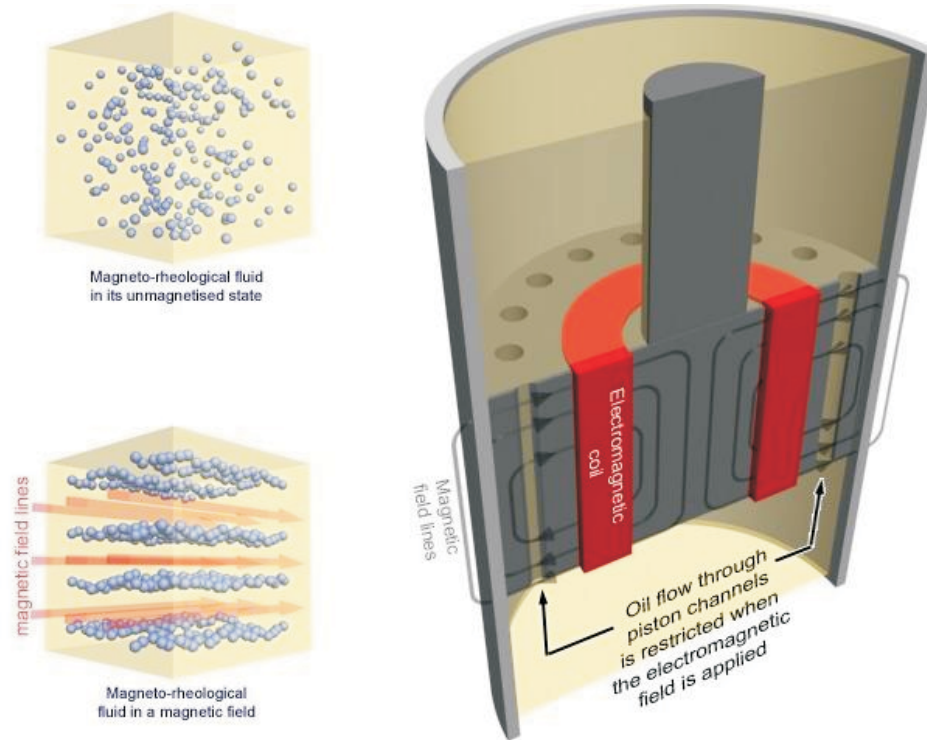
Figure 1.4: working principle of MR damper, figure from [36]

It should be pointed out that a semi-active system, like a passive system, can only dissipate the power. But it consumes some energy for changing system damping. The energy is needed to drive the sensors, damper valves and the controller, and not to provide the control force.

Other implemented semi-active suspensions

Porsche PASM (Porsche Active Suspension Management): A series of sensors monitors the body. A dedicated control unit provides real-time analysis and damping force adjustment as defined for the respective setup mode (Normal or Sport).

BMW EDC (Electronic Damper Control): Sensitive sensors constantly monitor all factors influencing the vehicle's behaviour and occupants comfort, including road

conditions, load changes and vehicle speed. In a fraction of a second, the signals are analysed by the EDC microprocessor and orders are sent to the actuators on the shock absorbers, which, with the help of magnetic valves, are variably adjusted to provide optimal suspension.

1.1.3 Active suspensions

Different from semi-active suspensions, an active suspension does not change the damper characteristics, but generally is implemented using an actuator that either replaces or acts in parallel with the suspension components. The great virtue of an active suspension system is its ability to adapt to variable road conditions, and to employ the full suspension working space (allowable suspension stroke) to satisfy ride comfort and handling requirements. To understand apparently the subtle difference between semi-active and active suspensions, consider a hypothetical conflict with a known pothole. A semi-active system will make the suspension softer when hitting the pothole and stiff after the pothole. An active suspension could feasibly lift the wheel over the pothole, and thereby will improve both ride comfort and safety.

An indispensable part of this type of suspensions are sensors and a microprocessor. Clearly, this type of technology typically appears on very expensive cars. But, rapid advances in microprocessor science, sensor and actuator technology may bring these features to a whole new range of vehicles.

Active suspension systems can be divided into two types of fast active and slow active. A detailed comparison of these types is given in [20].

fast active

In fast active (often referred to as fully active or high bandwidth suspension) systems the control actuator is mounted in parallel with a passive suspension. In some cases, there may be no passive damper or even no passive suspension. Typically discussed actuation systems, are hydraulic, hydropneumatic and pneumatic systems. In prac-

tical systems, the actuator usually placed in parallel with a passive spring so that it doesn't have to support the weight of the vehicle, thus greatly reducing the actuator static force [27]. But the actuator needs to have a large bandwidth to minimize the transmission of high frequency as well as low frequency loads/ disturbances to the vehicle. Clearly, this suspensions improve system performance in the whole desired frequency range.

Due to the complexity, costs and energy demand of these systems, no active systems got to the market, they have been realized only on research or prototype vehicles. A recently publicized fully active system is from Bose Corporation. The Bose suspension system, shown in Fig. 1.5, uses on each corner of car a single linear electromagnetic motor and power amplifier. These motors act both as sensors and as actuators. When a wheel moves up or down, the motor functions as a generator to send a signal to the control unit, announcing the presence of a bump or hole. The unit then sends the proper current to each motor to keep the car level [1].
One of the big advantages of an electromagnetic approach is speed. The linear electromagnetic motor responds quickly enough to counter the effects of bumps and potholes, thus allowing it to perform the actions previously reserved for shock absorbers.

slow-active

As mentioned above, the actuator bandwidth required for a fully active system is typically 15 Hz. This translates into an expensive actuator. One way to address this problem is to use slow active systems, in which the actuator is placed in series with passive springs. In this strategy, the actuator controls the low frequency (less than 3 Hz) motions, whilst the passive spring controls the higher frequency motions in the range where the actuator is essentially very stiff. It has been shown that slow active suspensions can provide asymptotically, with negligible reduction, the performance of fully active suspensions[43, 50].

A slow active suspension system in series production is the Active Body Control (ABC), introduced in 1999 on the Mercedes-Benz CL-Class. This system is standard on all Mercedes-Benz SL and CL class models and on some S Class models. Its
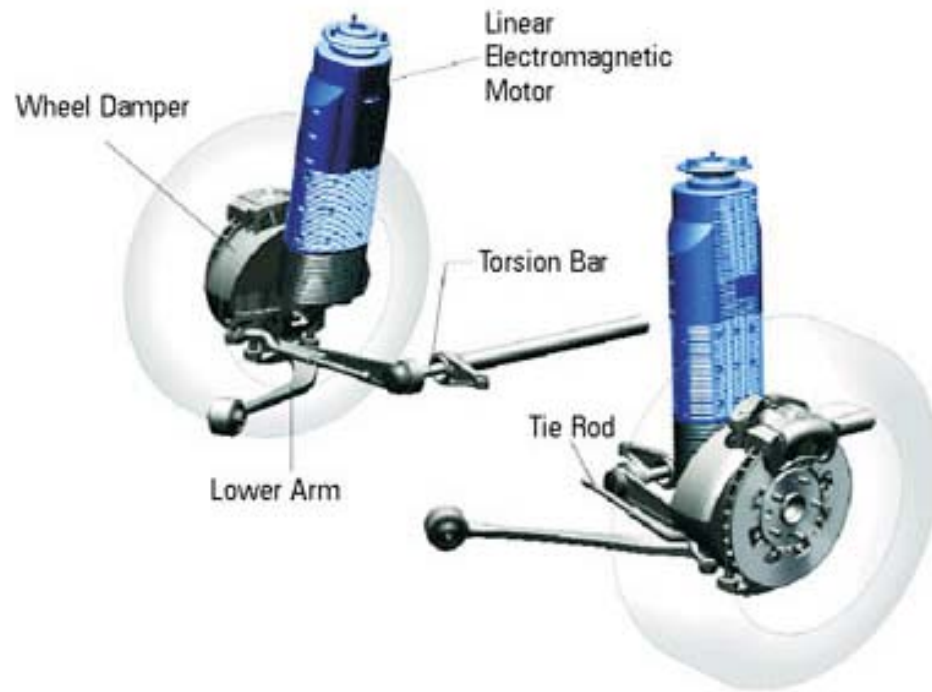
Figure 1.5: Bose suspension system

schematics is given in Fig. 1.6. In the ABC system, the control system detects body movement from 30 sensors located throughout the vehicle, and controls the action of the active suspension with the use of hydraulic servomechanisms.

The system also enjoys the level adjuster feature, which enables the vehicle level to be raised/ lowered manually and automatically depending on vehicle speed. The level control helps keep the vehicle level at the front and rear axle according to the driving/load condition in each case and keeps it constant.

At the end of this section, it should be pointed out that in the vehicle marketing the term active suspension system, also known as Computerized Ride Control (CRC), loosely refers to a wide range of both slow and fast active or even semi-active suspensions. Since the most companies haven't disclosed their CRC suspension structure, here we just mentioned examples of each suspension type and surveying all CRC
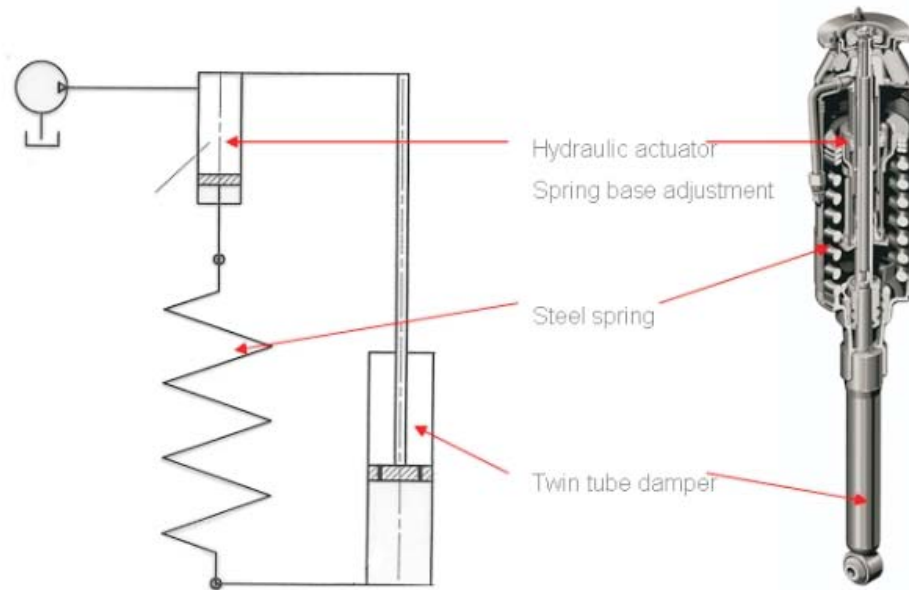
Figure 1.6: Active Body Control

products is behind the scope of this study.

1.2 Preview based active suspensions

Suspension performance of active suspensions can be further improved if preview, i.e., knowledge of the road surface in front of controlled axles, is used in the control strategy [26]. This is done by including a feedforward term (or preview control) in feedback controller. This scheme promises more improvements in system performance, compared to its pure feedback counterpart.

Two main reasons for exploiting the preview based active suspensions are:

1. To 'prepare' the system for oncoming disturbance. If preview information is used

by the controller, when facing a bump, the control system lifts the wheel over the bump, and thereby reduces the forces transmitted to the body. Compared to its non-preview active counterpart, even in the case of ideal sensors and actuators, preview active suspension reacts very fast. In fact, it reacts before hitting the bump, but the non-preview one after observing the effect of bump on vehicle motions.

2. To counteract the delays in the reaction of the system and actuator. In a non-preview active suspension, the control system must react very quickly to suppress the effect of disturbances that already have been encountered by the vehicle. In those cases where transients occur faster than the rate of response, some form of preparation strategy is clearly essential. This 'preparation strategy' implies the need for information describing disturbances before they are encountered by the vehicle [33].

This strategy since its emergence by Bender [5] has been investigated by a few researchers and some contributions are reported in the literature. They all have reported a considerable enhancement in system performance, when preview information is utilized by the control law. A survey of the these contributions is given in chapter 3 and here to give a perspective on motivating the current work, they will be generally and conceptually, with an emphasis on recent works, reviewed.

Years after the early proposed control approaches, which are mainly based on Wiener-Hof filter, Foag [18] made one of the major contributions in this field. He formulated the problem of active preview suspension as a multi-criteria one and used the optimization approach based on K-S functions to solve the problem. His formulation of the problem is the most perfect one presented so far, unfortunately this work is rarely recited in the literature of active suspension. This work, however, doesn't care for measurement noises in the design. Moreover, it solves the optimization problem for two inputs of step and half-sinus and therefore, the system may lose the performance encountering other types of inputs.

Later studies, to cope with these issues, utilized *LQ*-based optimization approaches. A detailed study of this scheme for all vehicle models from quarter car to full car, both slow active and fully active suspensions and discrete time as well as continuous time designs can be surveyed in the literature. *LQ*-based design provides an appealing design tool for active suspensions, and despite its simplicity gives insight into performance potentials and trade-offs. But it suffers from the following drawbacks:

1. It's a single objective design, but the active suspension design requires a multi-objective one. In LQ-based designs the output constraints, such as the ones on working space, are not treated explicitly. Constraint fulfillments are tested a posteriori with the help of so-called carpet plots which depict the closed loop behavior as a function of different LQ controller design parameters.

2. Optimization is done in time domain and just for the white-noise inputs. And it may not work satisfactorily for other types of disturbances. Moreover, it possesses lower stability margins.

3. It is based on state feedback design and system may deteriorate its performance when an estimator is included in the system. This has been shown for a typical suspension system in [59].

The study here tries to overcome these problems by employing an output feedback multi-objective preview control, where the optimization is done in the frequency domain for the worst case road disturbance (unknown spectra), and thereby addresses more stability. The design scheme is based on an LMI approach, which offers powerful design tools for multi-objective designs.

Output feedback nature of the design here makes it more convenient for practical implementation, furthermore, it avoids performance degradation, caused in LQ-based design by adding observer to the system.

To avoid performance degradation by discretizing the controller, the design is done in the discrete time domain.

Moreover, to ensure desired stability margins for the system, pole location constraints are considered in the design.

Clearly, generalization of multi-objective design to discrete time preview systems is also some part of this contribution.

The proposed approach is first evaluated numerically on a quarter car model with an insight to its extension to more precise models and finally it is implemented experimentally.

ABC Pre-sacn: realization of preview concept on a research car

we conclude this section with an overview on ABC Pre-scan. The research car F700 with pre-sacn presented to the public at IAA 2007, was the first to employ the active suspension with preview. Pre-scan merges the features of ABC suspension with preview. Laser sensors from SICK corporation are integrated in the headlights of the F700 and scan the road surfaces ahead. To detect road irregularities as accurate as possible, road is scanned at a few distances ahead of vehicle. To any measuring point, as illustrated in Fig. 1.7, an individual distribution function is assigned. This distribution function takes into account the beam expansion and the imprecision of the measurement procedure. Then road profile is computed through weighted averaging and iterative recursive reconstruction [49].

Pre-scan control system is based on modal perspective of the closed loop where the closed loop system is designed to track some prespecified desired dynamics. Comparison of the proposed control strategy here with that of the Pre-sacn is left for future works.

1.3 Synopsis

This thesis is organized as follows.
Chapter 2: Design requirements and problem formulation. The quarter car
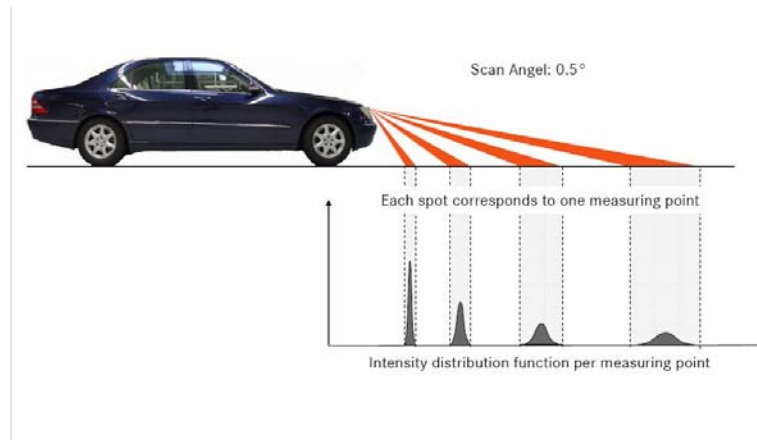
Figure 1.7: Disturbance detection scheme of ABC-Prescan [49].

as well as half car models used in the potential assessment part of the study are described in this chapter. Design requirements mainly based on the quarter car model are given and suitable system norms to formulate them mathematically are discussed in this chapter. The design framework is finally obtained and a guideline to extend this framework to half car and full car models concludes this chapter.

Chapter 3: look-ahead preview design. This chapter contains a survey on preview active suspensions and discusses why the preview idea and not feedforward controller has to be used for the active suspensions. It derives a unified design framework for (LQ-based and multi-objective) preview suspension design. This chapter, for the sake of comparison, gives a detailed compilation of discrete time LQ-based preview design and considers it for the quarter car model of chapter 2. Generalization of multi-objective design to discrete time preview systems is also given in this chapter. A comparison study details the benefits of multi-objective preview design compared to the LQ-based preview design.

Chapter 4: A perspective on wheelbase preview. There are two ways to obtain preview information, one using a look-ahead sensor, mounted on front bumper of the vehicle, and the other by estimating road profile from the system response, referring

to as wheelbase preview. This chapter gives some insight into the wheelbase preview design using the proposed approach. However, because of similarity to quarter car, to avoid duplication, it mainly highlights the robust estimation of the front wheel disturbance from system response.

Chapter 5: Experimental setup description and preview suspension design. Discussions in chapter 3 consider a linear system with an ideal actuator. Switching to a practical system requires considering actuator dynamics as well as the effect of nonlinearities on system performance. This chapter, after a short description of the test-rig, concerns with preview suspension design for the system addressing the above issues. The performance of both LQ-based and multi-objective preview controller, in presence of system nonlinearities are compared.

Chapter 6: Implementation and related challenges. This chapter deals with the challenges associated with the practical implementation of the preview suspension on the test-rig, and finally reports the results of the application.

Chapter 7: Conclusion and outlook. This chapter concludes this thesis and proposes some possible further research topics.

Chapter 2

DESIGN REQUIREMENTS

This chapter provides the preliminary steps for designing an active vehicle suspension. Firstly it introduces some simple, widely used models of automotive dynamics. Then requirements of the design which play a great role in any control system design, are given.

This study mainly deals with a quarter car model. Therefore, the focus will be on quarter car model, however, in any situation it will be discussed how it could be extended to be applicable to half car or even full car models.

2.1 System description

A mathematical description of a real world system may be obtained through various approaches, including multi-body, finite element or identification, however they all rely on some simplification, (probably linearization) and idealization.

The simplification degree of the model is primarily determined by the problem at hand. For economic reasons it should be as simple as possible, while reflecting the essential information about the system. Additionally, a simple model often has the benefit of leading to greater transparency of the studied phenomena [55].

For the purpose of vehicle suspension studies, multi-body systems have been widely used in the literature and proved to be valuable. In this way, the essential structural components of a vehicle, like wheels, axles, car body, motor, gearbox, etc. are modeled

as ideal rigid bodies or point masses. and these masses are connected by suspension system components (spring/ damper/ actuator), which are assumed to have no mass.

2.1.1 Quarter car model

Considering the vertical dynamics and taking into account the vehicle's symmetry, a suspension can be studied based on a quarter car model. Therefore, a 2-DOF vehicle suspension representing a quarter-car model, shown in Fig. 2.1, will be mainly used in this study. This linear model assumes damping in the tire and an ideal actuator between the wheel and car body. This model despite its simplicity, captures major characteristics of a real suspension system, and continues to be a useful tool for understanding the behavior of vehicle suspensions. Here, m_s denotes the portion of
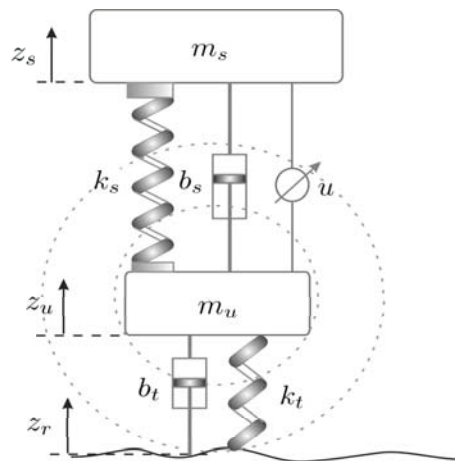
Figure 2.1: A quarter-car active suspension system

body mass (sprung mass) corresponding to one corner of the vehicle. The unsprung mass m_u is the mass of wheel and axle at one corner. k_s and b_s represent the suspension stiffness and damping coefficient respectively, and k_t and b_t model the tire stiffness and damping respectively. The nomenclature used and parameter values, which will be considered in chapter 3 of this study, are given in Table 2.1. These values are borrowed from [10].

As illustrated on Fig. 2.1, the variables z_s and z_u denote absolute vertical displacements of the sprung and unsprung masses measured from static equilibrium and z_r represents the road unevenness with respect to the static equilibrium case. The variable $u(t)$ denotes the actuator force, added to the system in the case of active suspension. According to these definitions and assuming a linear characteristics for stiffness and damping, the equations governing the motions of the sprung and unsprung masses are given by

$$\begin{cases} m_s\ddot{z}_s + b_s(\dot{z}_s - \dot{z}_u) + k_s(z_s - z_u) = u, \\ m_u\ddot{z}_u + b_s(\dot{z}_u - \dot{z}_s) + k_s(z_u - z_s) + k_t(z_u - z_r) + b_t(\dot{z}_u - \dot{z}_r) = -u \end{cases} \tag{2.1}$$

Choosing the set of state variables as

$$x_1(t) = z_u - z_r,$$
$$x_2(t) = \dot{z}_u,$$
$$x_3(t) = z_s - z_u,$$
$$x_4(t) = \dot{z}_s$$

the state space description of the system is obtained as

$$\dot{x}_c(t) = A_c x_c(t) + B_{c,u}u(t) + B_{c,w}w(t) \tag{2.2}$$

where

$$A_c = \begin{pmatrix} 0 & 1 & 0 & 0 \\ -k_t/m_u & -(b_s + b_t)/m_u & k_s/m_u & b_s/m_u \\ 0 & -1 & 0 & 1 \\ 0 & b_s/m_s & -k_s/m_s & -b_s/m_s \end{pmatrix}$$

$$B_{c,w}^T = \begin{pmatrix} -1 & -b_t/m_u & 0 & 0 \end{pmatrix}$$

$$B_{c,u}^T = \begin{pmatrix} 0 & -u_{max}/m_u & 0 & u_{max}/m_s \end{pmatrix}$$

where the control input u is defined as u_f/u_{max}, with u_{max} being the normalizing factor and u_f the actuator real force., and $w = \dot{z}_r$ (ground vertical velocity) is considered as disturbance input.

Model parameters	symbol	values	unit
sprung mass	m_s	320	kg
suspension stiffness	k_s	18000	N/m
suspension damping rate	b_s	1000	N/(m/sec)
Wheel assembly mass	m_u	40	kg
tire stiffness	k_t	200000	N/m
tire damping	b_t	170	N/(m/sec)
normalizing factor	u_{max}	1000	N

Table 2.1: Nomenclature and parameter values in a quarter car model (from [10])

A popular method of analyzing systems with elastic, mechanical elements is modal analysis. In this method, the so-called modal parameters are determined, which characterize the dynamic properties of the system under study. The modal parameters consist of system natural frequencies, damping factors and mode shapes. For the quarter car, described above, modal parameters under passive suspension, are given by

$$\omega_s = \sqrt{\frac{k_s}{m_s}}, \quad \zeta_s = \frac{b_s}{2m_s\omega_s}$$
$$\omega_u = \sqrt{\frac{k_t}{m_u}}, \quad \zeta_u = \frac{b_t}{2m_u\omega_u}$$

The unsprung mass mode is often referred to as wheel-hop mode and characterized by relatively light damping and natural frequency $f_{us} = \omega_{us}/2\pi$ between 8 and 12 Hz. Wheel-hop is a resonance mode where the wheels of the car move with large amplitude with respect to the road, while car body remains relatively still.

The principal body mode or sprung mass mode, is typically has a natural frequency $f_s = \omega_s/2\pi$ lying in the 1-2 Hz [31].

Invariant points on frequency response

Assume that the tire has no damping, i.e. $b_t = 0$, then side by side adding of equations

(2.1) gives

$$m_s \ddot{z}_s + m_u \ddot{z}_u + k_t(z_u - z_r) = 0 \qquad (2.3)$$

This equation is independent of both the passive and active suspension forces! This is the basic invariant equation for this vibration isolation problem and several interesting conclusions can be drawn from it. Taking Laplace transform from (2.3), assuming zero initial conditions one obtains

$$m_s \frac{\ddot{Z}_s(s)}{Z_r(s)} + \left(\frac{k_t}{s^2} + m_u\right) \frac{\ddot{Z}_u}{Z_r(s)} = k_t \qquad (2.4)$$

setting $s = j\omega$, it can be easily realized that the transfer function $\frac{\ddot{Z}_s(s)}{Z_r(s)}$, independent of suspension strategy, has an invariant point at wheel-hop frequency of $\omega_u = \sqrt{\frac{k_t}{m_u}}$, with the magnitude of $\frac{k_t}{m_s}$.

Similarly, one can show that the transfer function from road irregularity to suspension deflection has an invariant point at rattle-space frequency of $\omega_s = \sqrt{\frac{k_t}{m_u+m_s}}$. But the tire deflection transfer function possesses no invariant point.

These invariant points, which hold under zero tire damping, were firstly introduced by [29]. Although neglecting the tire damping is common in many studies about active suspensions, there are some studies that include it, e.g. [65], arguing that it allows the reduction of passenger acceleration at frequencies near the wheel-hop mode. This is because of the fact that taking the tire damping to be nonzero, yet small, couples the unsprung and sprung masses at all frequencies. In this study the latter case, i.e. nonzero tire damping, will be considered.

2.1.2   Half car model

A pitch-plane (bicycle) half-car model, which is a natural extension of the quarter car model, is given in Fig. 2.2. This structure will be employed in chapter 4 to give a perspective on wheelbase preview active suspensions. Moreover, it provides definitions to facilitate the extension of quarter car based designs to half car models.

It consists of the sprung (body) mass, two unsprung masses (wheel-axle assemblies)
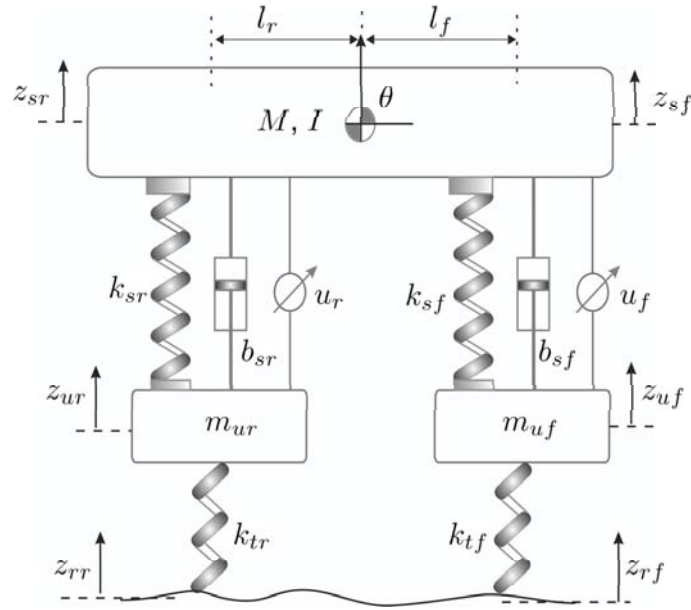
Figure 2.2: A typical half car model with active suspension

and the suspension system placed between them. The suspension system is assumed to be active, i.e., it comprises a spring/ damper pair parallel to an actuator. The nomenclature used and parameter values are given in Table 2.2. Parameter values, which will be employed in studies of chapter 4, are borrowed from [53].

The sprung mass is assumed to be rigid and has freedom of motion in heave and pitch directions. Either of unsprung masses has the freedom of motion in vertical direction. Thus the half car model has four degrees of freedom.

According to the variables defined on the figure, the equations governing the motions of sprung and unsprung masses are given by

$$M_s \ddot{q} = G B_s (\dot{z}_u - \dot{z}_s) + G K_s (z_u - z_s) + G u,$$
$$M_u \ddot{z}_u = B_s (\dot{z}_s - \dot{z}_u) + K_s (z_s - z_u) + K_t (z_r - z_u) - u \tag{2.5}$$

Model parameters (symbols)	values
sprung mass (m_s)	$730 \pm 40\%$ kg
pitch moment of inertia (I)	$1230\ kg.m^2$
distance between C.G. and front axle (l_f)	1.011 m
distance between C.G. and rear axle (l_r)	1.803 m
front suspension stiffness (k_{sf})	19960 N/m
rear suspension stiffness (k_{sr})	17500 N/m
front suspension damping rate (b_{sf})	1290 N/(m/sec)
rear suspension damping rate (b_{rf})	1620 N/(m/sec)
front unsprung mass (m_{uf})	40 kg
rear unsprung mass (m_{ur})	35.5 kg
front tire stiffness (k_{tf})	175500 N/m
rear tire stiffness (k_{tr})	175500 N/m
road roughness coefficient (G_0)	5.12×10^{-6} m
vehicle forward velocity (V)	20 m/s

Table 2.2: Nomenclature and values of the parameters in a half car model

where

$$q = \begin{pmatrix} z_c \\ \theta \end{pmatrix}, \quad z_s = \begin{pmatrix} z_{sf} \\ z_{sr} \end{pmatrix}, \quad z_u = \begin{pmatrix} z_{uf} \\ z_{ur} \end{pmatrix}, \quad z_r = \begin{pmatrix} z_{rf} \\ z_{rr} \end{pmatrix} \quad u = \begin{pmatrix} u_f \\ u_r \end{pmatrix} \tag{2.6}$$

and the matrices of sprung mass (M_s), unsprung mass (M_u), suspension stiffness (K_s), suspension damping (B_s), tire stiffness (K_t) and geometry (G),are given as

$$M_s = \begin{pmatrix} m_s & 0 \\ 0 & I_\theta \end{pmatrix}, \quad M_u = \begin{pmatrix} m_{uf} & 0 \\ 0 & m_{ur} \end{pmatrix},$$
$$K_s = \begin{pmatrix} k_{sf} & 0 \\ 0 & k_{sr} \end{pmatrix}, \quad B_s = \begin{pmatrix} b_{sf} & 0 \\ 0 & b_{sr} \end{pmatrix}, \tag{2.7}$$
$$K_t = \begin{pmatrix} k_{tf} & 0 \\ 0 & k_{tr} \end{pmatrix}, \quad G = \begin{pmatrix} 1 & 1 \\ l_f & -l_r \end{pmatrix}$$

Note that this description (except for the vectors/ matrices instead of scalars) coincides with that of the quarter car model and thus allows for extension of quarter car

design tools to half car models.

Assuming that the pitch motion is small enough, the following linear approximations can be applied

$$z_{sf} = z_c + l_f \theta,$$
$$z_{sr} = z_c - l_f \theta$$

which yields

$$z_s = G^T q$$

therefore, left-multiplying $G^T M_s^{-1}$ both sides of the first equation in 2.5, we arrive at

$$\ddot{z}_s = N[B_s(\dot{z}_u - \dot{z}_s) + K_s(z_u - z_s) + u]$$

where $N := G^T M_s^{-1} G$. Choosing the set of state variables as

$$x^T = \left((z_s - z_u)^T \quad \dot{z}_s^T \quad (z_u - z_r)^T \quad \dot{z}_u^T \right) \in \mathbb{R}^8$$

and $w = \left(w_f \quad w_r \right)^T = \dot{z}_r$ (ground vertical velocity) as disturbance input, the state space description matrices are given as

$$A_c = \begin{pmatrix} 0 & I & 0 & -I \\ -NK_s & -NB_s & 0 & NB_s \\ 0 & 0 & 0 & I \\ M_u^{-1}K_s & M_u^{-1}B_s & -M_u^{-1}K_t & -M_u^{-1}B_s \end{pmatrix}, B_{c,u} = \begin{pmatrix} 0 \\ N \\ 0 \\ M_u^{-1} \end{pmatrix} B_{c,w} = \begin{pmatrix} 0 \\ 0 \\ -I \\ 0 \end{pmatrix}$$

2.2   Design requirements and problem formulation

When designing a suspension system, the dual objective is to isolate car body from road disturbances and maximize the tire road contact. Good vibration isolation is required to secure the ride comfort, whereas good road holding is important for vehicle handling, which in general leads to enhanced safety. In real world car suspension

design, however, it should be noted that only a fixed and limited working space is permitted. The suspension working space (or suspension deflection) is defined as the relative distance between axle and vehicle body and is limited by constructional reasons. Moreover, in the case of active suspensions, the actuation should be run with as low energy as possible.

The goal of this section is to formulate mathematically these requirements. Let's start with a quarter car model. First of all, we need to give the criteria used in the literature to quantify the above requirements

2.2.1 Performance evaluation criteria

1. Ride Comfort: Previous researches (see [31] and references therein) have investigated the correlation between the ride comfort and vehicle body acceleration and have found that ride comfort of a vehicle, also known as vibration isolation ability, is judged by the RMS value of the acceleration, sensed by vehicle passengers. This is a widely used measure for ride comfort. On the other hand, according to ISO-2631 human body is more sensitive to frequencies near 4-8 Hz in the vertical direction [31]. This fact calls for more stress on minimizing the acceleration in these frequencies. Hence the RMS weighted body acceleration is used to evaluate the ride comfort, i.e., $z_{11} = W_{\ddot{z}_s}\ddot{z}_s$ where

$$W_{\ddot{z}_s} = \frac{50s + 500}{s^2 + 60s + 1412}$$

   This weight, which is in fact the transfer function from body acceleration to passenger-perceived acceleration, has its peak in the above frequency range to emphasize the importance of minimization in this frequency range. Note that the more recent VDI standard, gives higher order weighting function for assessing ride comfort, and the one used here can be considered as its simplified model.

2. Ride safety: Firm uninterrupted contact of wheels to road against road disturbances (good road holding) is necessary for vehicle handling and leads to ride

safety. Many authors in the literature, e.g. ([11, 25]), have relied on the idea that for ride safety, the dynamic tire load should not exceed the static one, i.e.,

$$k_t(z_u(t) - z_r(t)) + b_t(\dot{z}_u(t) - \dot{z}_r(t)) < (m_s + m_u)g, \quad \forall t \geq 0$$

But in practical situations, there are many forces acting on the wheel that can lift it off the road. This criterion in many situations will lead to losing the contact with the road, and hence losing the control of the vehicle, in either drive or steering senses. Therefore, it is desirable to keep the tire deflection as small as possible, and we define the second controlled output as

$$z_{12}(t) = z_u - z_r$$

The minimization of this variable, especially in the frequency range near wheel-hop frequency is of interest.

3. Control effort: Clearly, it is desirable to minimize the control effort of a system as far as possible. Therefore, we choose

$$z_{13}(t) = u$$

4. Suspension deflection limit: Suspension systems are placed between the chassis and wheel assembly, hence structural features of a vehicle impose a hard limit on the suspension stroke. Hitting the deflection limit not only results in deterioration of ride comfort, but also even may cause structural damage. Thus, it is important that the suspension stroke should not exceed a prespecified limit,

$$|z_s(t) - z_u(t)| < SS_{max}, \quad \forall t \geq 0$$

Remark 2.1: The measures discussed above, coincide with those of [18]. However, as it will be discussed in next subsections, here the worst case road irregularities will be considered, covering all road profiles.

2.2.2   Suitable design framework

The objective here is to cast the problem into a suitable design framework. It is clear that the design approaches impose some limitations on the formulation of the problem and avoid considering all requirements as they are. Based on what described above and due to simplicity of optimal control, LQ-based design has been an appealing design tool for active preview suspensions. In this design approach, all the above requirements are translated into finding the control input u, which minimizes the **single objective** of

$$J = \lim_{T \to \infty} \frac{1}{2T} \int_0^{+\infty} E \left\{ \ddot{q}^2 + \rho_1 (z_s - z_u)^2 + \rho_2 (z_u - z_r)^2 + \rho_3 u^2 \right\} dt$$

where for the case of quarter car model, $q = \ddot{z}_s$, and the ρ_i is the weighting used to penalize the corresponding effect in the performance index. Based on the discussion above, in reality we need to constrain suspension deflection within a prespecified range, not to minimize it. In the single objective design above, whether the constraints on suspension deflection are fulfilled or not, is checked for by a posteriori analyzing the closed loop, requiring many trials before a satisfactory control law is obtained.

To achieve the best possible performance, it is required to minimize RMS body acceleration, tire deflection and control signal while suspension deflection is allowed to vary freely within its prespecified bounds. Therefore, controller design for a vehicle suspension by is its nature a **multi-objective** design [2]. Multi-objective design [48] offers a very flexible and powerful design framework, in which control objectives are specified as different channels of the system and each channel is handled with an appropriate norm independently. Before formulating the problem in the desired framework, for the sake of completeness, we briefly review the systems norms will be used in this formulation.

2.2.3 System norms

in LQ-based design as well as K-S optimization, the optimization is carried out in time domain. The common drawback of time domain optimizations is that the design is done for a special class of inputs and it may deteriorate its performance, when encountering other inputs. Here a frequency domain optimization will be used to allow for consideration of a wide range of inputs. Optimization in the frequency domain requires norms for transfer functions. These norms are used for comparing systems. The system-norms which will be employed in this study include: H_2, H_∞ and GH_2 (Generalized H_2).

The **H_2 norm** of (sub)system T_1, where T_1 represents the transfer function from input w to output z_1, is defined by

$$\|T_1\|_2^2 = \frac{1}{2\pi} \int_{-\infty}^{\infty} |T_1(j\omega)|^2 d\omega \tag{2.8}$$

On the other hand, the Power Spectral Density (PSD) of the output of a system is given by

$$S_{z_1}(\omega) = |T_1(j\omega)|^2 S_w(\omega)$$

and therefore, the RMS value of the output is given by

$$z_{1,rms} = \left\{ \frac{1}{2\pi} \int_{-\infty}^{\infty} |T_1(j\omega)|^2 S_w(\omega) d\omega \right\}^{1/2}$$

For white noise inputs, $S_w(\omega) = 1$ for all frequencies. Hence, the system H_2 norm can be interpreted as the RMS value of the output when the system is driven by white noise input.

The **H_∞ norm** of (sub)system T_1, is defined as

$$\|T_1\|_\infty = \sup_{\omega \in \mathbb{R}} |T_1(j\omega)| \tag{2.9}$$

where T_1 is assumed to be stable. Clearly, it represents the peak on the bode (singular value) plots for the SISO (MIMO) systems. This norm in the time domain is given by

$$\|T_1\|_\infty = \sup_{w \in L_2} \frac{\|z_1\|_2}{\|w\|_2} \tag{2.10}$$

where $\| \cdot \|_2$ represents L_2 norm [1] for the signals, which can be interpreted as signal energy. Since this norm is defined as the ratio of the L_2 norms, it is also known as the L_2 gain of the system.

It can also be shown that

$$\|T_1\|_\infty \geq \frac{\left\{\int_{-\infty}^{\infty} S_{z_1}(\omega)d\omega\right\}^{1/2}}{\left\{\int_{-\infty}^{\infty} S_w(\omega)d\omega\right\}^{1/2}} = \frac{z_{1,rms}}{w_{rms}}$$

Hence, this norm is bounded below by the *rms gain* of the system.

The above discussion on H_2/ H_∞ norms for systems can be summarized as follows The H_∞ norm measures (minimizes) output energy (RMS) for the worst case input energy, whereas the H_2 is interpreted as the output energy when the system is driven by white noise input signals.

The **GH$_2$** (Generalized H_2) **norm** is defined as L_2-L_∞ induced norm (or 'energy to peak' norm) [47]

$$\|T_2\|_{GH_2} := \|T_2\|_{2,\infty} := \sup_{0 < w < \infty} \frac{\|z_2\|_\infty}{\|w\|_2} \tag{2.11}$$

The generalized H_2 norm measures the peak amplitude of the output signal for the worst case input. [Remember that ∞-norm of a signal (or vector) is defined as its maximum value.]

---

[1]see Glossary for the definition of signal norms and spaces

2.2.4 Problem formulation

Based on what is discussed above, we divide the controlled outputs into two parts of
to-be-minimized (z_1) and to-be-constrained (z_2) as

$$z_1 = \begin{pmatrix} \ddot{z}_s \\ z_u - z_r \\ u \end{pmatrix}$$

$$z_2 = z_s - z_u$$

To design a system to perform satisfactorily for a wide range of road irregularities
(not just white noises), calls for minimizing the H_∞ norm of the transfer function
from road disturbance to z_1. And in order to constrain the outputs z_2 within their
given bounds, for all kinds of road disturbances, the GH_2 norm of closed loop system
from disturbance to this output (vector) should be less than a positive scalar γ_2. This
guarantees that output ∞ norm (its max.) not to exceed a given maximum. Hence,
if we denote the channels from disturbance to the output z_1 and to the output z_2 as
T_1 and T_2 respectively, the problem can be formulated as

$$\text{Find a controller to minimize } \|T_1\|_\infty$$

$$\text{while } \|T_2\|_{GH_2} < \gamma_2$$

Remark 2.2: Similar formulations of the problem can be found in the literature, e.g.
[23, 53], which employ H_2/ GH_2 norms for the problem formulation. In such formu-
lations, whereas the minimization problem is solved for the white noise inputs, the
constrained problem is solved for the worst case input. Because of this contradiction
in the inputs classes, we formulated it based on H_∞/ GH_2 norms.

Remark 2.3: The requirements above also motivates the use of the constrained (opti-
mal, H_2 or H_∞) control. The approach is also based on multi-objective control. As all
multi-objective designs, using a single Lyapunov function to handle the performance
and the hard constraints, will lead to conservatism of the design. But constrained
scheme suffers from another source of conservatism resulting from the concept of

reachable sets and state space ellipsoids to capture perturbed state trajectories for all disturbances considered, see for more details [11]. Therefore, we adopted the formulation above.

Remark 2.4: In terms of different input signals, there are two interpretations of H_2 norm [8]. The one is the square root of total output energy in the impulse response of the system. The second is the asymptotic output variance when the input is a white noise. If the input signals are furthermore independent, the H_2 norm is then equal to the RMS (root mean square) value of the output. If all road irregularities could be classified as impulse or white noise, H_∞ norm based design appears to be conservative. However, to avoid the above mentioned contradiction in the inputs' classes, it is required to solve the constrained part of the problem for these types of inputs as well.

2.2.5 Extension to more precise models

A good understanding of active suspension capabilities can be obtained based on quarter car models [31]. But to include the additional mode of pitch, a half car model is needed. The new feature compared to the quarter car model is the angle θ and the moment of inertia I which gives rise to the pitch mode.

The formulation above, based on the definitions of (2.6, 2.7) can be readily extended to the half car models. Except for the performance output weighting functions, other constraints or requirements of the design are the same as quarter car models. In the case of using weighted outputs for judging the comfort, it is required to note that the human beings are more sensitive to rotational frequencies at 1-2 Hz and the weighting function corresponding to body rotational acceleration $\ddot{\theta}$ should emphasize this frequency range.

In order that the above formulations to be applicable to full car models, the variables

are defined as [24]

$$q = \begin{pmatrix} z_c \\ \theta \\ \phi \end{pmatrix}, \quad z_s = \begin{pmatrix} z_{s_{fl}} \\ z_{s_{fr}} \\ z_{s_{rl}} \\ z_{s_{rr}} \end{pmatrix}$$

$$z_u = \begin{pmatrix} z_{u_{fl}} \\ z_{u_{fr}} \\ z_{u_{rl}} \\ z_{u_{rr}} \end{pmatrix}, \quad z_r = \begin{pmatrix} z_{r_{fl}} \\ z_{r_{fr}} \\ z_{r_{rl}} \\ z_{r_{rr}} \end{pmatrix}$$

where ϕ represents the roll angle of the vehicle. When driving in a turn, the car will roll because of centrifugal force. θ is the pitch angle. When accelerating or braking, it will pitch respectively backward and forward. Subscripts f , r stand for front and rear, and r, l stand for right and left respectively.

With appropriate selection of state vector, the full vehicle suspension system with 7 DOF can be decoupled into heave-pitch (HP) and roll-warp (RW) subsystems using a similarity transformation [28, 62] and treated similar to a half car model.

2.3   Road disturbances

This section concerns with road profiles which will be used to evaluate the performance of the designed suspension systems.
In the context of vehicle ride and handling, road disturbances are generally classified as shock and vibration [11, 31].

2.3.1   Shock (single bump)

Shocks are discrete events of relatively short duration and high intensity, for example, an isolated bump or pothole in an otherwise smooth road surface. Such a disturbance

can be described as

$$
z_r(t) = \begin{cases} \frac{H}{2}(1 - \cos(\frac{2\pi V(t-T_p)}{L})), & T_p \leq t \leq T_p + \frac{L}{V} \\ 0, & Otherwise \end{cases}
$$

where H and L are the height and the length of the bump. In this study we choose $H = 0.06$ m, $L = 5$ m and the vehicle forward velocity as $V = 20$ m/s (=72 Km/h).

2.3.2 Vibration

Vibration, i.e., consistent road roughness, is typically specified as a random process. Two vibration type inputs will be used in this study

white noise

An often used approximation of road vertical displacement PSD for various terrains is given in the form [11, 31],

$$
G_{z_r}(q) = G_0(q_0) \left(\frac{q}{q_0}\right)^{-c} \tag{2.12}
$$

where q is the spatial frequency, and $q_0 = 0.1$ is the reference spatial frequency, G_0 provides a measure for road roughness, and c is the road roughness constant whose value for the most commonly used case equals 2. Related to the (time) frequency, we have $f = qV$, with V being the vehicle speed. By substituting this relation in (2.12) we arrive at

$$
G_{z_r}(f) = \frac{G_0 q_0^c V^c}{f^c}
$$

If $c = 2$, PSD of ground vertical velocity is given by

$$
G_{\dot{z}_r}(f) = (2\pi f)^2 G_{z_r}(f) = 4\pi^2 G_0 q_0^2 V^2
$$

which is independent of frequency, i.e., the ground vertical velocity can be described by white noise. In this study, we choose $G_0 = 128 \times 10^{-6}$ and $V = 20$ m/s. Moreover, as a complementary, we will also apply the real road profile described below.

Real road profile

The second vibration type road disturbance used in this study, is a real road profile whose time history and power spectral density is given in Fig. 2.3.
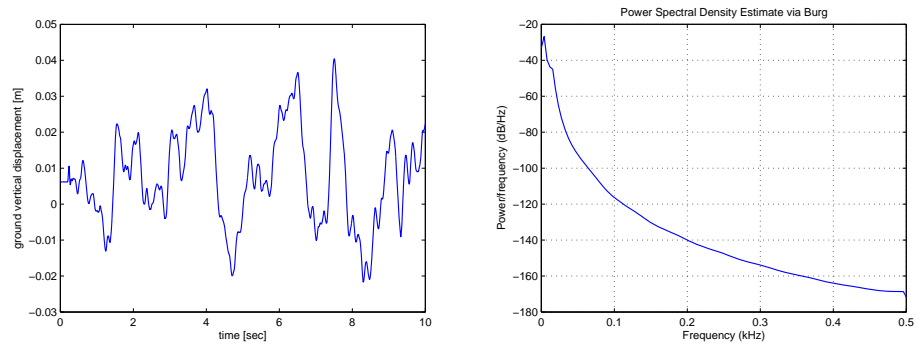
Figure 2.3: A real road profile; left: time history (ground vertical displacement), right: power spectral density corresponding to ground vertical velocity

Part II

Potential Assessment

Chapter 3

DESIGN SCHEME & LOOK-AHEAD PREVIEW DESIGN

This chapter mainly addresses a design scheme to achieve the design requirements formulated in the preceding chapter. The design requirements were described in a general form and are applicable to both cases of preview and non-preview, and so is the design scheme of this chapter. The main purpose of this chapter is to consider this scheme for active suspensions utilizing preview information, however for the sake of comparison, it is applied to non-preview case as well. Preview design of this chapter is also compared with an LQ-based preview design.

3.1 Why preview control

Let's first of all declare that with a preview control, we refer to feedback controller which utilizes preview information of road irregularities to enhance system performance. Accordingly, the non-preview control means a pure feedback control, and with a feed-forward control we mean a system whose the only measured variables are the road disturbances ahead of vehicle.

As discussed in chapter 1, a preview control, by preparing the control system for oncoming disturbances as well as compensating for system delays, compared to a non-preview one promises more improvement in system performance. Therefore, its superiority to pure feedback is clear. Moreover, it should be pointed out that using a feedback controller, because of the water-bed effect, system performance could be improved in a limited frequency range, whereas a preview control extends this
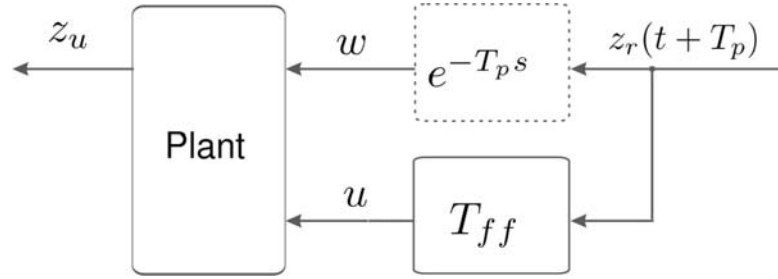
Figure 3.1: Feedforward control design scheme

improvement to a wider frequency range, if required. This section is to explain the reason for using preview control instead of feed-forward control.

At first view, it may seem that the design requirements of vehicle suspensions are fulfilled if we make the vertical position of the unsprung mass z_u follow road profile z_r. Thus, the design objective now is to enforce the transfer function from z_r to z_u to tend toward 1 or some desired transfer function. If the road profile T_p time units ahead of t is available, such an objective can be achieved by a feed-forward compensator. The simplest way to obtain this compensator is to use the model inversion technique. From Fig. 3.1, the feedforward controller T_{ff}, when T_p is set to 0, is obtained by

$$T_{z_u u} T_{ff} + T_{z_u w} = T_{desired}$$

Clearly, $T_p > 0$ leads to better results than $T_p = 0$. This is due to dynamic and delay time of actuators and reaction time of compensator. The value of T_p, by a rule of thumb, can be considered equal to actuator time constant.

But such a compensator cannot fulfill all requirements of active vehicle suspensions, because

1. It requires a large bandwidth actuator

2. It neglects the constraints on suspension deflection and actuator force

3. It is not clear if it could isolate satisfactorily the body from road disturbances

4. It is not robust against plant variations

5. It can lead to unstable compensators

In a try to obtain a feedforward controller for a quarter car model, for a few data sets we got either an unstable compensator or one with sparse coefficients which Matlab failed to analyze the overall system.

One remedy to deal with the items 2, 3 and 5 , is to consider the multi-objective approach of this chapter for the pure feedforward case, however it cannot cope with sensitivity against parameter changes and hence a feedforward controller has a risk of instability.

To conclude this section, the preview control combines benefits of both feedback and feedforward control.

3.2   A brief history on Preview control

The idea of utilizing the preview information in active vehicle suspensions was first proposed by Bender in 1968 [5], who used a single degree of freedom quarter car model to investigate numerically the effectiveness of preview control on active vehicle suspensions. He employed Wiener filter theory to find the optimum controller. Bender's results revealed a sixteenfold theoretical improvement.

There are two ways to obtain preview information, one using a "look-ahead" sensor mounted at front bumper of the vehicle and the other by estimating road profile from the response of front wheel, referring to as "wheelbase preview". Clearly, the above study considered the preview of the first type.

Bender's technique was extended by [46] and [32] to a two-dimensional model, having heave (bounce) and pitch freedoms. They treated a wheelbase preview and concluded that vibration levels could be reduced significantly.

The main difficulty with this approach is the implementation of the optimal controller.

Tomizuka [57, 58] recast the problem in a discrete time domain and derived the solution by dynamic programming. In this way he avoided the potential problems with implementing unstable transfer function in the controller. However, the application of this approach in practice was blocked by the complicated mathematics, requiring solution of a large set of regressive matrix equations to determine the optimal controller.

Thompson *et al.* [56] approached the problem as an extension of linear quadratic regulator theory to the case of preview included plant. From implementation point of view it is similar to that of Tomizuka [58].

The need to adapt to a wide range of speeds was treated by automatic switching of the preview time. They used a multi-stage fixed delay line, and relied on changing the point at which the input is fed to the controller. They refer to their system as a speed adaptive linear active vehicle suspension.

Foag [18] used a practical model of a half-car to investigate control problems of active vehicle suspensions with finite preview. He rejects the single scalar performance index as an adequate measure of system performance. Rather, He describes an active vehicle suspension design problem as a multi-criteria one. Much effort was expended in establishing a means of performance evaluation. In total, fourteen contributions to performance were considered. We believe that his formulation of the problem is the best one presented so far.

While he considers direct static feedback of some outputs for the feedback part, a parametric transfer function is used for the feedforward part, where the gain of feedback part as well as parameters of feedforward transfer function are selected by parameter optimization. He employs the package of **REMVG**[1], which is developed by the DLR-institut für Dynamik der Flugsysteme and is based on **K-S**[2] optimization technique.

---

[1]**R**egler**e**ntwurf **m**it **v**ektoriellem **G**ütekriterium

[2]Kreisselmaier-Steinhauser optimization technique: This technique combines all constraints and objective functions to form a single unconstrained composite function to be minimized

However he assumes a deterministic description of the road profile.

To consider the measurement noises in the design and to care for stochastic road profiles, the LQ-based control seems to be an appealing design method for active suspensions. Therefore, Yoshimura et al. [64] changed the problem into the LQG form by augmenting the dynamics of the original system and the road inputs. Hac [26] also solved the problem by the variational approach. He derived the optimal control and estimation schemes independently and then showed that a separation principle is satisfied with his solution to prove its optimality.

A similar work for the discrete time case was followed by [44]. In fact, an extension of LQG approach (extension of LQR synthesis and Kalman filter) was employed to obtain the preview controller.

Marzbanrad *et al.* in 2004, applied the results of [26] to a half car model to study the preview control from different aspects. They considered either of look-ahead and wheelbase preview, performed the synthesis and analysis under stochastic road profile and measurement noises for both cases of ride comfort or road holding preference . Their results substantiated the earlier findings on preview included suspensions. They showed that providing preview for only rear wheels is not as effective as providing it to both front and back wheels, but it offers significant performance advantages over active suspensions with no preview.

3.3   Objective

As we discussed in the previous chapter, a vehicle suspension design is by its nature a **multi-objective** design problem. This was firstly considered by [18]. However the deficiency of that study is that the optimization is done in time domain for fixed inputs of step function and half-sinus. There are in practice a wide range of road irregularities and it is not clear if the the designed system would work satisfactorily for other types of disturbances. To care for the mostly stochastic nature of road irregularities, all the

preview based active suspension systems, reported in the literature after this work, utilized *LQ*-based optimization approaches. The drawbacks of this approach include

1. Optimization is done in time domain for just white noise inputs. All time domain optimizations solve the problem for some given or a class of inputs and thus the designed system may deteriorate its performance for other types of inputs.

2. It is single objective design approach and some a posteriori analyses are required to prove the achievement of system constraints.

3. It is based on state feedback and unmeasured states need to be estimated. When vehicle parameters change, the resulted control may become unstable, unless conservative observers are used. Thus, the design of the observer also is usually done through an iterative process.

Therefore, *the objective of this study is to design and evaluate a suspension system utilizing an output feedback multi-objective preview control approach, based on the problem formulation of section 2.2.4 as*

$$Find\ a\ controller\ to\ minimize\ \|T_1\|_\infty$$

$$while\ \|T_2\|_{GH_2} < \gamma_2$$

This control scheme has two main aspects: firstly, it allows constrained outputs of the system to vary freely as long as they remain within their given bounds, in order that the best possible performance could be delivered. Secondly, the optimization as well as constraint fulfillment is done for the worst case road disturbances to cover all road types.

3.4   The unified design framework

This section addresses the preview design framework which will be used for both LQ-based design and LMI-based multi-objective designs. The control design problem is

formulated as in Fig. 3.2. The output vector z denotes the controlled (minimized and constrained) output.

In this chapter, we deal with the case of output feedback. It is assumed that
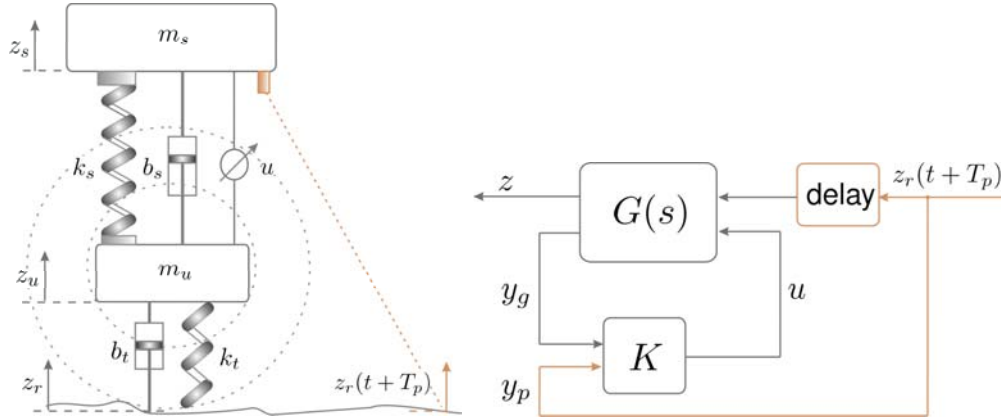
Figure 3.2: left: preview suspension concept, right: corresponding design framework

suspension deflection $(z_s - z_u)$ and vertical velocity of the sprung mass $(\dot{z}_s)$ are the measured outputs (y_g).

As it can be seen from the design framework of Fig. 3.2, road irregularities T_p time units ahead of t (T_p is referred to as preview time) is the additional measured output considered in preview design.

In practice the preview signal can be acquired from an ultrasonic, infrared or radar device. It should also be pointed out that a perceivable amount of effort has been expended in the development of suitable low cost sensors and actuators to make preview suspensions practically realizable. Nevertheless, there are some difficulties associated with practical application of these sensors, such as locating the sensor in an appropriate place or detection of road disturbance from sensor data, which are detailed in [18] and we will shortly discuss it in next chapter.

Recently publicized preview realization on the research car F700 [52] employs Laser sensors from SICK corporation (Fig. 3.3). Officially, the sensors are LIDAR, for Light Detecting and Ranging and has been carried across from military hardware. To detect

road irregularities as accurate as possible, road is scanned at a few distances ahead of vehicle. To any measuring point, an individual distribution function is assigned. This distribution function takes into account the beam expansion and the imprecision of the measurement procedure. Then road profile is computed through weighted averaging and iterative recursive reconstruction [49] and herewith partly manages the problems with the wrong detection of road disturbance from sensors' data.

Figure 3.3: Picture of a laser sensor from SICK corporation, employed by ABC-Prescan [49].

The main challenge in obtaining the control law in the above structure, is to absorb the time delay between sensing and excitation by the plant. One way to round this matter is to apply some approximation like Pade, what some authors have used [16, 21]. However, in this study, since the discrete time control problem will be considered, a discrete time state space description as in [58], also used in [43, 44, 54], will be employed to represent the delay.

It is firstly discussed why we approach the problem by a discrete time method.

3.4.1   Why discrete time approach?

The signals of interest in control systems are usually continuous-time signals and the performance specifications are readily formulated in continuous time. But since digital technology offers many benefits, the controllers are eventually implemented via microcomputers. Such a control system thus involves both continuous- and discrete-time signals. Two well-known approaches to design a controller for such a system include

- *Analog design, digital implementation:* The advantage of this approach is that the design is performed in continuous time, where the performance specifications are most natural. but discretizing the controller and adding A/D and D/A converters would result some performances degradation. Continuous-time specifications are recovered only for higher sampling rates. But in practice several technical issues preclude this assumption [12]. First, smaller sampling periods require faster and hence newer and more expensive hardware, so there is a trade-off between performance and cost in this sense. Secondly, performing all the control computations may not be feasible if the sampling is too fast. Thirdly, if a plant with slow dynamic is sampled very quickly, there will be little difference between successive samples, calling for large word size. This implies another performance/ cost trade-off.

- *discretize the plant, perform a digital design:* The design is done in a purely discrete time domain, avoiding any performance deterioration by implementation.

Moreover, it should be pointed out that one main drawback of classic direct digital controller synthesis is that it is more involved and complex to handle than its continuous time counterpart. But in the LMI-based design which will be employed in

this study, both are of the same degree of complexity. These facts motivate the use of discrete time design approach.

3.4.2 Augmented plant description

For a generality, it is assumed that the plant to be controlled, $G(z)$, is described by the following discrete-time state-space realization, where the equation of controlled outputs (z), since these outputs for the design approaches of this study differ from each other, for the moment has been dropped.

$$
\begin{aligned}
x_g(k+1) &= A_g x_g(k) + B_{g,w} w(k) + B_{g,u} u(k), \\
y_g(k) &= C_{g,y} x_g(k) + D_{g,yw} w(k)
\end{aligned}
\tag{3.1}
$$

This is the discrete time equivalent of the following continuous time description obtained by Zero Order Hold (ZOH) approach

$$
\left(
\begin{array}{c|cc}
A_c & B_{c,w} & B_{c,u} \\
\hline
C_{g,y} & D_{g,yw} & \mathbf{0}
\end{array}
\right)
\tag{3.2}
$$

In the discrete time description above, k is a counter for the samples and denotes the time kT_s, with T_s being the sampling time. $x_g(k) \in \mathbb{R}^n$ is the state vector of the plant, $w(k) \in \mathbb{R}^{m_1}$ is the vector of disturbances, $u(k) \in \mathbb{R}^{m_2}$ is the control input and $y_g(k) \in \mathbb{R}^{p_g}$ is the measured output vector. For the discrete-time plant, instead of subscript d, subscript g has been applied, to discriminate the plant dynamics from that of preview. This convention applies throughout this chapter. We will mainly deal with discrete time descriptions of plant and preview, and represent them respectively by subscripts g and p and therefore subscript d will be dropped.

Delay description

Let $x_p(k)$ denote the vector which represents the preview information which is avail-

able for control. We define this vector as

$$x_p(k) = \begin{pmatrix} w(k) \\ w(k+1) \\ \vdots \\ w(k+N_p) \end{pmatrix}$$

where $N_p = T_p/T_s$. It can be easily seen that

$$\begin{aligned} x_p(k+1) &= A_p x_p(k) + B_{p,w} w(k+N_p+1) \\ y_p(k) &= C_{p,y} x_p(k) = w(k+N_p) \end{aligned} \qquad (3.3)$$

where

$$A_p = \begin{pmatrix} 0 & & & \\ \vdots & & \mathbf{I} & \\ 0 & & & \\ \hline 0 & 0 & \cdots & 0 \end{pmatrix}, B_{p,w} = \begin{pmatrix} 0 \\ \vdots \\ 0 \\ 1 \end{pmatrix},$$

$$C_{p,y} = \begin{pmatrix} 0 & 0 & \cdots & 0 & 1 \end{pmatrix}$$

Augmented plant

To absorb the delay by the plant, a state augmentation technique is used. For this purpose, consider the augmented state and measured-output vectors as

$$x(k) = \begin{pmatrix} x_g(k) \\ x_p(k) \end{pmatrix}, y(k) = \begin{pmatrix} y_g(k) \\ y_p(k) \end{pmatrix}$$

Now the equations for the augmented system, by combining (3.1) and (3.3) is obtained as

$$x(k+1) = Ax(k) + B_w w(k+N_p+1) + B_u u(k),$$

$$y(k) = C_y x(k) + D_y \begin{pmatrix} w(k+N_p+1) \\ u(k) \end{pmatrix} \qquad (3.4)$$

where

$$A = \left(\begin{array}{c|cc} A_g & B_{g,w} & \mathbf{0} \\ \hline \mathbf{0} & & A_p \end{array} \right), B_w = \left(\begin{array}{c} \mathbf{0} \\ B_{p,w} \end{array} \right), B_u = \left(\begin{array}{c} B_{g,u} \\ \mathbf{0} \end{array} \right),$$

$$C_y = \left(\begin{array}{c|cc} C_{g,y} & D_{g,yw} & \mathbf{0} \\ \hline \mathbf{0} & & C_{p,y} \end{array} \right), D_y = \left(\begin{array}{c|c} D_{yw} & D_{yu} \end{array} \right) = \left(\begin{array}{c|c} \mathbf{0} & \mathbf{0} \\ \hline \mathbf{0} & \mathbf{0} \end{array} \right)$$

The block diagram of the discretized system with added measurement noises is shown in Fig. 3.4.

Figure 3.4: *P-K* formulation of the discretized system

3.5 LQ-based design

This section describes the procedure for the performance discretization and synthesis of an LQ-based preview controller. Once the discrete time augmented system and the discrete time performance specifications are available, for full state feedback, the optimal LQR-like (LQR preview) controller is given by the state feedback law $u(k) = -Kx(k)$, where K is obtained from steady state solution of a Riccati equation and for the Cy given above, the optimal LQG-like (LQG preview) controller is given by $u(k) = -K\hat{x}(k)$, where $\hat{x}(k)$ is the state estimate obtained from a Kalman filter with estimator gain L.

Although this theory is already broadly explained and employed in different references, we will give a very basic and brief description of the algorithm in order to have a compilation of algorithm and simplify the discussion of its different aspects. For a more detailed discussion of the discrete LQG synthesis based on continuous cost function see [4, 19, 44]. Since performance specifications are readily formulated in continuous time, we consider again continuous time description of (3.2), however with contaminant measurement (white) noises

$$
\begin{aligned}
\dot{x}_g(t) &= A_c x_g(t) + B_{c,u} u(t) + B_{c,w} w(t), \\
y_g(t) &= C_{g,y} x_g(k) + D_{g,yw} w(k) + v(t)
\end{aligned}
\tag{3.5}
$$

where $x \in \mathbb{R}^{n \times n}$ is the state vector, u is the control input and w is stationary Gaussian white noise with zero-mean and intensity of $Q_{c,o}$. The measurement noise v is also assumed to be stationary Gaussian white noise with zero-mean and intensity of $R_{c,o}$ and uncorrelated with w, i.e.,

$$
E\left\{ \begin{pmatrix} w(t) \\ v(t) \end{pmatrix} \begin{pmatrix} w^T(t) & v^T(t) \end{pmatrix} \right\} = \begin{pmatrix} Q_{c,o} & 0 \\ 0 & R_{c,o} \end{pmatrix}
$$

The objective is to find the optimal control input u so that the following performance index is minimized

$$
J = \lim_{T \to \infty} \frac{1}{2T} \int_0^T E\{\rho_1 \ddot{z}_s^2 + \rho_2 (z_s - z_u)^2 + \rho_3 (z_u - z_r)^2 + \rho_4 u^2\} dt
$$

where ρ's are weighting constants determined by designers. Defining the performance output of z as

$$z = \begin{pmatrix} z_s \\ z_s - z_u \\ z_u - z_r \\ u \end{pmatrix} = C_z x + D_z u$$

the integrand of performance index can be described by $z^T W z$ with W being the weighting matrix of $W = diag([\rho_1, \cdots, \rho_4])$ and thus the performance index can be written as the following quadratic form

$$J = \lim_{T \to \infty} \frac{1}{2T} \int_0^T E\{x_g^T Q_c x_g + 2 x_g^T N_c u + u^T R_c u\} dt$$

where

$$Q_c = C_z^T W C_z,$$
$$N_c = C_z^T W D_z,$$
$$R_c = D_z^T W D_z$$

The first step of discrete-time controller synthesis for a continuous system is to obtain a sampled-data version of continuous-time system and performance index.

3.5.1 Discretization of performance index and covariance matrices

Discretization of performance index

Assuming a zero order hold (ZOH) as a reconstruction filter, with the notation

$$\Phi(\tau) = e^{A_c \tau},$$
$$\Gamma(\tau) = \int_0^\tau \Phi(\eta) B_{c,u} d\eta$$

the weighting matrices for the equivalent discrete cost function are given by

$$\begin{pmatrix} Q_g & N_g \\ N_g^T & R_g \end{pmatrix} = \int_0^{T_s} \begin{pmatrix} \Phi^T(\tau) & 0 \\ \Gamma^T(\tau) & I \end{pmatrix} \begin{pmatrix} Q_c & N_c \\ N_c^T & R_c \end{pmatrix} \begin{pmatrix} \Phi(\tau) & \Gamma(\tau) \\ 0 & I \end{pmatrix} d\tau$$

Numerical hint to compute the discretized performance index

From matrix theory [60], for square matrices of M_{11} and M_{22} we have

$$exp\left\{ t \begin{pmatrix} M_{11} & M_{12} \\ 0 & M_{22} \end{pmatrix} \right\} = \begin{pmatrix} e^{tM_{11}} & \hat{M}_{12} \\ 0 & e^{tM_{22}} \end{pmatrix}$$

where $\hat{M}_{12} = \int_0^t e^{(t-\tau)M_{11}} M_{12} e^{\tau M_{22}} d\tau$ for $t \geq 0$. This result can be used to obtain weighting matrices for the equivalent discrete cost function numerically. To this goal, compute the following exponential matrix

$$\left(\begin{array}{c|c} \Psi_{11} & \Psi_{12} \\ \hline 0 & \Psi_{22} \end{array} \right) = exp \left\{ T_s \left(\begin{array}{cc|cc} -A_c^T & 0 & Q_c & N_c \\ -B_{c,u}^T & 0 & N_c^T & R_c \\ \hline 0 & 0 & A_c & B_{c,u} \\ 0 & 0 & 0 & 0 \end{array} \right) \right\}$$

It can be easily seen

$$\Psi_{22} = \begin{pmatrix} \Phi(T_s) & \Gamma(T_s) \\ 0 & I \end{pmatrix} = \begin{pmatrix} A_g & B_{g,u} \\ 0 & I \end{pmatrix}$$

where a zero order hold (ZOH) as a reconstruction filter is assumed. It should be pointed out that C_g and D_g matrices are the same as continuous time ones. Also

$$\Psi_{22}^T \Psi_{12} = \begin{pmatrix} Q_g & N_g \\ N_g^T & R_g \end{pmatrix}$$

Augmented performance index

The performance index for the augmented discrete time system is given by

$$J = \lim_{N \to \infty} \frac{1}{N+1} E \left\{ \sum_{k=0}^{N} x(k)^T Q x(k) + 2x(k)^T N u(k) + u(k)^T R u(k) \right\} \qquad (3.6)$$

where

$$Q = \begin{pmatrix} Q_g & \mathbf{0} \\ \mathbf{0} & \mathbf{0} \end{pmatrix}, N = \begin{pmatrix} N_g \\ \mathbf{0} \end{pmatrix}, R = R_g$$

Discretization of covariance matrices for observer design (Q_o and R_o)

The discretized process noise $w_d(k)$ (notice that this is an $n \times 1$ vector rather than a scalar) is a stationary Gaussian white noise sequence with zero mean and a covariance matrix of

$$Q_{g,o} = \int_0^{T_s} \Phi(\tau) B_{c,w} Q_{c,o} B_{c,w}^T \Phi^T(\tau) d\tau$$

This equation can be evaluated numerically with a matrix exponential function in a similar way to the above. It can approximated by

$$Q_{g,o} = Q_{c,o}/T_s$$

if T_s is much smaller than the dominant time constant of the system.

Based on the discussion above for the augmented plant we apply

$$Q_o = B_w \frac{Q_{c,o}}{T_s} B_w^T \tag{3.7}$$

$$R_o = \frac{R_{c,o}}{T_s} \tag{3.8}$$

3.5.2 LQR preview design scheme

Similar to classical LQG problem, it can be easily proved that the separation principle holds for the LQG preview problem too and its solution is the combination of a deterministic optimal state feedback regulator (LQR) and a stochastic optimal estimator (Kalman) [44]. This subsection highlights some points of the LQR preview design. Applying the LQR design approach to the augmented plant of (3.4) and augmented performance index of 3.6, the control signal is given by

$$u(k) = u_1(k) + u_2(k) = - \begin{pmatrix} K_1 & K_2 \end{pmatrix} \begin{pmatrix} x_g \\ x_p \end{pmatrix},$$

$$K_1 = \left(B_{g,u}^T P_{11} B_{g,u} + R_g \right)^{-1} \left(B_{g,u}^T P_{11} A_g + N_g^T \right),$$

$$K_2 = \left(B_{g,u}^T P_{11} B_{g,u} + R_g \right)^{-1} B_{g,u}^T \left(P_{11} H + P_{12} A_g \right)$$

where $H = \begin{pmatrix} B_{g,w} & 0 \end{pmatrix}$ and

$$P = \begin{pmatrix} P_{11} & P_{12} \\ P_{21} & P_{22} \end{pmatrix}$$

is the symmetric solution to the discrete algebraic riccati equation which results in

$$P_{11} = A_g^T P_{11} A_g + Q_g - \left(A_g^T P_{11} B_{g,u} + N_g\right)\left(B_{g,u}^T P_{11} B_{g,u} + R\right)^{-1}\left(B_{g,u}^T P_{11} A_g + N_g^T\right) \quad (3.9a)$$

$$P_{12} = A_g^T P_{11} H + A_g^T P_{12} A_p - K_1^T B_{g,u}^T P_{11} H - K_1^T B_{g,u}^T P_{12} A_p \quad (3.9b)$$

$u_1(k)$ and $u_2(k)$ denote state feedback and preview control parts of control signal respectively. It can be seen that

1. K_1 equation as well as P_{11} riccati equation coincides with that of non-preview case. It means that preview control doesn't influence the feedback part of the control.

2. neither K_1 nor K_2 depends on P_{22}, and that's why its expression above has been excluded .

Moreover, P_{12} may be expressed in terms of P_{11} as follows

Let $P_{12} := \begin{pmatrix} P_1 & P_2 & \cdots & P_{N_p} \end{pmatrix}$, where each P_i is an $n \times n$-matrix. With A_F being the closed loop system matrix for the non-preview case, defined by $A_F = A_g - B_{g,u}K_1$, P_{12} given by (3.9b) can be rewritten as

$$P_{12} = A_F^T P_{11} H + A_F^T P_{12} A_P$$
$$= \begin{pmatrix} A_F^T P_{11} B_{g,w} & 0 & \cdots & 0 \end{pmatrix} + \begin{pmatrix} 0 & A_F^T P_1 & A_F^T P_2 & \cdots & A_F^T P_{N_p-1} \end{pmatrix}$$

Hence,

$$P_1 = A_F^T P_{11},$$
$$P_2 = A_F^T P_1 = \left(A_F^2\right)^T P_{11} B_{g,w},$$
$$\vdots$$
$$P_{N_p} = \left(A_F^{N_p-1}\right)^T P_{11} B_{g,w},$$

Therefore,

$$P_{12} = \begin{pmatrix} A_F & \left(A_F^2\right)^T & \cdots & \left(A_F^{N_p-1}\right)^T \end{pmatrix} \cdot P_{11}$$

The gain matrix for the preview control part, K_2, can now be expressed in terms of only P_{11}

$$K_2 = -L \begin{pmatrix} P_{11}B_{g,w} & A_F^T P_{11}B_{g,w} & \cdots & \left(A_F^{N_p-1}\right)^T P_{11}B_{g,w} \end{pmatrix} \tag{3.10}$$

where $L = \left(B_{g,u}^T P_{11}B_{g,u} + R\right)^{-1} B_{g,u}^T$. Thus, all gains of the optimal preview control law can be derived from the solution of the non-preview case, as shown originally in [37]. Note that since the feedback system is stable, A_F^T is also stable and the powered A_F^T in (3.10) will decrease with time. Thus the influence of the knowledge of future inputs on $u_2(k)$ will diminish with time and the knowledge of inputs from distant future will be irrelevant for system performance. To give an insight to preview contributions to the control signal, we have computed K_2 for a typical quarter car model for a preview time of 0.5 sec. Considering that all the modal frequencies of the system is less than 12 Hz, sampling time for this computation was set to 5 msec. For a preview time of 0.5 sec (100 samples), K_2 will have the dimension of 1×100. Fig. 3.5 shows the elements of K_2 for inputs of different times ahead of wheel. This figure
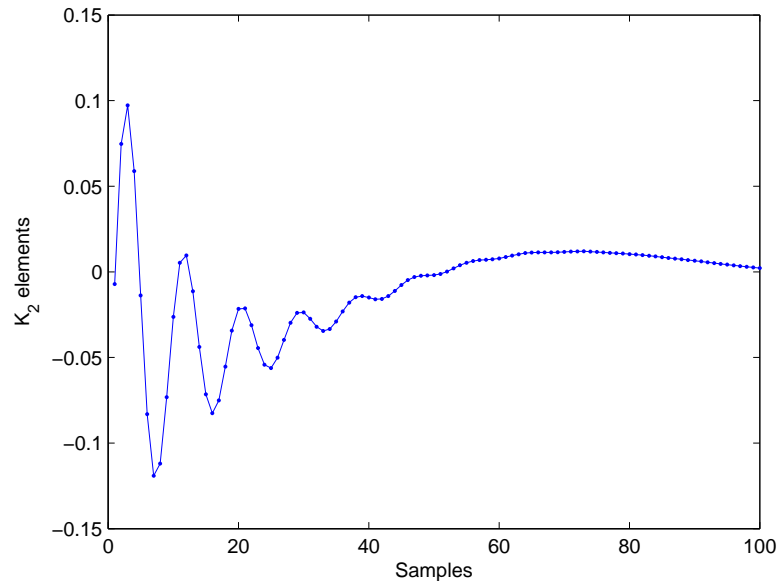
Figure 3.5: Coefficients of preview signals of different times ahead of wheel

shows up to which preview time a measurable benefit can be gained from preview control. As it can be seen, no significant benefit can be achieved by increasing the preview time over 0.35 s (70 samples).

3.5.3   Kalman Filtering with preview

In vehicle suspension control all the state variables cannot be measured and therefore to realize a preview control, since all measurements including the preview signal are noisy, an optimal estimator is necessary. Given the augmented plant of (3.4), the objective is to construct a state estimator that minimizes the steady state error covariance. The optimal solution is the Kalman filter with equations [19]

$$\hat{x}(k+1|k) = A\hat{x}(k|k-1) + B_u u(k) + L(y(k) - C_y\hat{x}(k|k-1) - D_{yu}u(k))$$

In discrete time, one may use for the LQG regulator, either the 'prediction' $\hat{x}(k|k-1)$ of $x(k)$ based on measurements up to $y(k-1)$, or the 'current' state estimate $\hat{x}(k|k)$ based on all available measurements including $y(k)$. In the latter case, the following equations are used to generate 'current' output and state estimates

$$\begin{pmatrix} y(k|k) \\ \hat{x}(k|k) \end{pmatrix} = \begin{pmatrix} C_y(I - MC_y) \\ I - MC_y \end{pmatrix} \hat{x}(k|k-1) + \begin{pmatrix} (I - C_yM)D_{yu} & C_yM \\ -MD_{yu} & D \end{pmatrix} \begin{pmatrix} u(k) \\ y(k) \end{pmatrix}$$

Where gain matrices L and M are derived by solving a discrete time riccati equation. Matlab functions *Kalman* and *lqgreg* provide a user-friendly environment for synthesis of a discrete time Kalman filter and its utilization for LQG control. While the regulator

$$u(k) = -K\hat{x}(k|k-1)$$

is always well-defined, the current regulator

$$u(k) = -K\hat{x}(k|k)$$

is causal only when $I - KMD$ is invertible. In addition, practical implementations of the current regulator should allow for the processing time required to compute $u(k)$, once the measurements $y_(k)$ become available (this amounts to a time delay in the feedback loop).

3.5.4   Application to the problem

Let's first determine the sampling frequency of the system. Considering that all the modal frequencies of the system is less than 12 Hz, a sampling time of 5 msec seems to be sufficient, however, the lower the sampling time, the more accurate approximation of the continuous time performance in discrete time domain is obtained. The main precluding factor in increasing the sampling frequency of the system is the processor speed. As long as the processor could process the control algorithm and compute the control signal between sampling instants, we are allowed to increase the sampling frequency of the system. Therefore, for both designs of LQ-based and multi-objective the sampling time of 1 msec is considered.

It is assumed that a preview sensor is mounted in the front bumper of vehicle and could capture road irregularities $N_p = 20$ samples ahead of wheel. Clearly, the longer the preview length, the better the performance is improved, however to meet a realistic situation this assumption is made. This assumption, under vehicle speed of 25 m/s, will lead to preview length of $L_p = 0.5$ m. In next sections, we will discuss how this choice facilitates the use of the controller for other speeds.

LQR preview design

The above compilation, concisely shows how an LQ-based preview design can be performed. It has been shown in the literature how the design parameters for an active suspension system can be tuned. The LQR preview design and a posteriori simulation is repeated by varying the performance index weights W and results are reflected in the so-called 'carpet plots'. These plots which represent the performance index terms for different values of weights, help the designer to decide for the best possible trade-off between conflicting requirements. For more details see for example [30]. Obtaining these carpet plots is not the topic of this study which mainly concerns with multi-objective preview design. In this study, we skip obtaining these carpet plots and simply adopt the following parameters for the ride comfort preference design from

[55]

$$\rho_1 = 1,$$
$$\rho_2 = 1000,$$
$$\rho_3 = 10000,$$
$$\rho_4 = 0,$$

Now, the performance index is discretized and the discrete time LQR design algorithm is used to obtain the controller.

Observer design

It is well known that LQR solution has excellent stability margins, however since all system states are not available it requires an estimator. Adding this estimator may deteriorate system performance. Doyle and Stein [14] showed that under certain conditions LQG can asymptotically recover the LQR properties. In order to prevent system performance degradation, caused by adding the observer, observer design also similarly should be done through an iterative process. If statistical information of the noise processes R_o are available, the only parameter to be tuned is Q_o. We set R_o intuitively to the following value and obtained Q_o through trials. The higher the value of Q_o, the closer the LQG system comes to LQR performance. However, it should be noted that greater values of Q_o may lead to unreasonably large values for the filter(observer) gain L, and make the system more sensitive to noise and uncertainties. By a posteriori analyses for various Q_o's and checking for system time and frequency responses we obtained the appropriate values for the observer design as

$$R_{c,o} = \begin{pmatrix} 2 \times 10^{-4} & 0 & 0 \\ 0 & 6 \times 10^{-6} & 0 \\ 0 & 0 & 2 \times 10^{-4} \end{pmatrix},$$
$$Q_{c,o} = 0.1I$$

These covariance matrices were discretized and augmented according to equation (3.8) and the estimator is obtained using discrete Kalman filter design approach.

To assess the designed system performance, frequency responses of the system from $w(k + N_p + 1)$ to performance outputs are given in Fig. 3.6. The simulation results compare a preview-based design with a non-preview one. The frequency response of the passive system is also presented for reference. It should be noted that the frequency response of the pure feedback and passive systems coincide with the frequency responses from $w(k)$ to performance outputs, because $|z^{-N_p-1}| = 1$ (z is the z-transform variable). As it can be seen, inclusion of the preview information leads to
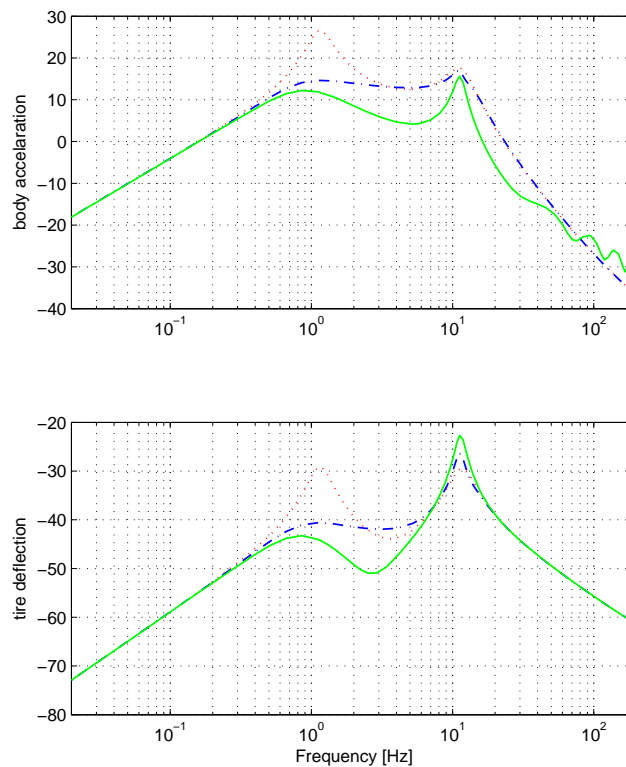
Figure 3.6: Frequency Response of the LQ-based design: Preview (–), Pure feedback (-.), Passive (..)

a significant reduction in the body acceleration magnitude, especially in the frequency range 4-8 Hz, and thereby improves passenger's ride comfort. However, compared to

non-preview case, it destroys the low pass behavior of the passive system. We believe this degradation at higher frequencies is immaterial, because

1. Human body is not sensitive to higher frequency accelerations.

2. Shuffle behavior of the tire in practice, would suppress the higher frequency disturbances before they enter the system, as described in [18]. Note that the shuffle behavior of the tire hasn't been included in system model.

3. Transfer function of a sampled data system $T_d(z)$ produces the same output as continuous time one at sampling times, but their frequency responses are not the same and the following relation applies

$$|T_c(j\omega) - T_d(e^{j\omega T_s})| < \omega T_s \int_0^\infty |T_c(\tau)| d\tau$$

At lower frequencies ($\omega < 0.1\omega_s$), a good match there exists.

The frequency responses considered above, don't contain the performance outputs of control signal u and suspension deflection. The control signal is missing, because the design doesn't penalize it, meaning that the control signal for the design here is irrelevant. The suspension deflection is missing, because the requirements on suspension stroke is a time domain specification, and whether the constraints on suspension stroke are fulfilled or not, should be proved through time domain simulations.

It should also be pointed out that even though these frequency responses provide an intuitive measure for performance evaluation, which is particularly useful for comparison purposes, they don't provide an ideal measure to evaluate system performance, because they don't reflect the effect of the measurement noises. As a complementary, we will perform some time domain simulations in the next sections. Time domain analysis has the capability of considering noises. It could also be used to check whether system constraints are fulfilled.

3.6   Multi-objective preview control

In this section we derive a multi-objective preview solution to the problem formulated in chapter 2, based on LMI optimization.

As discussed in chapter 2, the system controlled outputs consist of two parts of to-be-minimized (z_1) and to-be-constrained (z_2). These outputs in the augmented plant appear as

$$
\begin{aligned}
x(k+1) &= Ax(k) + B_w w(k+N_p+1) + B_u u(k), \\
z_1(k) &= C_1 x(k) + D_{11} w(k+N_p+1) + D_{12} u(k), \\
z_2(k) &= C_2 x(k) + D_{21} w(k+N_p+1) + D_{22} u(k), \\
y(k) &= C_y x(k) + D_{yw} w(k+N_p+1)
\end{aligned}
\tag{3.11}
$$

Where for $i = 1, 2$

$$
\begin{aligned}
C_i &= \left(\begin{array}{c|cc} C_{g,i} & D_{g,i1} & \mathbf{0} \end{array} \right), \\
D_i &= \left(\begin{array}{c|c} D_{i1} & D_{i2} \end{array} \right) = \left(\begin{array}{c|c} \mathbf{0} & D_{g,i2} \end{array} \right)
\end{aligned}
$$

with $C_{g,i}$ and $D_{g,ij}$ being the corresponding matrices for the discrete time plant (without preview dynamics).

Now the control problem is to find a controller such that the H_∞ norm of the closed loop system from $w(k+N_p+1)$ to $z_1(k)$ is minimized, while GH_2 norm from $w(k+N_p+1)$ to $z_2(k)$ is kept less than a prespecified positive number γ_2. Henceforth, we deal with a discrete-time multi-objective control problem and what follows is, in fact, an extension of the [13, 48] to discrete-time case with preview. Consider again the system described by (3.11) and let the controller K to be designed be represented in state space form by

$$
\begin{aligned}
x_k(k+1) &= A_k x_k(k) + B_k y(k), \\
u(k) &= C_k x_k(k) + D_k y(k)
\end{aligned}
$$

Then closed loop system has a state space realization with the following matrices

$$\mathcal{A} := \begin{pmatrix} A + B_u D_k C_y & B_u C_k \\ B_k C_y & A_k \end{pmatrix}$$

$$\mathcal{B} := \begin{pmatrix} B_w + B_u D_k D_{yw} \\ B_k D_{yw} \end{pmatrix}$$

$$\mathcal{C}_i := \begin{pmatrix} C_i + D_{i2} D_k C_y & D_{i2} C_k \end{pmatrix}$$

$$\mathcal{D}_i := D_{i1} + D_{i2} D_k D_{yw}$$

(3.12)

Let us denote the channels from disturbance to the output z_1 and to the output z_2 as T_1 and T_2 respectively.

- H_∞ control of channel T_1

Lemma 3.1: : It is known [from [66] with slight modification] that above discrete time system is quadratically stable and $\|T_1(z)\|_\infty < \gamma_1$ if and only if there exists some $\mathcal{X}$ such that

$$\mathcal{X} \succ 0 \tag{3.13a}$$

$$\begin{pmatrix} \mathcal{X} & 0 & \mathcal{A}\mathcal{X} & \mathcal{B} \\ * & \gamma_1 I & \mathcal{C}_1 \mathcal{X} & \mathcal{D}_1 \\ * & * & \mathcal{X} & 0 \\ * & * & * & \gamma_1 I \end{pmatrix} \succ 0 \tag{3.13b}$$

where * represents the transpose of the elements across the diagonal. This lemma is, in fact, the discrete time equivalent of the Bounded Real lemma [7].

- GH_2 control of channel T_2

GH_2 norm, given by 2.11, for a discrete time system satisfies

$$\|T_2\|_{GH_2} = \lambda_{max}^{1/2} \left\{ \frac{1}{2\pi} \int_0^{2\pi} T_2(e^{j\theta}) T_2^*(e^{j\theta}) d\theta \right\}$$

By restating the term between brackets [12], this norm can can be computed as (Note that in the case of preview $\mathcal{D}_2 = 0$ and it is dropped in the relation)

$$\|T_2\|_{GH_2} = \lambda_{max}^{1/2}(\mathcal{C}_2\mathcal{X}_0\mathcal{C}_2)^T$$

where $\mathcal{X}_0$ is the solution of Lyapunov equation

$$\mathcal{X}_0 = \mathcal{A}\mathcal{X}_0\mathcal{A}^T + \mathcal{B}\mathcal{B}^T$$

It can be readily verified that $\|T_2\|_{GH_2} < \gamma_2$ if and only if there exists a symmetric matrix $\mathcal{X}$ such that

$$\lambda_{max}^{1/2}(\mathcal{C}_2\mathcal{X}\mathcal{C}_2^T) < \gamma_2,$$
$$\mathcal{X} - \mathcal{A}\mathcal{X}\mathcal{A}^T + \mathcal{B}\mathcal{B}^T > 0$$

These inequalities can be restated as the following LMI's

$$\begin{pmatrix} \mathcal{X} & \mathcal{A}\mathcal{X} & \mathcal{B} \\ \mathcal{X}\mathcal{A}^T & \mathcal{X} & 0 \\ \mathcal{B}^T & 0 & I \end{pmatrix} \succ 0 \tag{3.13c}$$

$$\begin{pmatrix} \gamma_2 I & \mathcal{C}_2\mathcal{X} \\ \mathcal{X}\mathcal{C}_2^T & \mathcal{X} \end{pmatrix} \succ 0 \tag{3.13d}$$

As usual in multi-objective design framework [48], we have used the same decision matrix $\mathcal{X}$ of H_∞ design for the above constraint.

- Pole location constraint

In order to ensure desired stability margins for the system, the poles of the closed loop system are constrained to be inside the disc with radius $\rho = exp(-\alpha T_s)$ centered at the origin. This ensures a minimum damping coefficient of α. All eigenvalues of $\mathcal{A}$ lie in a disk with radius ρ centered at the origin if and only if there exists a matrix $\mathcal{X}$ satisfying [13]

$$\begin{pmatrix} -\rho\mathcal{X} & \mathcal{A}\mathcal{X} \\ * & -\rho\mathcal{X} \end{pmatrix} \prec 0 \tag{3.13e}$$

After substitution of calligraphic matrices in the LMI's (3.13) with their values of (3.12), for an unknown controller, we arrive at a matrix inequality which involves nonlinear terms (Bilinear matrix inequalities in $\mathcal{X}$ and controller matrices). BMI's cannot be solved by numerically tractable methods. To manage this problem, we apply the linearizing idea of [13, 48] with slight changes. To this goal, partition $\mathcal{X}$ and $\mathcal{X}^{-1}$ as

$$\mathcal{X} = \begin{pmatrix} X & M \\ M^T & \star \end{pmatrix}, \mathcal{X}^{-1} = \begin{pmatrix} Y & N \\ N^T & \star \end{pmatrix}$$

where $\star$ represents that the block is arbitrary. X and Y are symmetric and of the same size as A. Observe that $\mathcal{X}\mathcal{X}^{-1} = I$ implies

$$MN^T = I - XY$$

Also define

$$\mathcal{Y} = \begin{pmatrix} Y & I \\ N^T & 0 \end{pmatrix}$$

Let us now define the change of controller variables as follows

$$\begin{aligned}
\hat{A} &:= Y(A + B_u D_k C_y)X + YB_u C_k M^T + NB_k C_y X + NA_k M^T, \\
\hat{B} &:= YB_u D_k + NB_k, \\
\hat{C} &:= D_k C_y X + C_k M^T, \\
\hat{D} &:= D_k
\end{aligned} \tag{3.14}$$

If M and N have full row rank and if A, B, C, D, X, Y are given, we can always compute controller matrices A_k, B_k, C_k, D_k satisfying (3.14). If M and N are square and invertible, then A_k, B_k, C_k, D_k are unique. For full order design one can always assume that M and N have full row rank. Hence the variables A_k, B_k, C_k, D_k can be replaced by $\hat{A}$, $\hat{B}$, $\hat{C}$, $\hat{D}$ without loss of generality.

Proposition 3.1: for a given controller K, closed loop system (3.12) is quadratically stable and achieves H_∞ performance of the $\|T_1(z)\|_\infty < \gamma_1$, while it also satisfies $\|T_2(z)\|_{GH_2} < \gamma_2$, if and only if there exist positive definite symmetric matrices X and Y and rectangular matrices M and N such that the following LMI's hold

$$\begin{pmatrix} Y & I \\ I & X \end{pmatrix} \succ 0, \tag{3.15a}$$

$$\begin{pmatrix} \Psi_{11} & \Psi_{12} \\ \Psi_{12}^T & \Psi_{22} \end{pmatrix} \succ 0 \tag{3.15b}$$

where

$$\Psi_{11} = \Psi_{22} = \begin{pmatrix} Y & I & 0 \\ I & X & 0 \\ 0 & 0 & \gamma I \end{pmatrix},$$

$$\Psi_{12} = \begin{pmatrix} YA + \hat{B}C_y & \hat{A} & YB_w + \hat{B}D_{yw} \\ A + B_u\hat{D}C_y & AX + B_u\hat{C} & B_w + B_u\hat{D}D_{yw} \\ C_1 + D_{12}\hat{D}C_y & C_1X + D_{12}\hat{C} & D_{11} + D_{12}\hat{D}D_{yw} \end{pmatrix}$$

$$\begin{pmatrix} Y & I & YA + \hat{B}C_y & \hat{A} & YB_w + \hat{B}D_{yw} \\ * & X & A + B_u\hat{D}C_y & AX + B_u\hat{C} & B_w + B_u\hat{D}D_{yw} \\ * & * & Y & I & 0 \\ * & * & * & X & 0 \\ * & * & * & * & I \end{pmatrix} \succ 0 \tag{3.15c}$$

$$\begin{pmatrix} \gamma_2 I & C_2 + D_{22}\hat{D}C_y & C_2X + D_{22}\hat{C} \\ * & Y & I \\ * & * & X \end{pmatrix} \succ 0 \tag{3.15d}$$

$$\begin{pmatrix} -\rho Y & -\rho I & YA + \hat{B}C_y & \hat{A} \\ * & -\rho X & A + B_u\hat{D}C_y & AX + B_u\hat{C} \\ * & * & -\rho Y & -\rho I \\ * & * & * & -\rho X \end{pmatrix} \prec 0 \tag{3.15e}$$

Proof: After substituting closed loop matrices in (3.13) with their values of (3.12) and applying change of variables of 3.14, If we perform a congruence transformation

on obtained LMI's with

$$\mathcal{Y}$$
$$diag(\mathcal{Y}, I, \mathcal{Y}, I)$$
$$diag(\mathcal{Y}, \mathcal{Y}, I)$$
$$diag(I, I, \mathcal{Y})$$
$$diag(\mathcal{Y}, \mathcal{Y})$$

respectively, only some manipulation is required to obtain the LMI's (3.15). Utilize the mappings listed below for this purpose

$$\mathcal{Y}^T \mathcal{X} \mathcal{Y} = \begin{pmatrix} Y & I \\ I & X \end{pmatrix},$$

$$\mathcal{Y}^T (\mathcal{A} \mathcal{X}) \mathcal{Y} = \begin{pmatrix} YA + \hat{B}C_y & \hat{A} \\ A + B_u \hat{D} C_y & AX + B_u \hat{C} \end{pmatrix},$$

$$\mathcal{Y}^T \mathcal{B} = \begin{pmatrix} YB_w + \hat{B}D_{yw} \\ B_w + B_u \hat{D} D_{yw} \end{pmatrix},$$

$$(\mathcal{C}_i \mathcal{X}) \mathcal{Y} = \begin{pmatrix} C_i + D_{i2}\hat{D}C_y & C_i X + D_{i2}\hat{C} \end{pmatrix}$$

Now we can formulate discrete-time multi-objective control design for a given γ_2 by the following optimization problem in LMI's

$$\min_{\gamma_1, \hat{A}, \hat{B}, \hat{C}, \hat{D}, X, Y} \gamma_1, \text{subject to LMI's(3.15)} \tag{3.16}$$

Given any solution of this LMI, compute via SVD a full-rank factorization of the matrix $I - XY$ and then solve the system of linear equations (3.14) for D_k, C_k, B_k and A_k (in this order).

3.6.1   application to the problem

In any robust control design, according to requirements of performance, some weights are added to normalize the exogenous inputs and controlled outputs. For the con-

trolled (to-be-minimized) outputs, a dynamic weight expresses the desired frequency content in the corresponding output channel, and for a exogenous input reflects its frequency content. In this stage, which comparison to the LQ-based preview controller is intended, because of performing a fair comparison, the design is carried out under static weights of

$$\begin{aligned}
W_{z_{11}} &= 1; \\
W_{z_{12}} &= \frac{k_t}{(m_s+m_u)g}; \\
W_u &= 0.01; \\
W_d &= 0.15; \\
n_g &= n_p = 0.01;
\end{aligned}$$
(3.17)

To normalize the exogenous inputs, it is assumed that road disturbance has the maximum magnitude of 0.15 m/s and measurement noises a maximum magnitude of 0.01. The tire deflection is normalized by $\frac{k_t}{(m_s+m_u)g}$, which neglecting the damping of tire, this output represents the ratio of dynamic to static tire load. To design a controller to lead to similar results of LQ-based design, for comparison purposes, we chose a small weight for control signal. Moreover, because of ride comfort preference $W_{z_{11}} = 1$ was chosen.
Assuming a maximum suspension stroke of $SS_{max} = 8$ cm, the output z_2 was normalized by the weighting of 1/0.08.

Noting the definition of GH_2 norm of (2.11), to determine a suitable value for γ_2, a priori knowledge on road disturbances may be useful. For a given road disturbance energy, a greater γ_2 value will allow for more variation of constrained outputs. Considering normalized constrained outputs implies that γ_2 value be less than the inverse of the worst case disturbance energy. Since we have tried to normalize all inputs and outputs, we considered a γ_2 value of 1.

The controller was obtained by solving the above LMI optimization, using Matlab LMI toolbox [22]. The design lead to the γ_1 value of 0.8717, ensuring achievement of system performance under input magnitudes defined by (3.17).

The approach described above, apart from the inclusion of preview related parts, is also used to design a pure feedback multi-objective controller for the system. We obtained the results shown in Fig. 3.7. They represent frequency response from $w(k + N_p + 1)$ to body acceleration and tire deflection for both pure feedback and preview controlled suspensions as well as passive one. The results are very similar to those of LQ-based preview design (Fig. 3.6).
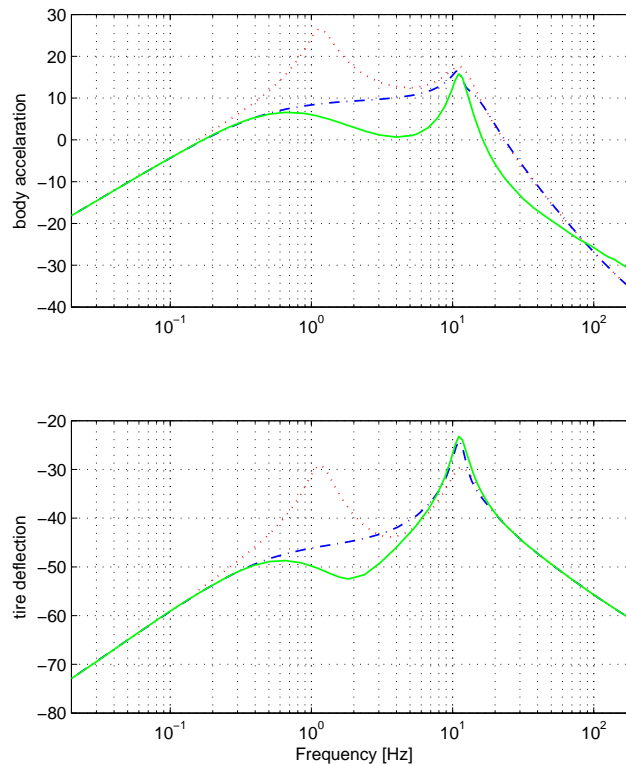
Figure 3.7: Frequency Response of the Multi-objective design: Preview (−), Pure feedback (-.), Passive (..)

Similar to LQ-based design, the figure shows some deterioration in ride comfort at higher frequencies, which is of less importance, because of the reasons stated for LQ-based case in section 3.5.4.

Fig. 3.8 shows the designed multi-objective systems' response to the real road profile introduced in chapter 2. The response of the passive suspension is also given for reference. It should be pointed out that for all time domain simulations of this chapter, the measured variables are contaminated with noises. For this purpose, three uncorrelated white noise sequences have been generated to simulate them. It can be easily seen that in presence of preview, ride comfort, compared to pure feedback case, is considerably improved. When preview information is used by the controller, the control system reacts very fast, and thereby reduces the forces transmitted to the body.
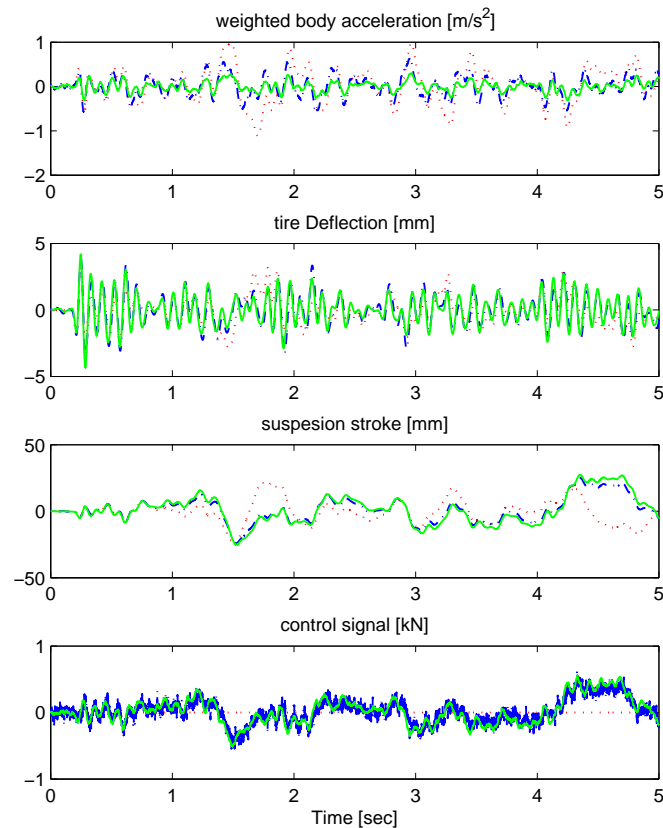
Figure 3.8: Real road response of the Multi-objective design: Preview (–), Pure feedback (-.), Passive (..)

RMS values of weighted body acceleration ($W\ddot{z}_s$, passenger perceived acceleration), tire deflection (TD), suspension deflection (SS) and power consumption, for 3 suspension systems, are listed in Table 3.1, where for the power consumption the following relation has been applied

$$P(t) = [-b_s(\dot{z}_s - \dot{z}_u) + u(t)](\dot{z}_s - \dot{z}_u)$$

The results reveal that inclusion of preview, reduces the passenger perceived acceleration of pure feedback suspension up to 65%, and thereby provides 65% more comfort for the passengers. It can be easily seen that this improvement doesn't sacrifice the ride safety, but even a slight improvement (9%) in the ride safety is observed. This is done at the expense of an increase of 20% in suspension stroke. The time domain plots of Fig. 3.8 show that for the first 5 sec against this increase, suspension stroke is far from its bounds. Let's check if this increase for the whole simulation time (10 sec) is allowed or not. To determine whether the constraints on suspension stroke are fulfilled from the Table 3.1 data may be confusing . Thus constraints on the output are translated into constraints on its RMS value. If we assume a normal distribution and use the statistical 3σ rule, $z_2^{rms} = m$ implies that $z_2 < 3 \cdot m$, 99.7% of time. Therefore, based on the maximum value we considered for suspension stroke, its RMS value should not exceed 0.0267. Data of this table confirm that these requirments are satisfied.

System	RMS $W\ddot{z}_s$	RMS TD	RMS SS	RMS power
Passive	0.471	0.00128	0.0109	0
Multi-objective	0.336	0.00111	0.0104	24.024
Multi-objective preview	0.118	0.00104	0.0126	25.458

Table 3.1: Components of performance index for multi-objective designs, for a real road input

3.7   Comparison to LQ-based design

3.7.1   For various road disturbances

In the following, the performance of the designed controllers is assessed for three road irregularities described in chapter 2.

First of all, it should be pointed out that both preview controllers are of the same degree as augmented plant, namely, $n + N_p = 24$.

Here, since it seems that the numbers speak louder than the plots, the plots are neglected to be included in the analyses. RMS values of system performance components for both preview designs for all three road inputs are given in table 3.2. The simulations for the shock input are carried out for the time interval 0-2 sec and for the vibration inputs for the time interval 0-10 sec. First we consider the case of white noise input. As expected, the suspension stroke of the multi-objective preview design is more than that of LQG-preview design. This is because of the first aspect of the multi-objective design, which allows the suspension stroke to vary freely as along as it remains within its given bounds, to deliver the best possible performance. But the results for the white noise input reveal that both strategies provide the same degree of ride safety and ride comfort. It means that the multi-objective design is conservative, and it is because of the second aspect of the design, i.e., the minimization is done for the worst case inputs.

Now we consider other inputs of chapter 2. For a real road profile, the multi-objective preview design provides 31% more driving comfort, without relinquishing other performance specifications. Similarly, for a single bump, passenger perceived acceleration, in comparison to LQ-based, 32% more is reduced, however in this case a 7% deterioration in ride safety is seen.

In a summary, the performance of the LQ-based preview design for white noise inputs is better than that of multi-objective one. However, it deteriorates its performance

road disturbace	preview control strategy	RMS $W\ddot{z}_s$	RMS TD	RMS SS	RMS Power
white noise	LQG	0.1112	0.00178	0.00474	26.693
	Multi-objective	0.1104	0.00175	0.00627	25.909
single bump	LQG	0.3264	0.00120	0.0137	186.820
	Multi-objective	0.2080	0.00128	0.0135	184.640
real road	LQG	0.1737	0.00105	0.0117	25.122
	Multi-objective	0.1183	0.00104	0.0126	25.458

Table 3.2: Components of performance index for both preview designs, for different road irregularities

compared to multi-objective one for other types of inputs.

3.7.2   Robustness against parameter changes

To evaluate the robustness characteristics of the designed suspensions, we observed the RMS values of passenger perceived acceleration for different values of vehicle body mass (m_s), when systems are excited with the real road profile.

For a fair comparison, the relative RMS value of passenger perceived acceleration defined with respect to the RMS values corresponding to the nominal preview suspensions (LQ-based or multi-objective) have been computed. Fig. 3.9 shows the results. This figure reveals that the passenger perceived acceleration for the multi-objective preview design has lower changes against parameter variations and hence possesses more robustness. Variations in car body mass occur when loadings on the vehicle vary either from passengers or payloads [39].

This study shows that a multi-objective preview is only slightly robuster than LQ-based, in other words, the LQ-based design possess good robustness properties. In
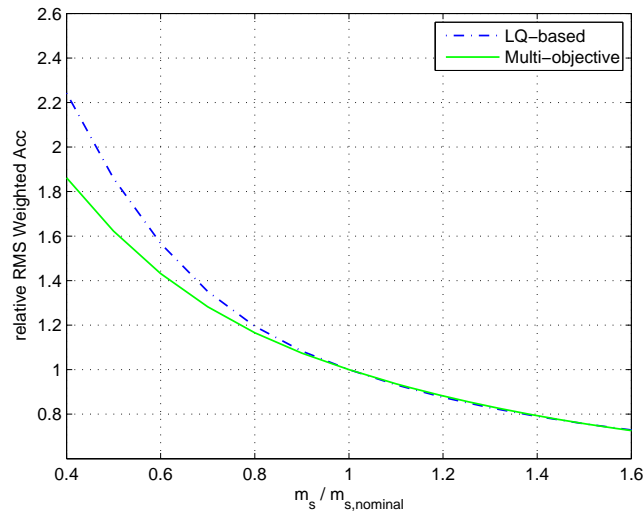
Figure 3.9: relative RMS weighted acceleration: multi-objective preview(−), LQ-based preview(-.)

fact, we expected less robustness for the LQ-based design, however since in the design of observer we tried to retrieve LQR properties, the obtained LQ-based system is robust.

3.7.3   Concluding remarks

Remark 3.1: Based on the unified design scheme employed in this study for preview design, the design approaches can be viewed as feedback designs. Designing an LTI feedback controller calls for a trade-off between nominal performance and robustness. Nominal performance and robustness specifications cannot be improved simultaneously using an LTI controller. In the case of white noise input, slight performance degradation of multi-objective design (requiring more suspension stroke), compared to LQ-based is because that the multi-objective design cares for all kinds of exogenous inputs and solves the optimization problem for the worst case, thus a more robust system, yet conservative for white noise input, is obtained.

Remark 3.2: The proposed multi-objective design approach reduces the number of a posteriori analyses or even eliminates the need for these simulations. All we need is to normalize the exogenous inputs and controlled outputs. However, as we will see in this case of study in next section, it may require few trials before a satisfactory performance is obtained.

Remark 3.3: Whereas the proposed multi-objective design is a dynamic output feedback based design and the design is done in one step, the LQ-based design requires full-state feedback, and hence a observer design.

Remark 3.4: The multi-objective design has been formulated in LMI's, and therefore could be easily extended to LPV designs, to retain system performance against parameter changes. This is done using self scheduled controllers, if system varying parameters could be easily measured [3].

3.8   A multi-objective design with improved ride safety

One main deficiency of both LQ-based and multi-objective preview designs above, is the amplification of tire deflection at the wheel-hop frequency, which translates into reduction in ride safety, at some situations. In order to improve the ride stability, it is important to keep the tire in contact with the road surface and therefore to decrease the resonance peak near the resonance frequency of the wheel, known as wheel-hop frequency, (for the problem of this study, around 11 Hz). To improve the ride safety of the system in multi-objective design, one could readily apply the following dynamic weighting function to the corresponding minimized output

$$W_{z2} = \frac{k_t}{(m_s + m_u)g} \cdot \frac{s^2 + 200s + 4780}{s^2 + 100s + 4780}$$

which has its peak value around 11 Hz to emphasize the importance of minimization at these frequencies.

Remark 3.5: Whereas frequency dependent weights can be readily utilized to penalize

system performance at some given frequency range in the multi-objective design of this study, in the LQ-based design utilization of dynamic weights is not common.

The results of the new design are given in Fig. 3.10. As it can be seen the adding of this weight hasn't improved the ride safety of non-preview case significantly. This is due to the inherent property of the feedback controller, where the performance of the controller should be balanced along the frequency domain. This feedback control characteristics is known as water-bed effect in the literature and referred to as Bode sensitivity integral as well. Therefore, one of other benefits of the preview control is to provide a framework that could improve performance over whole frequency range. Finally, it should be pointed out that as in the previous design, we didn't increase the
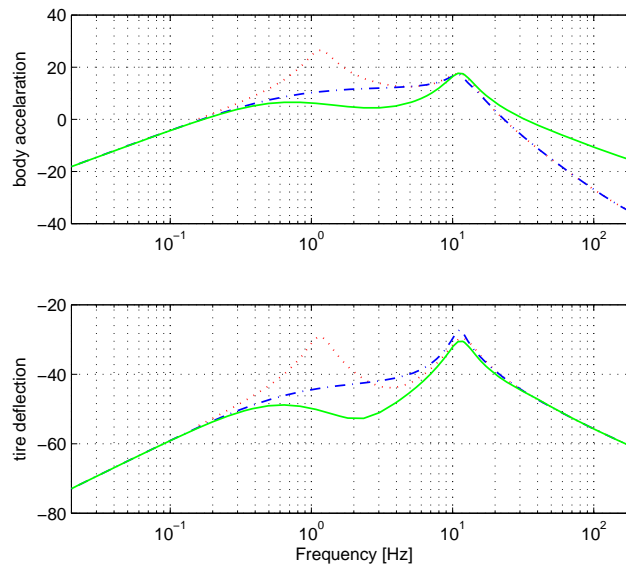
Figure 3.10: Frequency Response of the Multi-objective design with improved safety: Preview (−), Pure feedback (-.), Passive (..)

weighting of the control signal. Since preview design has improved both comfort and safety characteristics of the design, one could easily improve power consumption of the preview system as well, just by increasing the corresponding weighting function, however at the cost of small deterioration of other performance specifications.

3.8.1   System performance at other speeds

Now, we examine the performance of the designed system under vehicle speeds other than the nominal one (25 m/s).

We consider the vehicle speed interval of $20 - 30$ m/s. Fig. 3.11 shows preview system performance, normalized with respect to corresponding values of active pure feedback system, for the given speed range. Note that the speed range $\frac{500}{21} < v \leq \frac{500}{20}$ corresponds to $N_p = 20$ and hence nominal performance and any change in the performance level represents one unit change in N_p value. It can be seen that the designed preview controller, over whole this speed range, is surprisingly robust against changes in vehicle speed and maintains its superiority to pure feedback one and therefore we can claim that it can be used for speeds ranging from 20 to 30 m/s, without severe performance degradation. To use the so-called gain scheduling, a set of speeds may
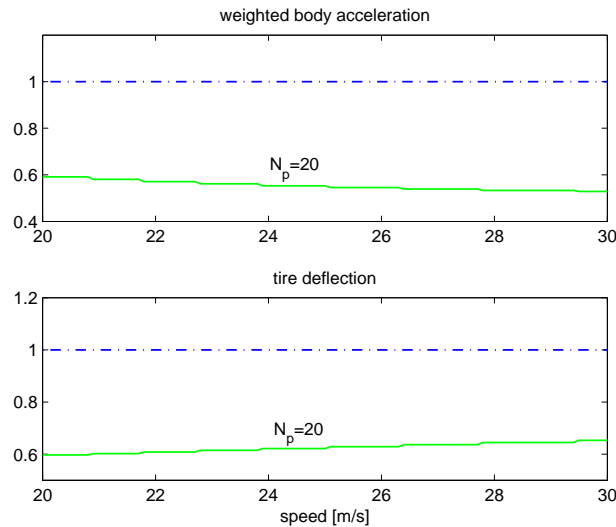
Figure 3.11: Components of performance index for varying vehicle speeds

be selected so that the preview controller based on these speeds could be used over the whole speed range. It will greatly reduce calculation cost of the system.

Holding performance using a delay line and switching

If view (capture) angle of the sensor could change with vehicle speed so that at any

speed it could capture a speed-dependent preview length of $L_p = 0.02 * V$, leading to $N_p = 20$ samples ahead of time, no deterioration in performance would appear.

However, if the sensor is fixed and captures irregularities $L_p = 0.5$ m ahead of vehicle, for vehicle speeds less than nominal ($V < 25$), we have $N_p = [\frac{0.5}{0.001*V}] > 20$ and road irregularities $N_p = 20$ samples ahead of time can be used as input to the controller and hence no deterioration in performance occurs, This can be done by adding an additional delay of $\frac{L_p}{V} - T_p$ (here $L_P = 0.5$ m and $T_p = 20$ msec) between the sensing and the preview signal entering the controller. This can be easily implemented using a tapped delay line and changing the point at which the input is fed to the controller, as in [56].

However if vehicle speed is greater than the nominal one, the difference between actual and nominal values of vehicle speed will lead to some performance degradation, as was shown above. Higher vehicle speed translates into lower preview length L_p, and hence lower N_p.

From the discussion above, one could easily conclude that if $L_p = 1$ m is considered, the designed controller is valid for $V = 50$ m/s (180 km/h) and therefore using the delay line and switching, it can be used for almost all speeds without any performance degradation

3.9   Inclusion of actuator dynamics

In the above sections, we showed that the preview information improves the control system performance. In addition to the potential improvements in ride quality and handling performance, preview control could offer lower power consumption. Moreover, in a non-preview active suspension, the control system must react very quickly to suppress disturbances that already have been encountered by the vehicle. In those cases where transients occur faster than the rate of response, some form of preparation strategy is clearly essential. This 'preparation strategy' implies the need for

information describing disturbances before they are encountered by the vehicle [33]. Hence, one other advantage of the preview control is that it can compensate for the time delays in the reaction of the system and the actuators. This means that with the inclusion of actuator in the plant, the superiority of preview suspension to its non-preview counterpart will be clarified even more. Let's postpone investigation of performance of preview suspension with inclusion of actuator dynamics to chapter 5.

Chapter 4

A PERSPECTIVE ON WHEELBASE PREVIEW DESIGN

Wheelbase preview suspension is based on the estimation of road profile from system response. Once the front wheel encounters a road irregularity, this irregularity is detected by analyzing system response and is utilized by the controller of the rear suspension to provide the system to counteract its effect as far as possible. This chapter gives a perspective on wheelbase preview control design.

4.1 Wheelbase preview

As discussed in the preceding chapter, suspension performance can be improved if preview, i.e., knowledge of the road surface in front of controlled axles, is utilized by the control strategy. Among two preview concepts, look-ahead preview was extensively investigated in previous chapter. In this concept, the road information, obtained by a look-ahead sensor, is used to control both the front and rear suspension. Look-ahead preview systems, even though have been shown to lead to enhanced system performance compared to their pure feedback counterpart, they suffer the drawback of **wrong detection/ interpretation of road irregularities when facing pseudo-obstacles**. They recognize a heap of leaves or paper as a serious obstacle, while a pothole filled with rain water will not be detected at all. These situations may lose vehicle road holding and hence its stability. Moreover, its steering cannot be accomplished as desired.

An alternative to round this problem is to assume that the road surface at rear wheel

is the same as at front wheels (except for the time delay) and to reconstruct it from on-line measurements of system accelerations and deflections and then to use this information for the rear wheel suspension. This preview scheme is referred to as wheelbase preview.

From this point of view, **wheelbase preview is more promising** and reliable. Moreover, it imposes no additional costs for the sensor. Even in comparison to the pure feedback active suspensions, it doesn't increase the overall cost of the system. Because the only difference is the control algorithm, and both of the algorithms are implemented using high speed processors, which are available at low costs nowadays.

The control problem with wheelbase preview consists of the following two steps:

- To design a controller improving ride comfort without sacrificing handling requirements, assuming that front wheel disturbance is available.

- To estimate the disturbance applied to the front wheel from system response.

Both disturbance detection and controller design problems are formulated and solved using LMI techniques which allow considering many other constraints, leading to enhancement in system performance.

Since the first step can be carried out in a similar way to that of preceding chapter, this chapter will not expend much time on it. Rather, it will mainly focus on the second step, which cannot be traced in the literature.

At the end, it should be pointed out that even though the wheelbase preview appears cheaper and more reliable than look-ahead preview, it has also some drawbacks, for example, the track of the rear wheels may differ from that of the front wheels, especially in cornering; or a brick, detected by the front wheels, might be thrown away so that the rear wheels doesn't encounter it.

4.2   Controller design scheme

Wheelbase preview has already been studied in few papers, e.g., [16, 38], in which the LQ-based designs have been employed. Based on the benefits of multi-objective preview design, presented in the previous chapter, here we give guidelines for applying this design scheme to wheelbase preview design.

As discussed above, in the controller design stage, it is assumed that the front wheel disturbance (w_f) is already available, and w_r, rear wheel disturbance, is a delayed version of w_f. Based on this assumption the controller design design scheme has been shown in Fig. 4.1. Here l represents the distance between front and rear wheels and v is the vehicle speed.
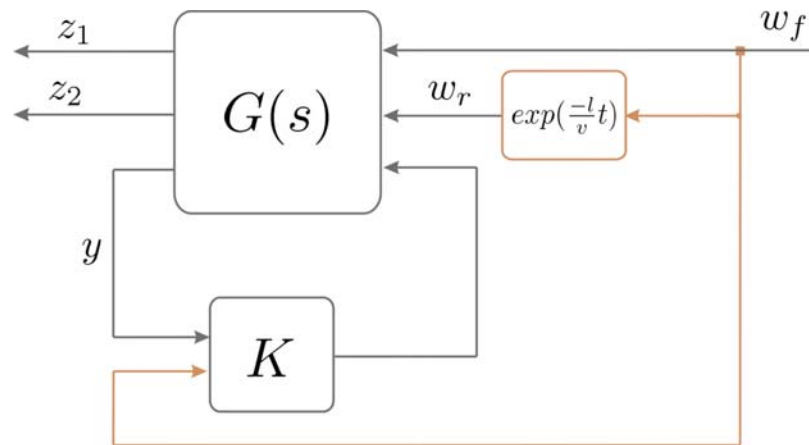
Figure 4.1: Wheelbase preview design framework

The control problem can then be stated as

$$\text{Find a controller to minimize } \|\frac{z_1}{w_f}\|_\infty$$

$$\text{while } \|\frac{z_2}{w_f}\|_{GH_2} < \gamma_2$$

As in the look-ahead preview, z_1 is the to-be-minimized output vector, which consists of (weighted) body vertical and rotational accelerations, as measure of ride comfort;

tire deflection, as measure of ride safety; and control signal

$$z_1 = \begin{pmatrix} q \\ z_u - z_r \\ u \end{pmatrix}$$

(Note the notations and definitions of chapter 2.) and z_2 is the vector of to-be-constrained outputs

$$z_2 = z_s - z_u$$

This formulation minimizes worst-case RMS value of z_1, so that $\|z_2\|_\infty$ (its max.) doesn't exceed a prespecified maximum.

With the above definitions, the approach of preceding chapter, is easily extended to wheelbase preview and considering appropriate measured outputs, the controller is obtained by solving the optimization problem of 3.16.

4.3 Detection of front wheel disturbance

All the studies dealing with the wheelbase preview concept in the literature, as the best knowledge of the author, assume that road data of the front wheel is already available. Therefore, the objective of this section is to fill the gap between and obtain a robust estimation of the road disturbance applied to the front wheel from system response.

To care for the wide range of road irregularities, an H_∞-norm based scheme is used to design the estimator. The problem is formulated using LMI's and allows consideration of parameter variations in the design, in fact a self-scheduled LPV estimator is obtained in this study. Moreover, to ensure desired transient dynamics for the estimator, some pole location constraints are considered. It is also worthwhile to mention that the design scheme allows the designer to emphasize on specific states to get more accurate estimation of road disturbance.

This study is also useful for adaptive (gain scheduled) active suspensions where the

road type is the scheduling variable. In addition, noting that the approach is based on state estimation, it can also be utilized in state feedback suspensions.

The half car model used in this study is the one described in chapter 2, however without loss of generality, the suspension system here is assumed to be passive, i.e., the actuator is removed from system.

The goal of this section is to estimate the road disturbance applied to the front wheel (w_f) from system response. The estimator design framework is depicted in Fig. 4.2 . In this framework, suspension deflections $(z_s - z_u)$ and vertical accelerations of the sprung mass $(\ddot{z}_s)$ are considered as measured outputs (y). These outputs can be readily measured in practice using suitable displacement sensors and accelerometers respectively.

The performance output of z, noting the relation

$$w_f = \dot{z}_{rf} = \dot{z}_{uf} - \dot{x}_5 = x_7 - \dot{x}_5$$

is assumed to comprise only these relevant states, i.e., x_5 and x_7. Clearly the more precise estimation of these states, the more accurate detected road disturbance.
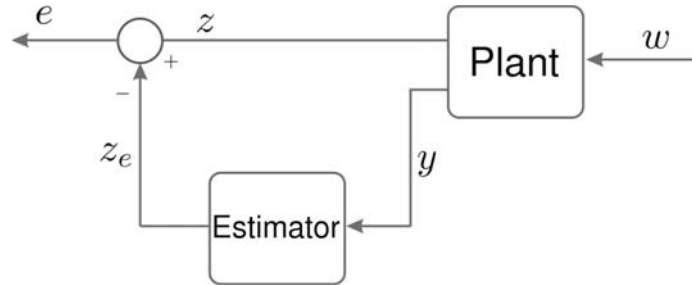
Figure 4.2: Estimator design framework

4.3.1   Estimator design scheme

This section gives a brief overview of estimator design approach employed in this study. For a generality, it is assumed that the system, $G(s)$, is described by the

following parameter-dependent state-space realization

$$\dot{x}(t) = A(p)x + B(p)w,$$
$$z(t) = C(p)x, \qquad\qquad\qquad (4.1)$$
$$y(t) = C_y(p)x + D_y(p)w$$

where $x(t) \in \mathbb{R}^n$ is the state vector, $w(t) \in \mathbb{R}^m$ is exogenous input, $z(t) \in \mathbb{R}^p$ is the performance output vector and $y(t) \in \mathbb{R}^{p_y}$ is the measured output vector. The vector $p = (p_1, p_2, \cdots, p_q)$ represents uncertain parameters of the system, and is assumed that

1. Each uncertain parameter p_i varies in some interval $[\underline{p}_i, \overline{p}_i]$, then the parameter vector p takes values in a parameter box (polytope) with corners $\theta_1, \theta_2, \cdots, \theta_r$, where $r = 2^q$, i.e.,

$$p \in \Theta = Co\{\theta_1, \theta_2, \cdots, \theta_r\}$$
$$= \{\sum_{i=1}^{r} \alpha_i \theta_i : \alpha_i \geq 0, \sum_{i=1}^{r} \alpha_i = 1\}$$

2. The parameter dependence of the system is affine, i.e., the state-space matrices $A(p)$, $B(p)$, $C(p)$, $C_y(p)$ and $D_y(p)$ depend affinely on p.

Thus, it is clear that system matrices range in a polytope of matrices whose vertices are images of the parameter box vertices $\theta_1, \theta_2, \cdots, \theta_r$, i.e.,

$$\begin{pmatrix} A(p) & B(p) \\ C(p) & 0 \\ C_y(p) & D_y(p) \end{pmatrix} \in Co\left\{ \begin{pmatrix} A_i & B_i \\ C_i & 0 \\ C_{y,i} & D_{y,i} \end{pmatrix} \right.$$
$$:= \begin{pmatrix} A(\theta_i) & B(\theta_i) \\ C(\theta_i) & 0 \\ C_y(\theta_i) & D_y(\theta_i) \end{pmatrix}, i = 1, 2, \cdots, r \left. \right\}$$

Now, as in Fig. 4.2 interconnect the system (4.1) with the following estimator

$$
\begin{aligned}
\dot{x}_e &= A(p)x_e + L(p)(C_y(p)x_e - y), \\
z_e &= C(p)x_e
\end{aligned}
\tag{4.2}
$$

The goal is to find an Estimator matrix $L(p)$ such that $z - z_e$ is kept as small as possible, for all disturbances w. Defining $\tilde{x} = x - x_e$, the overall system equations are given by

$$
\begin{aligned}
\dot{\tilde{x}} &= (A(p) + L(p)C_y(p))\tilde{x} + (B(p) + L(p)D_y(p))w, \\
e &= z - z_e = C(p)\tilde{x}
\end{aligned}
\tag{4.3}
$$

To design an estimator to perform satisfactorily for a wide range of road irregularities, not just white noises, calls for employing L_2-norm as a measure of estimation quality. Therefore, the objective is to find $L(p)$ such that the resulting system is internally stable, and the L_2 gain (H_∞ norm) of the system from w to e is smaller than γ, a specified positive number, i.e.,

$$
\sup \frac{\|e\|_2}{\|w\|_2} < \gamma
\tag{4.4}
$$

By virtue of bounded real lemma [7, 48], achieving internal stability and the satisfaction of H_∞-constraint (4.4) are jointly equivalent to the existence of symmetric positive definite matrix P such that

$$
\begin{pmatrix}
\mathcal{A}^T(p)P + P\mathcal{A}(p) & * & * \\
\mathcal{B}^T P & -\gamma I & * \\
\mathcal{C}(p) & \mathcal{D}(p) & -\gamma I
\end{pmatrix} \prec 0
\tag{4.5}
$$

where * represents the transpose of the elements across the diagonal and calligraphic letters represent the matrices of the overall system (4.3).

In addition, in order to guarantee desired transient dynamics for the system, some pole placement constraints are imposed. Here we consider the desired pole location of Figure 4.3 , the combination of the following pole constraints
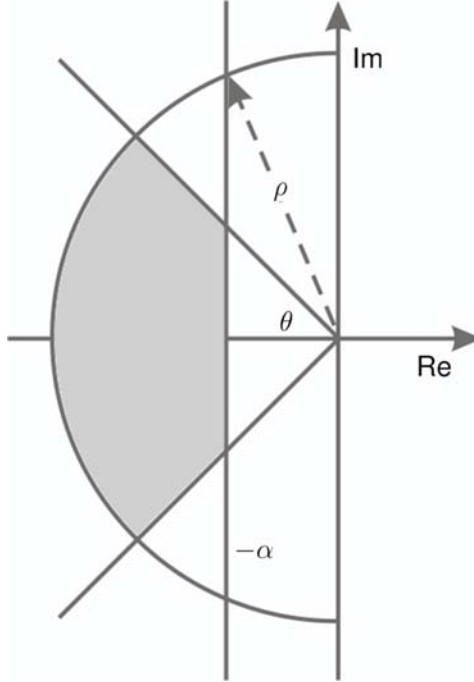
Figure 4.3: Desired pole location

1. Disk region ($|s| < \rho$), which can prevent fast estimator dynamics and therefore makes it easier to implement using digital computers. All eigenvalues of $\mathcal{A}$ lie in a disk with radius ρ centered at the origin if and only if there exists a matrix P satisfying [13]

$$\begin{pmatrix} -\rho P & P\mathcal{A}(p) \\ * & -\rho P \end{pmatrix} \prec 0 \tag{4.6}$$

2. α-stability region ($Re(s) < -\alpha$), which ensures a minimum damping coefficient of α and is represented by the following LMI

$$\mathcal{A}^T(p)P + P\mathcal{A}(p) + 2\alpha P \prec 0 \tag{4.7}$$

3. Conic sectors $\angle s \in [\pi - \theta, \pi + \theta]$, which guarantees a minimum damping ratio of $\zeta = cos(\theta)$, if and only if the following LMI is satisfied

$$\begin{pmatrix} \sin\theta(P\mathcal{A}(p) + \mathcal{A}^T(p)P) & \cos\theta(P\mathcal{A}(p) - \mathcal{A}^T(p)P) \\ -\cos\theta(P\mathcal{A}(p) - \mathcal{A}^T(p)P) & \sin\theta(P\mathcal{A}(p) + \mathcal{A}^T(p)P) \end{pmatrix} \prec 0 \tag{4.8}$$

After substitution of calligraphic matrices in the above LMI's (4.5-4.8) with their values of (4.3) and change of matrix variables as

$$Y(p) = PL(p) \tag{4.9}$$

and noting the affine dependence of the system on p, based on the vertex property of polytopic LPV systems [3], the above inequalities are satisfied for all p in parameter box if and only if there exist $P = P^T \succ 0$ and Y_i, $i = 1, 2, \cdots, r$ such that

$$\begin{pmatrix} A_i^T P + PA_i + Y_i C_{y,i} + C_{y,i}^T Y_i^T & * & * \\ B_i^T P + D_{y,i}^T Y_i^T & -\gamma I & * \\ C_i & D_i & -\gamma I \end{pmatrix} \prec 0$$

$$\begin{pmatrix} -\rho P & PA_i + Y_i C_{y,i} \\ * & -\rho P \end{pmatrix} \prec 0 \tag{4.10}$$

$$A_i^T P + PA_i + Y_i C_{y,i} + C_{y,i}^T Y_i^T + 2\alpha P \prec 0$$

$$\begin{pmatrix} \sin\theta(A_i^T P + PA_i + Y_i C_{y,i} + C_{y,i}^T Y_i^T) := M_{11} & -M_{21} \\ \cos\theta(A_i^T P - PA_i - Y_i C_{y,i} + C_{y,i}^T Y_i^T) := M_{21} & M_{11} \end{pmatrix} \prec 0$$

Now we can formulate estimator design by the following optimization problem in LMI's

$$\min_{\gamma, P, Y_i} \gamma, \text{subject to LMI's}(4.10) \tag{4.11}$$

Given any solution of this LMI, vertex estimator matrices are obtained by

$$L_i = P^{-1} Y_i, \ i = 1, 2, \cdots, r \tag{4.12}$$

then the LPV estimator is defined as an 'interpolant' of the L_i's [3], based on the position of p in the box Θ, i.e., for parameter values of

$$p = \sum_{i=1}^{r} \alpha_i \theta_i$$

the estimator is given by

$$L(p) = \sum_{i=1}^{r} \alpha_i L_i$$

Recall that parameter vector of p is measured on-line. While vertex estimator matrices are computed off-line, the LPV estimator matrix must be updated on-line based on the parameter measurements.

4.3.2   Application to the problem

Now the proposed approach is applied to design an LPV estimator for the problem described at the beginning of this section. The problem has already been cast into desired design scheme. But noting the fact that the sprung mass varies in an interval $m_{s1} \leq m_s \leq m_{s2}$, system matrices are nonlinear functions of this uncertain parameter. Now in accordance with the procedure described above, all we need is to obtain an affine parameter dependent system. To this goal, the parameter p is defined as $p = \frac{1}{m_s}$, which leads to a two-vertex parameter polytope as

$$p = \frac{1}{m_s} = \alpha_1 \frac{1}{m_{s1}} + \alpha_2 \frac{1}{m_{s2}}$$

where

$$\alpha_1 = \frac{1/m_s - (1/m_{s2})}{1/m_{s1} - (1/m_{s2})},$$
$$\alpha_2 = 1 - \alpha_1$$

In the design process, for the pole placement constraints the following values are considered

$$\alpha = 8, \ \rho = 150, \ \zeta = 0.7$$

Remark 4.1: It is worth mentioning that some other parametric uncertainties (e.g., tire stiffness) can be considered in the system and then treated in similar way. However the number of generators (parameter box vertices r) should be finite and appropriate to get less conservative results.

Remark 4.2: Clearly, the self-scheduled scheme, described above, is very useful for an LPV system, but since over the entire operating range a single Lyapunov function is used, the resulting estimator tends to be conservative, when number of generators r is high. A less

conservative design is obtained using parameter dependent Lyapunov functions similar to the approach of [23].

By applying the procedure in the preceding subsection in Matlab environment [22], the vertex estimator matrices are computed and a γ value of 0.29 is obtained.

To demonstrate the effectiveness of the obtained estimator, also a Kalman estimator is designed to solve the problem under study. A fair comparison requires the design of both estimators under similar design requirements. Since in the design of the LPV H_∞ estimator we ignored the measurement noise (clearly it can be readily included in the design without any complication), in the design of Kalman estimator, matrices Q (disturbance covariance) and R (measurement noise covariance) are assumed as I and $0.1 * I$ respectively, to represent the accuracy of measurements.

The designed estimators will be compared in the next subsection.

4.3.3 Simulation Results

To evaluate the effectiveness of the proposed estimator, in the following some time domain simulations are carried out.
In the following, the performance of the designed estimators is assessed for both types of disturbances, described in chapter 2.
Let's first expose the system to the bump input. It is assumed that the rear wheel disturbance is a delayed version of front wheel disturbance, i.e.,

$$z_{rf}(t) = \begin{cases} \frac{H}{2}(1 - \cos(\frac{2\pi V}{L}t)), & 0 \le t \le \frac{L}{V} \\ 0, & t > \frac{L}{V} \end{cases}$$
$$z_{rr}(t) = \begin{cases} \frac{H}{2}(1 - \cos(\frac{2\pi V}{L}(t - \frac{l}{V}))), & \frac{l}{V} \le t \le \frac{L+l}{V} \\ 0, & \text{otherwise} \end{cases}$$

where $l = l_f + l_r$ is the length of the half-car. Fig. 4.4 shows the error in estimation of front wheel disturbance using both LPV H_∞ and Kalman estimators. The results reveal that even though the Kalman estimator works well for the nominal value of the sprung mass, its performance deteriorates considerably, when sprung mass changes, but the proposed estimator shows immaterial degradation in performance for different values of sprung mass.

The ratio of RMS error to RMS disturbance signal for the above simulations are given in table 4.1. It can be easily seen that the LPV H_∞ estimator has almost the same performance level for all values of sprung mass, assuring stability and performance against mass variations, whereas the performance index using Kalman estimator, with change of mass, increases up to 3.25 times of the nominal case.
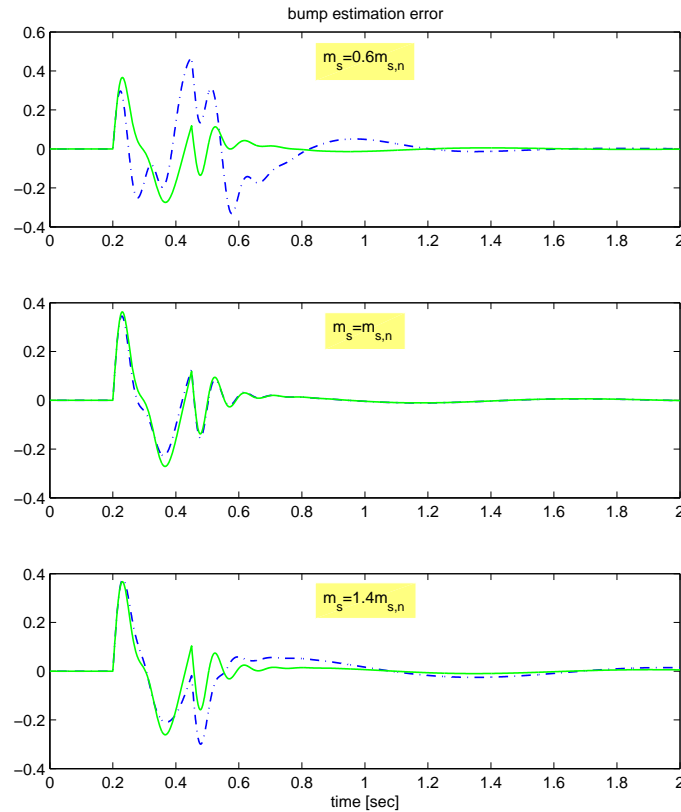
Figure 4.4: Performance of estimators for the bump input: LPV-H_∞ (–), Kalman (-.)

Now, we consider the case of vibration input. To assess system performance for this type of road disturbance, we consider the real road profile of Fig. 2.3. The results of applying this input to the system are given in Fig. 4.5 and Table 4.2. The results detailed in the table have been computed for the simulation time of 10 sec, but the figure is confined to show the results for the first 5 sec just for clarity. It should also be pointed out that shown inputs describe road vertical displacement, whereas the results show the error in detection

system	$m_s = 0.6m_{s,n}$	$m_s = m_{s,n}$	$m_s = 1.4m_{s,n}$
LPV H_∞	0.1119	0.1068	0.1065
Kalman	0.2685	0.0822	0.1598

Table 4.1: Performance of estimators for the bump input

of disturbance considered in this study, i.e., road vertical velocity. The results are more or

system	$m_s = 0.6m_{s,n}$	$m_s = m_{s,n}$	$m_s = 1.4m_{s,n}$
LPV H_∞	0.1215	0.1218	0.1393
Kalman	0.3409	0.1169	0.3099

Table 4.2: Performance of estimators for the vibration input

less similar to those of above and confirm the above expressions.

4.3.4 Summary

To estimate the disturbance applied to the front wheel a self-scheduled H_∞ estimator was designed to deal with the LPV system. Pole location constraints are also considered to care for the transient dynamics of the system. Moreover, the estimator suggested here, allows the designer to emphasize on specific states, even though its effect in this case of study is not remarkable. The designed estimator was compared with a Kalman one. The results showed that the designed LPV estimator has slightly worse performance than the Kalman estimator for the nominal plant, but unlike the Kalman estimator, maintains its performance over the entire range of uncertainty.
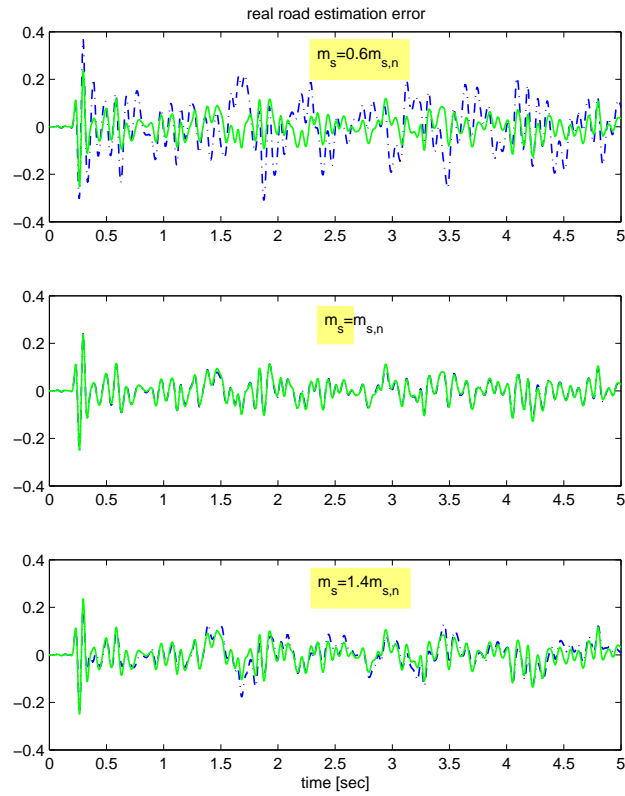
Figure 4.5: Performance of estimators for the vibration input: LPV-H_∞ (–), Kalman (-.)

Part III

Experimental verification

Chapter 5

EXPERIMENTAL SETUP DESCRIPTION AND PREVIEW SUSPENSION DESIGN

This chapter first shortly describes the test-rig used for verification of the results obtained in chapter 3 and then both LQ-based and multi-objective preview suspensions are designed and simulated.

5.1   Description of the test rig

The test rig used for the experimental investigation of the multi-objective preview is shown in Fig. 5.1. It emulates the behavior of a quarter vehicle. The sliding steel plate here resembles one corner of the vehicle body. The suspension system, placed between wheel assembly and vehicle body, consists of a spring/damper pair, and a linear motor in parallel, which is off for the passive case and is driven in the active case. The tire is excited at the bottom, by a linear motor, imitating the road irregularities. Moreover, at the bottom, springs are used to support the static load (weight) of the body and wheel assembly.

5.1.1   Linear model

The linear model of a quarter vehicle, discussed in chapter 2, applies to this system as well, however with parameter values given in Table 5.1. These values have been obtained through physical modeling of the system as well as some identification processes performed on the system by [51].

Figure 5.1: A picture of the test-rig

5.1.2   Nonlinear model

The linear system describes the system model sufficiently accurate for controller synthesis purposes, however one should not neglect the system nonlinearities in the analysis of the designed system, before getting it implemented. System nonlinearities, detected through some tests and white/gray box identification processes by [51], include the following

- Nonlinear damper characteristics: Damper coefficients in tension and compression differ from each other, furthermore in either case the force-velocity relation is not linear. Therefore, the force produced by the damper is obtained through a look-up

Model parameters	symbol	values	unit
sprung mass	m_s	89.56	kg
suspension stiffness	k_s	8375	N/m
suspension damping rate	b_s	769	N/(m/sec)
Wheel assembly mass	m_u	23.92	kg
tire stiffness	k_t	149063	N/m
tire damping	b_t	100	N/(m/sec)

Table 5.1: Nomenclature and parameter values corresponding to the test-rig

table. Coulomb friction is also modeled nonlinearly.

- Nonlinear Coulomb friction between the sliding plate (body) and its base, mounted on the wall.

- Nonlinear tire stiffness: The force describing the tire stiffness, in addition to the linear term, includes a quadratic term, i.e.,

$$F_{tire-stiffness} = k_{t1}(z_u - z_r) + k_{t2}(z_u - z_r)^2$$

- Nonlinear tire damping: tire damping is modeled by a linear damper, having nonlinear Coulomb friction.

- The damper/spring pair is not perpendicular to the body and wheel masses and therefore not all the force produced by them affects these masses. This is another source of nonlinearity.

5.1.3   Actuator dynamics

Suspension actuator used in the test setup is a permanent magnet (PM) linear synchronous motor (LSM). The PM synchronous motor is an electric machine which consists of an active classic three phase (stator) winding in one side of the air gap and array of alternate-pole permanent magnet (rotor) on the other side of air gap. The air gap magnetic field is produced by the permanent magnet (rotor). A PM synchronous motor is driven by three

phase sine wave voltage coupled with the given rotor position. The generated stator flux together with the rotor flux defines the force and thus speed of the motor. Clearly, to get the maximum generated force, the sine wave voltage has to be applied to the 3-phase winding system in a way that angle between the stator flux and the rotor flux is kept close to 90°. To meet this criterion, the motor requires referencing when switching from stop to run.

The PM synchronous motor lacks a commutator and is therefore more reliable than the DC motor. But can we control its speed/ force as easily as a DC motor ones? The answer is yes, it is possible through a closed-loop PM synchronous motor drive using a Vector Control technique. Vector Control is an elegant control method of a PM synchronous motor, where the coordinate system of space vectors of magnetic flux, current, and voltage (a,b,c coordinate) is transformed into a magnetic field-generating part and a force-generating part (d,q coordinate). The structure of the motor controller (Vector Control controller) is then almost the same as for a separately-excited DC motor, which simplifies the control of PM synchronous motor. This Vector Control technique was developed specifically to achieve a similar dynamic performance of DC motors in PM synchronous motors.

The field oriented control principle of a PM-SM has been illustrated in Fig. 5.2. As it can be seen, the force of the actuator can be easily controlled by varying the input voltage. The drive board of the PM-LSM in the laboratory, implements this control strategy.

The dynamic of this actuation system has been identified by [40] as

$$
\begin{aligned}
\dot{x}_{mot} &= \begin{pmatrix} A_{mot} & 0 \\ 1/T_{mot} & -1/T_{mot} \end{pmatrix} x_{mot} + \begin{pmatrix} b_{mot} \\ 0 \end{pmatrix} u_{[v]}, \\
u_{[N]} &= \begin{pmatrix} 0 & K_f C_{mot} \end{pmatrix} x_{mot}
\end{aligned}
$$

where

$$
\begin{aligned}
A_{mot} &= -15.784 \\
T_{mot} &= 0.003 \\
b_{mot} &= 0.0606 \\
K_f C_{mot} &= 100 \cdot 809.9
\end{aligned}
$$

The bode diagram of the actuator has been given in Fig. 5.3. As it can be seen, based on
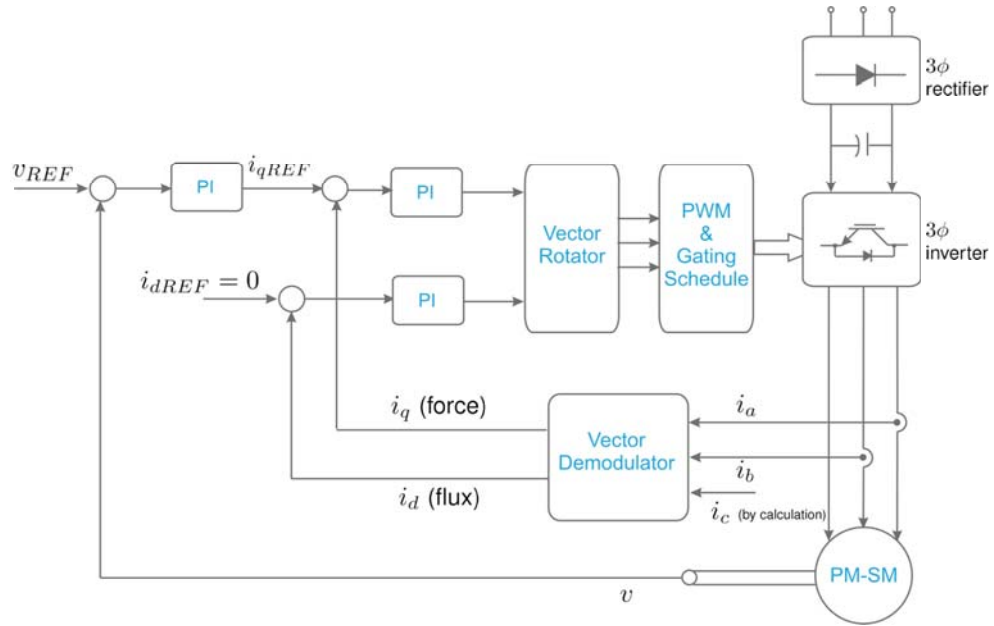
Figure 5.2: Field oriented control of a PM-SM

the '-3 dB' rule, the actuator has a bandwidth of about 3 Hz.

5.2   Preview suspension design

In the suspension designs of chapter 3, it was assumed that the actuator is ideal. However in reality any actuator has a dynamic. To implement a controller designed this way in the control loop, a sub-loop referring to mostly as force-tracking loop, is added to drive the actuator force to approach the desired value quickly. Although this approach is common, it suffers from two drawbacks:

1. In the design of the main loop it is not taken into account and therefore inclusion of this sub-loop may require re-design of the main loop.

2. If the sub-loop is open-loop, the actual force is not guaranteed to track the desired value, And if it is closed-loop, a force sensor maybe required.
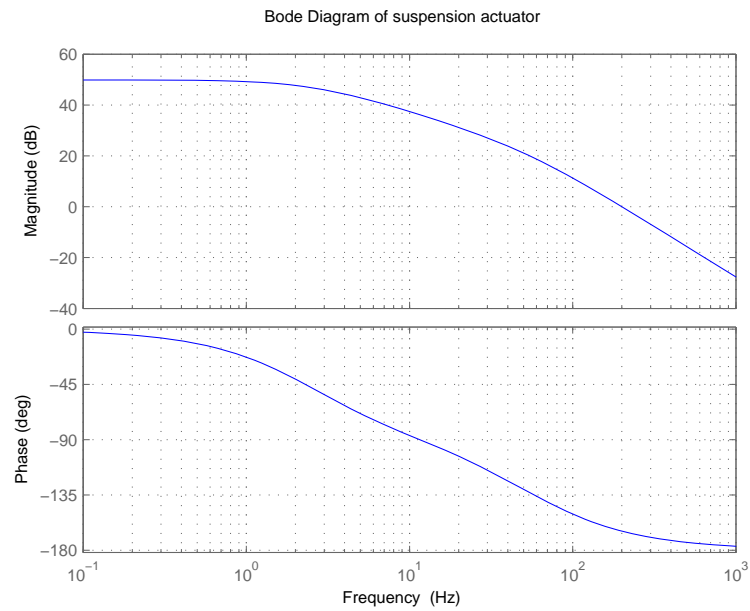
Figure 5.3: Bode diagram of the suspension actuator

To address these problems, several researchers have proposed to include the actuator dynamics to form an enhanced plant model [15, 41]. Moreover, since one of the main benefits of the preview control is to counteract the delays due to reaction time of the actuator, it seems that considering the actuator dynamics in the design of preview, lead to more efficient design. The new control input thus becomes an electrical signal that could be manipulated much more quickly and precisely and therefore eliminates the need for the sub-loop design.

Combining the actuator equation with the equations of ideal-actuator system of chapter 2, the enhanced system in continuous time domain can be described by the following state space matrices

$$A_c = \begin{pmatrix} 0 & 1 & 0 & -1 & 0 & 0 \\ -k_s/m_s & -b_s/m_s & 0 & b_s/m_s & 0 & K_f C_{mot}/m_s \\ 0 & 0 & 0 & 1 & 0 & 0 \\ k_s/m_u & b_s/m_u & -k_t/m_u & -b_s/m_u & 0 & -K_f C_{mot}/m_u \\ 0 & 0 & 0 & 0 & A_{mot} & 0 \\ 0 & 0 & 0 & 0 & 1/T_{mot} & -1/T_{mot} \end{pmatrix},$$

$$B_c = \begin{pmatrix} B_{c,w} & B_{c,u} \end{pmatrix} = \begin{pmatrix} 0 & 0 \\ 0 & 0 \\ -1 & 0 \\ 0 & 0 \\ 0 & b_{mot} \\ 0 & 0 \end{pmatrix}$$

For the synthesis of both preview and non-preview controllers, the same performance out-puts of z are considered, however measurement output comprises vertical accelerations of body $\ddot{z}_s$ and wheel $\ddot{z}_u$. The following weights and design parameters are applied to design the multi-objective controllers

$$W_{z_{11}} = 3.5,$$
$$W_{z_{12}} = 1,$$
$$W_u = 0.1 \frac{s/(50\pi)+1}{s/(5000\pi)+1},$$
$$W_d = 0.15,$$
$$n_g = n_p = 0.1,$$
$$\gamma_2 = 1$$

Discretization is done under the sampling time of 0.5 msec and then the optimization prob-lem of (3.16) is solved to compute the controllers.

At first try, we applied the same weights of ideal actuator case of chapter 3, however the designed multi-objective controller, through nonlinear simulations, was found to be sensitive to measurement noises. Therefore, the weights corresponding to measurement noises were increased. Moreover, since the bandwidth of the applied actuator is low, we reject to consider

a dynamic weight to penalize the tire deflection. This will increase only the controller degree without perceivable improvement in the ride safety. The first order lead term is used to penalize the control signal to retrieve low pass behavior of the passive suspensions. It should also be pointed out that due to specifications of suspension actuator, the suspension stroke here is limited to 5 cm.

Similarly, for comparison purposes, an LQ-based preview system is also designed. Design parameters are obtained after some trials as

$$\rho_1 = 1.2 \times 10^6,$$
$$\rho_2 = 10,$$
$$\rho_3 = 7 \times 10^4,$$
$$\rho_4 = 0,$$

and

$$R_{c,o} = \begin{pmatrix} 25 \times 10^{-4} & 0 & 0 \\ 0 & 25 \times 10^{-4} & 0 \\ 0 & 0 & 25 \times 10^{-4} \end{pmatrix},$$
$$Q_{c,o} = 1I$$

Remark 5.1: A note on sampling time (T_s) and preview horizon (N_p) selection
As in the potential assessment part of this study, first we applied the sampling time of 1 msec for the discretization of the plant. For the system designed under $T_s = 1$ msec, whereas the simulation results on linear model show a good performance, simulation results on nonlinear model for the system, showed that this sampling time is not sufficiently small and results in a perceivable degradation in system performance. The lower the sampling time, the better performance is delivered.
On the other hand, a physical limit on the sampling rate, is set by the operation speed of the control computer (dSPACE Power PC here). The processor has to carry out all the calculation required by the control algorithm within one sampling interval. While a sampling time of 0.5 msec with $N_p = 40$ leads to good performance, by controller implementation on dSPACE task-overrun error was occurred, which means that a task is requested to start, but the previous execution has not finished yet. This calls for increasing the sampling time or reducing the controller complexity. Another remedy, clearly is to reduce the controller degree using order reduction approaches, which is beyond the scope of this study.

Therefore, finally as a compromise $T_s = 0.5$ msec and $N_p = 25$ were adopted. This applies to both preview designs and both controllers will be of degree $n + N_p = 31$.

5.3 Simulation results

Numerical analyses are carried out for the real road profile of chapter 2. The measured variables are assumed to be contaminated with uncorrelated white noises. This section compares the designed multi-objective preview system with a pure feedback one as well as an LQ-based preview system in presence of nonlinearities.

5.3.1 Comparison to pure feedback

We observe here how a preview system improves the performance, when actuator dynamics is also included in the system. Response of the multi-objective preview, non-preview as well as passive suspensions to the real road profile is shown in Fig. 5.4. These simulations are based on the nonlinear model of system. The RMS values of the performance outputs associated with this figure, are given in Table 5.2. The results detailed in the table have been computed for the whole simulation time of 25 sec, but the figure is confined to show the results for the first 5 sec just for clarity. The DTL here stands for dynamic tire load. The results reveal a significant improvement in performance. Inclusion of preview leads

System	RMS $\ddot{z}_s$	RMS DTL	RMS SS	RMS u
Passive	1.53	220.55	0.0054	0
Multi-objective	1.02	194.44	0.013	1.30
Multi-objective preview	0.51	152.65	0.015	1.10

Table 5.2: RMS values of performance outputs for multi-objective designs, for a real road input

to 50% improvevement in ride comfort and 21% in ride safety comared to its non-preview counterpart. As the plots show, the constraint on suspension stroke, for the first 5 sec is
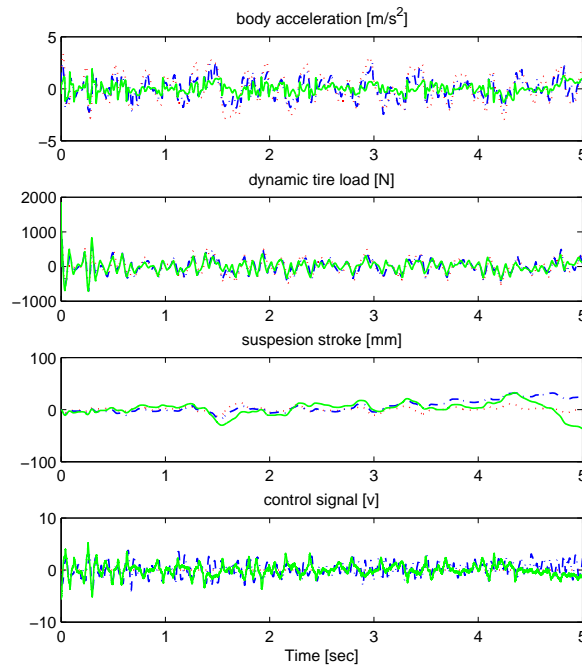
Figure 5.4: Real road response of the Multi-objective design considering actuator dynamics, based on nonlinear model simulations: Preview (–), Pure feedback (-.), Passive (..)

also fulfilled, and the results of the table, based on discussions in chapter 3, confrim that this fulfillment is achieved for the whole simulation time.

It can be easily seen that performance improvement from non-preview to preview for the actuator included system, is not perceivably different from that for the ideal-actuator system. This is mainly because the actuator possesses a low bandwidth. Otherwise, since the preview compensates for actuator's delay, it would show a great improvement. The lower preview horizon of this design also requires some attention.

5.3.2   Comparison to LQ-based preview suspension

In designing the LQ-based preview controller, through a posteriori analyses and redesigning both LQR preview controller and observers, lots of time was expended to obtain similar performance of the multi-objective preview controller. The real road response of both designs, based on the linear model of the system with noise-contaminated measurements, are given in Fig 5.5. This figure shows that from all aspects of performance, both LQ-based and multi-objective preview strategies behave similarly. The corresponding RMS values are given in Table 5.3, which confirm the above observations.
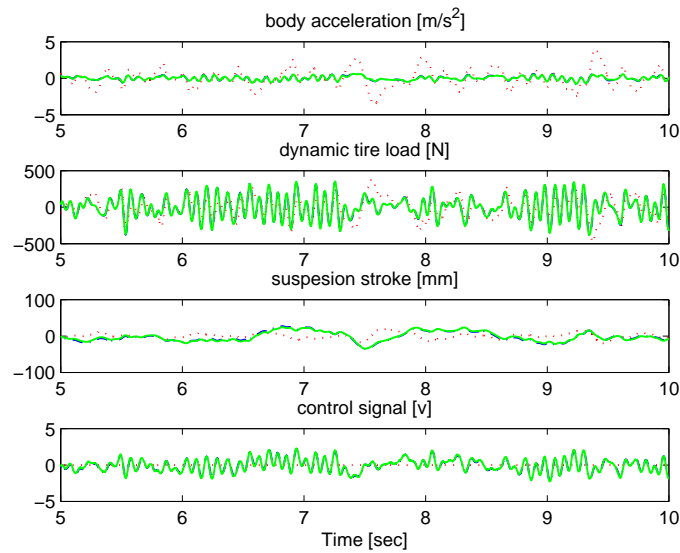
Figure 5.5: Real road response of the preview design considering actuator dynamics, based on linear model simulations: multi-objective (–), LQ-based (-.), Passive (..)

System	RMS $\ddot{z}_s$	RMS DTL	RMS SS	RMS u
LQG preview	0.30	144	0.012	0.779
Multi-objective preview	0.28	140	0.011	0.774

Table 5.3: RMS values of performance outputs, based on linear model simulations

Now we proceed to nonlinear simulations. We compare the performance of multi-objective preview and LQ-based preview suspensions based on the nonlinear model of the system. The results of Fig. 5.6 compares both strategies, for the real road profile of chapter 2. This figure reveals that multi-objective preview suspension behaves more robustly than the LQ-based against system nonlinearities. The RMS values of performance outputs for both designs corresponding to the nonlinear simulations are given in Table 5.4. The results of the Table confirm the above claims. First of all, they reveal that time domain constraint on suspension stroke in the LQ-based design is no longer fulfilled (greater than 0.0267). The multi-objective preview design is superior than the LQ-based one from all other aspects of performance, It provides about 38% more comfort, about 15% more safety and consumes about 12% less power.
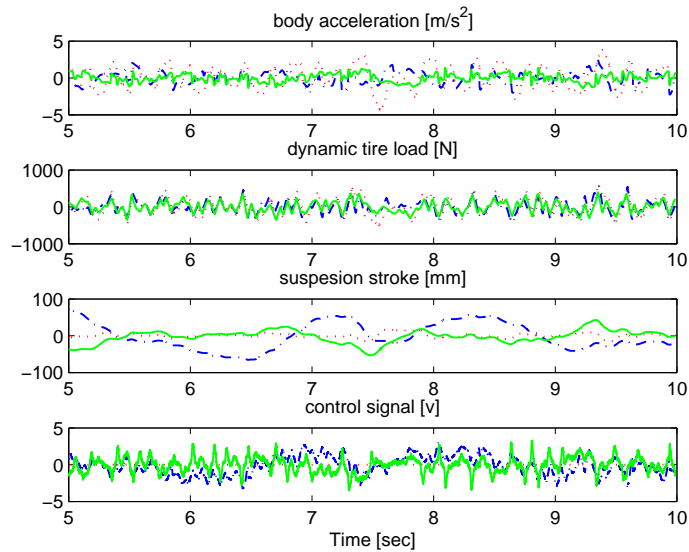

Figure 5.6: Real road response of the preview design considering actuator dynamics, based on nonlinear model simulations: multi-objective (–), LQ-based (-.), Passive (..)

System	RMS $\ddot{z}_s$	RMS DTL	RMS SS	RMS u
LQG preview	0.860	176.65	0.032	1.24
Multi-objective preview	0.51	152.65	0.015	1.10

Table 5.4: RMS values of performance outputs, when nonlinearities are included in the analysis

Chapter 6

IMPLEMENTATION AND RELATED CHALLENGES

This chapter first gives an introduction to dSPACE real time environment and then addresses the challenges associated with the implementation of multi-objective preview suspension, discussed in preceding chapter, in practice . In fact, it mainly deals with providing the preview signal for the controller and finally reports the implementation results.

6.1   An introduction to dSPACE real-time environment

The controller here is implemented using Matlab/Simulink-dSPACE. The dSPACE is a very flexible and powerful system, which features high computational capability and comprehensive I/O periphery, as well as a SIMULINK interface software that allows all applications to be developed in the Matlab/Simulink friendly environment.

dSPACE PPC

dSPACE I/O board (DS1104) allows the processor to interact directly with the sensors and actuators during real-time simulation. When operating in real-time, the variables are transferred between the controller and the controlled system using A/D and D/A converters, encoders and etc. The I/O resources of DS1104 are split between two processors on the board, the master PPC (Power PC) and the slave DSP. The most commonly used elements for the control, such as A/D, D/A and encoders are contained in the master PPC.

Real Time workshop (RTW)

The blocks corresponding to the above converters are already available at Simulink/ RTI1104

Library. The controller containing these I/O blocks is implemented in Simulink environment. The Real-Time Interface tool (RTI) connects Simulink and the Real-Time Workshop (RTW) with dSPACE to form a ready-to-use environment for real-time applications. The RTW is used to convert the Simulink models to real-time C code and automatically builds programs that can be run from the real-time system environment. The RTW includes a tool called Target Language Compiler (TLC), which works as a text processor used to transform an intermediate form of a Simulink model (*.rtw) and the the target files (*.tlc) into C code. The generated C code for the model is then compiled and linked by the Power PC compiler to produce a single executable object file with .ppc (or .sdf: system description file) extension. All these are done by the *build* process of Simulink/RTW.

dSPACE software (ControlDesk)

An experimenting software called ControlDesk, allows real-time management of the running process by providing a virtual control panel with instruments and scopes. In this environment, the executable file obtained through build process (either of *.sdf or *.ppc) is downloaded on the dSPACE board and one could start running the program (i.e, executing the controller). Instrument variables can be linked to certain variables of simulink model, allowing the designer to modify variables during real-time running.

6.2 Preview signal

The excitation signal of the bottom actuator, which serves as a simulator of road unevenness, is generated in Matlab-dSPACE. This signal at T_p time units ahead of time, contaminated with noise (representing measurement noise of reality), can be considered as preview signal entering the controller (a fictitious preview signal). However, the effective disturbance acting on the system (at tire), is not equal to the signal described above. The above signal fails to consider the dynamics of bottom actuator, and neglects the influence of top (suspension) actuator on the bottom actuator. The bottom actuator here, against the forces from suspension actuator, is not sufficiently strong and it may fail to imitate road irregularities as desired. In other words, from preview point of view, in fact, it simulates a soft road.

These effects have been illustrated in Fig. 6.1. It should be noted that the description of chapter 5 relates the inputs w_{eff} and u to the outputs z and y. We may refer to bottom and top actuators as road-imitator and suspension actuator repectively.
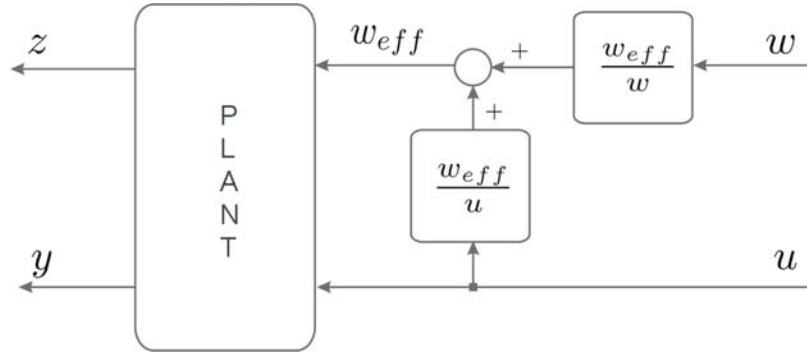

Figure 6.1: Effect of actuators on road disturbance at tire

Clearly, the preview signal entering the controller should reflect the effective disturbance at N_p samples ahead of time, namely $w_{eff}(k+N_p)$. In the following, we will discuss how these effects could be considered to compute the $w_{eff}(k + N_p)$.

6.3   Handling the dynamics of bottom actuator

If we neglect the influence of suspension actuator on imitated road disturbances, the controller designed in previous chapter can be easily, as shown in Fig. 6.2, implemented. The only unknown block, for controller implementation, in this figure is the transfer function of the bottom actuator, i.e., $\frac{w_{eff}}{w}$. For identification of bottom actuator, the real road profile of chapter 2, was used as excitation signal. The effective road unevenness (vertical displacement of the actuator shaft) is captured using the incremental encoder of the linear motor. The time histories of both the input signal and the effective road unevenness are recorded using Matlab-dSPACE environment.

Subspace identification is a convenient identification method for control system applications [34, 61], and is employed for identification of bottom actuator. This method is based on an
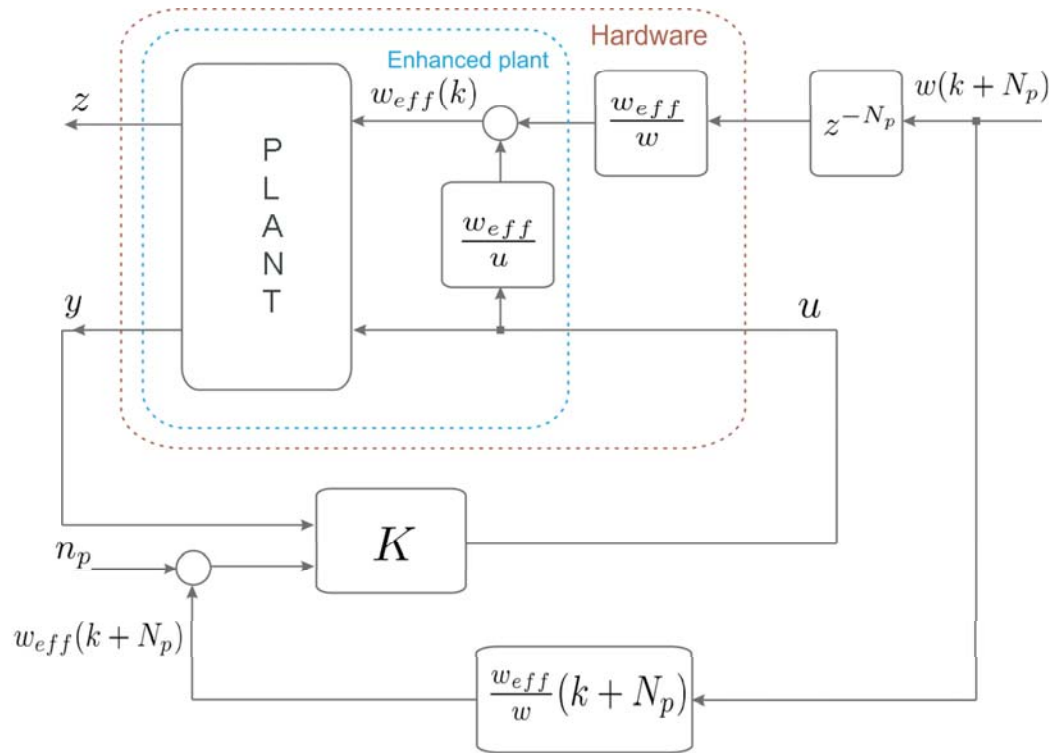
Figure 6.2: Implementation block diagram of preview controller

estimation of a state space model of the structure. Let's the system be described by

$$x_i(k+1) = A_i x_i(k) + B_i u_i(k) + K_i e_i(k)$$
$$y_i(k) = C_i x_i(k) + D_i u_i(k) + e_i(k)$$

where 'i' stands for road-imitator, $u_i(k)$ represents the input (excitation) signal and $y_i(k)$ the measured signal. The idea behind subspace method can be explained as follows [35]: Once the sequence of state vectors $x_i(k)$ are known, together with $y_i(k)$ and $u_i(k)$, the above equation would be linear regression, and C_i and D_i could be estimated by least squares method. This gives also $e_i(k)$. Now similarly A_i, B_i and K_i can be obtained.

But how to compute $x_i(k)$. All states $x_i(k)$ can be formed as linear combinations of the l-step-ahead predicted outputs ($l = 1, 2, \cdots, n$). Thus, the matter is finding these predictors and selecting a basis among them. The subspace methods form an efficient and numerically reliable way of determining the predictors by projections directly on the observed data

sequences.

Matlab command *n4sid* implements this algorithm and it will be employed here to obtain the actuator model.

The excitation and observation is done for 25 seconds. We split the data into two halves, one for estimation and one for validation. A close-up of the input and output is given in Fig. 6.3. Applying the sub-space method, the following state space description is identified
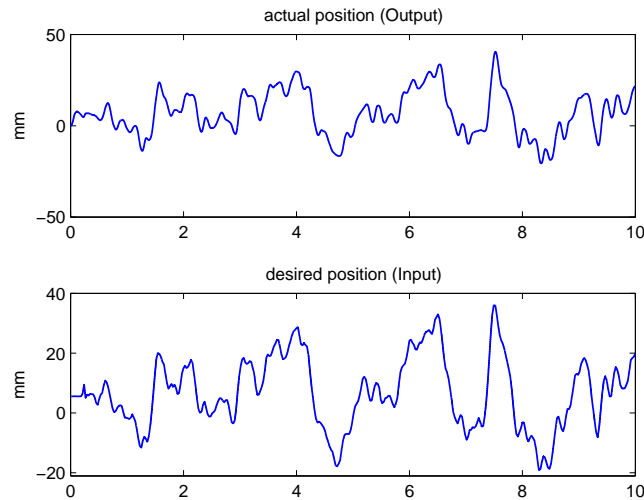
Figure 6.3: A part of the experiment data used for identification of the bottom actuator

for the bottom actuator

$$
A_i = \begin{pmatrix} 0.99578 & -0.02587 \\ 0.010139 & 0.99312 \end{pmatrix}, B_i = \begin{pmatrix} 1.609e - 005 \\ -4.4691e - 005 \end{pmatrix},
$$
$$
C_i = \begin{pmatrix} 226.74 & -2.3329 \end{pmatrix}, D_i = 0
$$

The identification process was lead to a Loss function of 8.74×10^{-5} and FPE (Final Prediction Error) of 8.75×10^{-5}. The obtained model was validated using the second half of the data. The results are given in Fig. 6.4. As it can be seen validation of the obtained system shows a 93.6% data fit.
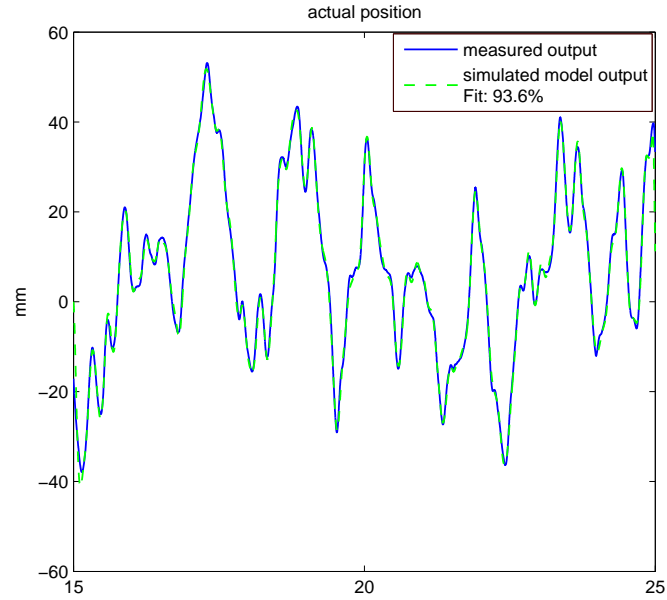
Figure 6.4: Validation of the obtained model for bottom actuator

6.4   Handling the influence of top actuator on imitated road irregularities

To handle this influence on the implementation of preview controller, the following two approaches were investigated:

1. Different observations showed that this effect would not exceed 25% of the applied disturbance through bottom actuator.
   On the other hand, simulations based on nonlinear model of the system, when considering a measurement error of up to 30% for preview signal, showed a maximum 12% deterioration in system performance. Therefore, the first approach to round this problem, is to neglect this effect in the controller synthesis and to consider it as measurement error on capturing preview signal.

2. The second approach is based on identifying the corresponding transfer function

(w_{eff}/u), and performing the controller design for the enhanced plant shown in Fig. 6.2.

To identify this influence , we recorded the control signal during pure feedback control of the system and applied it as excitation signal in the identification process. We also applied some other inputs, however, we found out that the system is strongly nonlinear and can not accurately described by a linear system (transfer function).

Fig 6.5 shows the input/output pair used for the identification. Here the ARX (Auto-Regressive with eXogenous input) model was found to describe the system dynamics better. To find a good structure for the data, Matlab commands *arxstruc* and *selstruc* were used. Simulating the model using the validation data, showed a 40% fit. This percentage, because of the nonlinearites in the system, unreasonably reduces when other data sets are used as validation data.
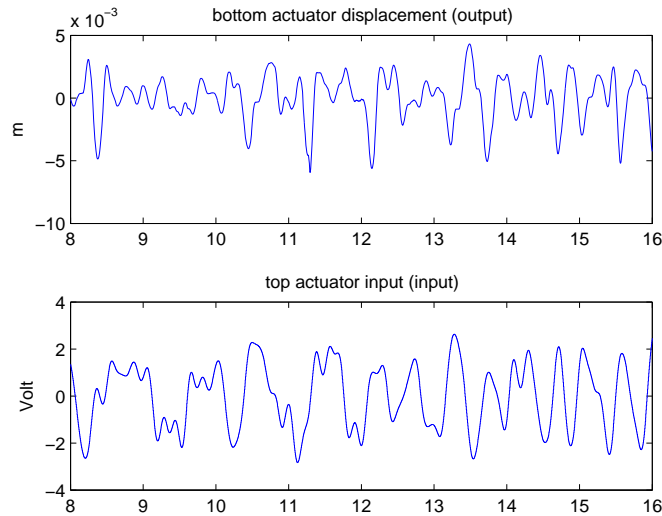

Figure 6.5: Input/ output pair for identification of suspension actuator

Implementation of both designs showed that the second design leads to worse results than the first one. This is because the identified model for $\frac{w_eff}{u}$ has less accuracy.

6.5 Preview control application and results

Based on the discussion in preceding section, to handle the effect of suspension actuator on imitated road irregularities, we employed the first approach, i.e., its effect was considered as measurement error of preview signal. The algorithm of Fig. 6.2 was implemented in Matlab/Simulink-dSPACE.

As mentioned in previous chapter, the measured signals for control consist of vertical accelerations of body and wheel, which are captured by two accelerometers. The body acceleration observed this way, is also used to evaluate the ride comfort. To evaluate ride safety, a force sensor is mounted at the bottom of tire, which measures dynamic tire load.

For the real road profile of chapter 2 as the system excitation, a close-up of measured performance outputs is given in Fig. 6.6 and the results for the whole time of 25 sec are detailed in Table 6.1. As it can be seen, the dynamic tire deflection for all three suspension system is identical, probably mainly because of low bandwidth of the actuator, which can not affect system frequency response magnitude at wheel-hop resonance frequency. The pure feedback system improves the ride comfort about 19% and the preview shows an improvement of 22% with respect to pure feedback.

System	RMS $\ddot{z}_s$	RMS DTL
Passive	1.82	217.63
Multi-objective	1.48	217.63
Multi-objective preview	1.14	217.63

Table 6.1: RMS values of measured performance outputs for multi-objective designs, for a real road input
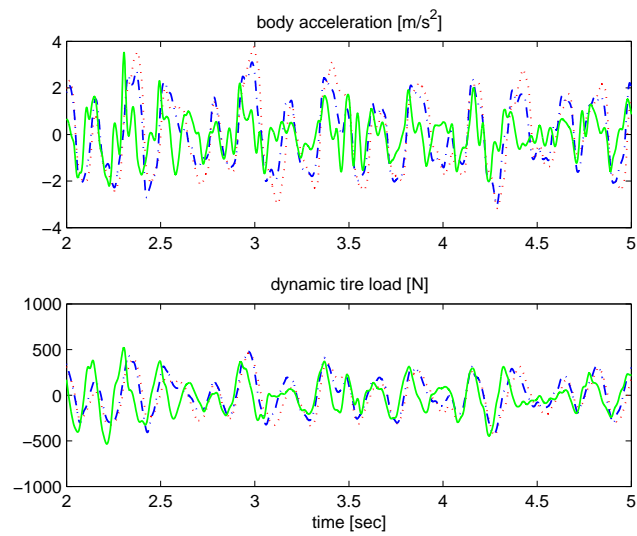
Figure 6.6: Real road response of the Multi-objective implementation: Preview (–),
Pure feedback (-.), Passive (..)

Chapter 7

CONCLUSION AND OUTLOOK

In this study, the preview suspension design was formulated as a multi-objective design problem, where performance outputs are divided into two parts of to-be-minimized and to-be-constrained. The best possible performance could be obtained if constrained outputs are allowed to vary freely as long as the constraints are fulfilled. To this goal, an H_∞/GH_2 design scheme was proposed for preview suspensions which provides a multi-objective design framework.

The main feature of this scheme is performing the design for the worst case disturbance input, and thereby providing more robustness for the system. To design a system to perform satisfactorily for a wide range of road irregularities, L_2-gain of system is minimized wherever minimization is required. Also, for the constrained outputs, the GH_2 norm measure is used which fulfills the constraints for the worst case disturbance input.

Preview control of the active vehicle suspensions has been extensively studied in the literature. The state-of-the-art control algorithm is the LQ-based one (LQG preview), which is a single objective design and is based on the time domain optimization of the objective for just white noise inputs.

Therefore, the main motivation for employing the multi-objective preview control of this study for active vehicle suspensions was the improvement of system performance for all road types as well as constraining suspension working space, not minimizing it. The simulation results for different road profiles, showed the superiority of multi-objective preview controller to LQG preview controller, However some other benefits of the multi-objective preview design to LQG preview are

- The design is done in one-step and it requires no observer design. In LQG preview design, adding the observer, which itself should be obtained through trials, may also call for re-design of the controller.

- It requires no aposteriori analyses to check for fulfillment of constraints, whereas in the LQG design, design of both controller and observer is done through iterative processes.

- This design is robuster than LQ-based one. The simulation results of chapter 3 proved the robustness against parameter changes, and those of chapter 5, robustness against nonlinearities.

- Dynamic weighting functions can be easily considered in the design procedure to emphasize on certain frequency range in performance outputs.

- LMI formulation of the problem allows for considering pole location constraints to guarantee sufficient stability margins for the system.

- It could be easily extended to design a self-scheduled LPV controllers to guarantee system performance against parameter variations.

We believe that the presented results point out the efficiency of the proposed scheme and it seems that H_∞/GH_2 preview to be a convenient approach for preview suspension design.

Future works

H_2/GH_2 design scheme

If all road irregularities can be modeled by white noise or impulse, The H_∞/GH_2 preview design scheme, employed in this study, appears to be conservative. Therefore to enjoy the benefits of this design scheme and simultaneously obtain a less conservative design, based on the 2-norm interpretation of the chapter 2, an H_2-based optimization seems to be a proper choice and more promising. However, the constrained part of the problem should also be solved for white noise inputs. It can be investigated and compared with results of this study.

Semi-active preview

Clearly, fully-active suspensions provide the best trade-off between conflicting objectives of comfort, required working space and handling, but it is far more complex, expensive, less failure safe and can lead to an unacceptable increase of fuel consumption. The intermediate solution between conventional and fully-active is the semi-active control. When the control system fails, the semi-active system can still work in passive condition. Compared with active and passive suspension systems, the semi-active suspension system combines the advantages of both active and passive suspensions; i.e., it provides good performance compared to passive suspensions and is economical, safe, and doesn't require either higher-power actuators or large power supply [63]. However, the control studies of fully active suspension systems are usually the first step in design of control strategies for less expensive and more reliable semi-active dissipative suspensions [45]. developing the results of this study to the semi-active preview suspension would help to develop a more practical and economical suspension.

Wheelbase preview

It was discussed in Chapter 4 that the wheelbase preview, i.e., the reconstruction of the preview information from measurements at the front wheels of vehicle, even though could not deliver the same performance improvement of look-ahead preview, is more reliable and promising in the sense of detecting pseudo-obstacles and imposes no additional sensing costs to the system. However,we gave just an insight on wheelbase preview control in this study. A complete study of the multi-objective (H_∞/GH_2) wheelbase preview control with employment of the detector designed in chapter 4, could be considered in future works.

Order reduction of the controller

Clearly, the greater the preview horizon, the more improvement in system performance could be observed. But, the longer the preview horizon, leads to increased controller complexity and hence arising implementation problems.
As we experienced, implementation of such a controller, calls for higher speed processors, and hence increases system costs. One remedy to deal with this problem, is to apply the order reduction approaches to the obtained controller and implement the reduced order controller. This could be seen in the future works.

GLOSSARY

Abbrevations

A/D: analog to digital converter

D/A: digital to analog converter

ISE: integral square error

LTI: linear time invariant

LMI: linear matrix inequality

LQR: linear quadratic regulator

LQG: linear quadratic gaussian

LTR: loop transfer recovery

MIMO: multiple input multiple output system

SISO: single input single output system

PSD: power spectral density

RMS: root mean square

LPV: linear parameter varying

SS: suspension stroke

W$\ddot{z}_s$: weighted body acceleration

TD: tire deflection

vs.:   versus

SVD: singular value decomposition

General symbols

$\mathbb{R}$:   set of real numbers.

$\mathbb{C}$:   set of complex numbers.

$tr(A)$: trace A.

$\lambda_i(A)$: i_{th} eigenvalue of A.

$\overline{\sigma}(A)$: the largest singular value of A.

$\underline{\sigma}(A)$: the smallest singular value of A.

$\sigma_i(A)$: i_{th} singular value of A.

$\rho(A) = \max_i |\lambda_i(A)|$: spectral radius of A.

$\mathcal{RH}_\infty$: The set of all real rational (prefix $\mathcal{R}$) functions bounded on $Re(s) = 0$ (including at ∞) and analytic in $Re(s) > 0$.

Subscripts

subscript: *represents components related to*

s, u: sprung, unsprung mass

t: tire

r, l: right, left half

f, r: front, rear part

Systems' Notation

The whole closed loop, discrete time system:

$$\mathcal{S}: \begin{cases} \dot{x}(t) = Ax(t) + Bu(t) \\ y(t) = Cx(t) + Du(t) \end{cases} = \left[\begin{array}{c|c} A & B \\ \hline C & D \end{array}\right] = C(sI - A)^{-1}B + D$$

where, u_i could be any possible input of the system like reference signal r, input disturbance d_i, output disturbance d_o or measurement noise n.

$$\text{Plant} \qquad G = \left[\begin{array}{c|c} A_g & B_g \\ \hline C_g & D_g \end{array}\right]$$

$$\text{Preview} \qquad \left[\begin{array}{c|c} A_p & B_p \\ \hline C_p & D_p \end{array}\right]$$

$$\text{Controller} \quad K = \left[\begin{array}{c|c} A_k & B_k \\ \hline C_k & D_k \end{array}\right]$$

For description of continuous time plant, subscript 'c' is used and subscript 'o' is used to represent covariance matrices for observer design. The subscript 'mot' represents the suspension actuator (a PM-LSM) and the subscript 'i' stands for the bottom actuator (road imitator)

Signal Norms & Spaces

The concept of *norm* is the mathematical equivalent of ordinary notion of size, which is used to compare different objects (vectors, signals and systems). Every object can be thought of as a member of a set. A set armed with some operations and properties is called a *space*.

There are a variety of norms for different objects. Here we will review the norms for the vectors and signals.

Norms of vectors in $\mathbb{C}^n$

Suppose that $x = \begin{pmatrix} x_1 & x_2 & \cdots & x_n \end{pmatrix}$ is an n-dimensional complex-valued vector, i.e., $x \in \mathbb{C}^n$, then for $1 \le p \le \infty$, the p-norm is defined as

$$\|x\|_p = \begin{cases} \left(\sum_{i=1}^n |x_i|^p\right)^{1/p}, & 1 \le p < \infty \\ \max_{i=1,2,\cdots,n} |x_i|, & p = \infty \end{cases}$$

mostly used special cases are the norms

$$\|x\|_1 = \sum_{i=1}^n |x_i|, \quad \|x\|_2 = \left(\sum_{i=1}^n |x_i|^2\right)^{1/2}, \quad \|x\|_\infty = \max_{i=1,2,\cdots,n} |x_i|$$

Norms of signals

For $1 \le p \le \infty$, the p-norm or L_p-norm of a continuous time scalar-valued signal z,

$\|z\|_p$, is defined as

$$\|z\|_p = \begin{cases} \left(\int_{-\infty}^{\infty} |z(t)|^p dt \right)^{1/p}, & 1 \le p < \infty \\ \sup_{t \in \mathbb{R}} |z(t)|, & p = \infty \end{cases}$$

if $z(t)$ is vector-valued, i.e., for each time t, $z(t)$ is a vector in $\mathbb{C}^n$, this defintion is generalized to [6]

$$\|z\|_p = \begin{cases} \left(\int_{-\infty}^{\infty} \|z(t)\|^p dt \right)^{1/p}, & 1 \le p < \infty \\ \sup_{t \in \mathbb{R}} \|z(t)\|, & p = \infty \end{cases}$$

where $\|.\|$ is any norm on the n-dimensional space $\mathbb{C}^n$. When the above norm is finite, the signal is said to belong to L_p space.

The signal norms that we mostly need are L_2 and L_∞ norms. The L_2 is defined as

$$\|z\|_2 = \left(\int_{-\infty}^{\infty} |z(t)|^2 dt \right)^{1/2} = \left(\frac{1}{2\pi} \int_{-\infty}^{\infty} |z(j\omega)|^2 d\omega \right)^{1/2}$$

The second equality is the statement of Parseval's theorem. The L_2 space is the space of square integrable signals.

The L_∞ norm is defined as

$$\|z\|_\infty = \sup_{t \in \mathbb{R}} \|z(t)\|_\infty = \sup_{t \in \mathbb{R}} \max_i |z_i(t)|$$

The L_∞ space is the space of bounded signals.

The square of L_2 norm, $\|z\|_2^2$, is often called the energy of the signal z, and L_∞ norm its amplitude peak value.

BIBLIOGRAPHY

[1] . Easy ride. *IEEE Spectrum*, pages 12–14, May 2005.

[2] Abdellahi, E., Mehdi, D. and M'Saad, M. On the design of active suspension system by H_∞ and mixed H_2/H_∞ . In *Proceedings of American Control Conference*, pages 4041–4045, 2000.

[3] Apkarian, P., Gahinet, P. and Becker, G. Self-scheduled H_∞ control of linear parameter-varying systems: a design example. *Automatica*, 31(9):1251–1261, 1995.

[4] Aström, K.J. and Wittenmark, B. *Computer controlled systems*. Prentice-Hall, Inc., Englewood Cliffs, 1984.

[5] Bender, E.K. Optimum linear preview control with application to vehicle suspension. *ASME, Jounal of Basic Engineering*, 100:213–221, 1968.

[6] Bosgra, O.H. and Kwakernaak, H. *Design methods for the control systems*. DISC Lecture Note, Dutch Inst. Syst. Control, 2001.

[7] Boyd, S., Ghaoui, L.E., Feron, E. and Balakishnan, V. *Linear Matrix Inequalities in system and control*. SIAM, Philadelphia, 1994.

[8] Burl, J.B. *Linear optimal control: H_2 and H_∞ methods* . Addison- Wesley, 1998.

[9] Causemann, P. *Kraftfahrzeugstossdämfer*. MI-Verlag, 1999.

[10] Chen, H. and Guo, K. An LMI approach to multiobjective RMS gain control for active suspensions. In *Proc. American Contr. conf.*, pages 2646–2651, 2001.

[11] Chen, H. and Guo, K. Constrained H_∞ control of active suspensions: an LMI approach. *IEEE Transactions on Control Systems Technology*, 13:412–421, 2005.

[12] Chen,T. , Francis, B.A. *Optimal Sampled-Data Control Systems*. Springer, 1995.

[13] Chilali, M. and Pascal, G. H_∞ design with pole placement constraints: an LMI approach. *IEEE Transactions on Automatic Control*, 41 (3):358–367, 1996.

[14] Doyle, J.C. and Stein, G. Robustness with observers . *IEEE Transactions on Automatic Control*, 24:607–611, 1979.

[15] Engelman, G.H. and Rizzoni, G. Including the force generation process in active suspension control formulation . In *Proceedings of American Control Conference*, 1993.

[16] Fan, Y. and Crolla, D.A. Wheelbase preview optimal control for active vehicle suspensions. *Chinese Journal of Mechanical Engineering*, 2, 1998.

[17] Fischer, D. and Isermann, R. Mechatronic semi-active and active vehicle suspensions. *Control engineering practice*, 12:1353–1367, 2004.

[18] Foag, W. *Regelungstechnische Konzeption einer aktiven PKW-Federung mit 'Preview'*. Fortschritt-berichte VDI, 1990.

[19] Franklin, G.F. , Powell, J. D. and Workman, M. L. *Digital control of dynamic system*. Addison-Wesley, 1989.

[20] Fritsch, O. and Akbari, A. *Vergleich vollaktiver und langsamaktiver Federungsysteme mit LQ-Regelung*. Semesterarbeit, TU Munich, 2007.

[21] Kasper, R. Frühhauf, F. and Lückel, J. Design of an active suspension for a passenger vehicle model using input processos with time delays. *Vehicle System Dynamics*, 15:126–138, 1986.

[22] Gahinet, P., Nemirovski, A., Laub, A.J. and Chilali, M. *LMI control toolbox*. The Mathworks Inc., 1995.

[23] Gao, H., Lam, J. and Wang, C. Mutiobjective control of vehicle active suspension systems via load-dependent controllers. *Journal of Sound and Vbration*, 290:654–675, 2006.

[24] Szaszi, I. Gaspar, P. and Bokor, J. Design of robust controllers for active vehicle suspension using the mixed μ synthesis . *Vehicle System Dynamics*, 40 (4):193–228, 2003.

[25] Marsh, C. Gordon, T. and Milsted, M. A comparison of adaptive LQG and nonlinear controllers for vehicle suspension systems. *Vehicle System Dynamics*, 20:321–340, 1991.

[26] Hac, A. Optimal linear preview control of active vehicle suspension. *Vehicle System Dynamics*, 21:167–195, 1992.

[27] Hansen, C.H. and Snyder, S.D. *Active control of noise and vibration* . E&FN Spon, London, 1997.

[28] Hayakawa, K., Matsumoto, K., Yamashita, M., Suzuki, Y., Fujimori, K. and Kimura, H. Robust H_∞ control of decoupled automobile active suspension systems. *IEEE Transactions on Automatic Control*, 44:392–396, 1999.

[29] Hedrick, J. K. and Butsuen, T. Invariant properties of automotive suspensions. *Proceedings of the Institution of Mechanical Engineers. Pt.D. Journal of Automobile Engineering*, 204:21–27, 1990.

[30] Hrovat, D. Optimal suspension performance for 2-D vehicl emodels. *Journal of Sound and Vibration*, 146(1):93–110, 1991.

[31] Hrovat, D. Survey of advanced suspension system developements and related optimal control applications. *Automatica*, 33:1781–1817, 1997.

[32] Iwata, Y. and Nakano, M. Optimum preview control of vehicle air suspension. *Bulletin of the JSME*, 19(138):1485–1489, 1976.

[33] Langlois, R.G. and Anderson, R.J. Preview control algorithms for the active suspension of an Off-Road vehicle. *Vehicle System Dynamics*, 24:65–97, 1995.

[34] Ljung, L. *System identification - Theory for the user*. Prentice Hall, 1999.

[35] Ljung, L. *System identification toolbox, for use with Matlab*. The Mathworks Inc., 2005.

[36] Longhurst, C.J. The suspension bible. In *http://www.carbibles.com*.

[37] Wilson, D.A. Louam, N. and Sharp, R.S. Optimal control of vehicle suspension incorporating the time delay between front and rear wheel inputs . *Vehicle System Dynamics*, 17:317–336, 1988.

[38] Marzbanrad, J., Ahmadi, G., Zohoor, H. and Hojjat, Y. Stochastic optimal preview control of vehicle suspension. *Jounal of Sound and Vibration*, 275:973–990, 2004.

[39] Moran, A. and Nagai, M. Analysis and design of active suspensions by H_∞ robust control theory . *JSME International journal*, 35 (3):427–437, 1992.

[40] Pellegrini, E. and Koch, G. *Modellierung, Ansteuerung und Regelung eines hochdynamischen Linearmotors zur aktiven Schwingungsdmpfung eines Kfz-Fahrwerks.* Semesterarbeit, TU Munich, 2008.

[41] Peng, H., Strathearn, R. and Ulsoy, A.G. A novel active suspension design technique–simulation and experimental results. In *Proceedings of American Control Conference*, pages 709–713, 1997.

[42] Pressnell, J. *Citroen DS: The complete story.* Crowood Press, 1999.

[43] Prokop, G. and Sharp, R.S. Performance enhancemnet of limited-bandwidth active automotive suspensions by road preview. *IEE proceedings on Control Theory Applications*, 142 (2):140–148, 1995.

[44] Roh, H.S. and Park, Y. Stochastic optimal preview control of an active vehicle suspension. *Jounal of Sound and Vibration*, 220(2):313–330, 1999.

[45] Sammier, T., Sename, O. and Dugard, L. Skyhook and H_∞ control of semi-active suspensions: Some practical aspects. *Vehicle System Dynamics*, 39(4):279–308, 2003.

[46] Sasaki, M., Kamiya, J. and Shimogo, T. Optimal preview control of vehicle suspension. *Bulletin of the JSME*, 19(129):265–273, 1976.

[47] Scherer, C.W. and Weiland, S. *Linear Matrix Inequalities in control.* DISC Lecture Note, Dutch Inst. Syst. Control, 2000.

[48] Scherer, C.W., Gahinet, P. and Chilali, M. Multi-objective output-feedback control via LMI optimization. *IEEE Transactions on Automatic Control*, 42:896–911, 1997.

[49] Schindler, A., Strieter, R. and Bretthauer, G. Integraler Ansatz fuer eine Fahrzeugregelung mit Preview. In *Chassis tech. Munich*, page , 2007.

[50] Sharp, R.S. and Hassan, S.A. On the performance capabilities of active automobile suspension systems of limited bandwidth. *Automatica*, 30:1717–1729, 1994.

[51] Spirk, S. and Koch, G. *Identifikation des vertikaldynamischen Verhaltens eines Kfz-Fahrwerks an einem Viertelfahrzeugprfstand.* Semesterarbeit, TU Munich, 2008.

[52] Streiter, R. Active preview suspension system: ABC Prescan in the F700. *ATZ*, 110:4–11, 2008.

[53] Sun, P.Y. and Chen, H. Multi-objective output-feedback suspension control on a half-car model. In *IEEE Conference on Control Applications.*

[54] K. Takaba. A tutorial on preview control systems. In *SICE Annual Conference in Fukui*, pages 1388–1393, 2003.

[55] Thiele, B. and Akbari, A. *Optimal preview control of vehicle suspensions.* Semesterarbeit, TU Munich, 2007.

[56] Thompson, A.G., Davis, B.R. and Pearce, C.E.M. An optimal linear active suspension with finite road preview. *Society of Automotive Engineers Inc.*, page Paper No. 800520, 1980.

[57] Tomizuka, M. Optimal continuous finite preview problems. *IEEE Transactions on Automatic Control*, 20:362–365, 1975.

[58] Tomizuka, M. Optimal preview control with application to vehicle suspension. *ASME, Jounal of Dynamic Systems Measurement and Control*, 98 (3):309–315, 1976.

[59] Ulsoy, A. G., Hrovat, D. and Tseng, T. Stability robustness of LQ and LQG active suspensions. *ASME Jounal of Dynamic Systems, Measurement and Control*, 116(1):123–131, 1994.

[60] Van Loan, C.F. Computing integrals involving the matrix exponential. *IEEE Transactions on Automatic Control*, 23:395–404, 1978.

[61] VanOverschee, P. and DeMoor, B. *Subspace identification of linear systems: theory, implementation, applications.* Kluwer Academic Publishers, 1996.

[62] Wang, J. , Wilson, D. A. and Halikias, G. D. H_∞ robust performance control of decoupled active suspension systems based on LMI method . In *Proceedings of American Control Conference*, pages 2658–2663, 2001.

[63] Chen, G. Li, W.H. Yao, G.Z., Yap, F.F and Yeo, S.H. MR damper and its application for semi-active control of vehicle suspension system. *Mechtronics*, 12:963–973, 2002.

[64] Yoshimura, and Edokoro, K. An active suspension model for rail/vehicle systems with preview and stochastic optimal control. *Journal of Sound and Vibration*, 166:507–519, 1993.

[65] Zaremba, A., Hampo, R. and Hrovat, D. Optimal active suspension design using constrained optimization. *Jounal of Sound and Vibration*, 207(3):351–364, 1997.

[66] Zhou, K., Khargonekar, P. P., Stoustrup, J. and Niemann, H. H. Robust performance of systems with structured uncertainties in state space. *Automatica*, 31 (2):249–255, 1995.

Relevant papers:

- Yousefi, A., Akbari, A. and Lohmann, B., Reduced order robust controllers for active vehicle suspensions, *IEEE Conference on Control Applications*, 2006, pp. 693 - 698

- Akbari, A. and Lohmann, B., Static output-feedback H_∞ design for vehicle suspensions based on an Iterative Linear Matrix Inequality algorithm, European Control Conference, 2007, pp. 1249-1256

- Akbari, A. and Lohmann, B., Robust detection of front wheel disturbance using LPV H_∞, *27th IASTED International Conference on Modelling, Identification and Control (MIC 2008)*, Innsbruck, 11-13 Feb.

- Akbari, A. and Lohmann, B., output feedback H_∞ preview control of active vehicle suspensions, *27th IASTED International Conference on Modelling, Identification and Control (MIC 2008)*, Innsbruck, 11-13 Feb.

- Akbari, A. and Lohmann, B., GL_2 estimation of steer wheel disturbance, *IFAC World Congress 2008*, Seoul, South Korea, , pp. 10750-10755

- Akbari, A. and Lohmann, B., Multi-objective preview control of active vehicle suspensions, *IFAC World Congress 2008*, Seoul, South Korea, pp. 3398-3403

- Akbari, A. and Lohmann, B., Output feedback H_∞/GH_2 preview control of active vehicle suspensions: A comparison study to LQG preview, submitted to *Vehicle System Dynamics*

- Output feedback multi-objective preview control of active vehicle suspensions: Experimental results, to be submitted to *Control Engineering Practice*